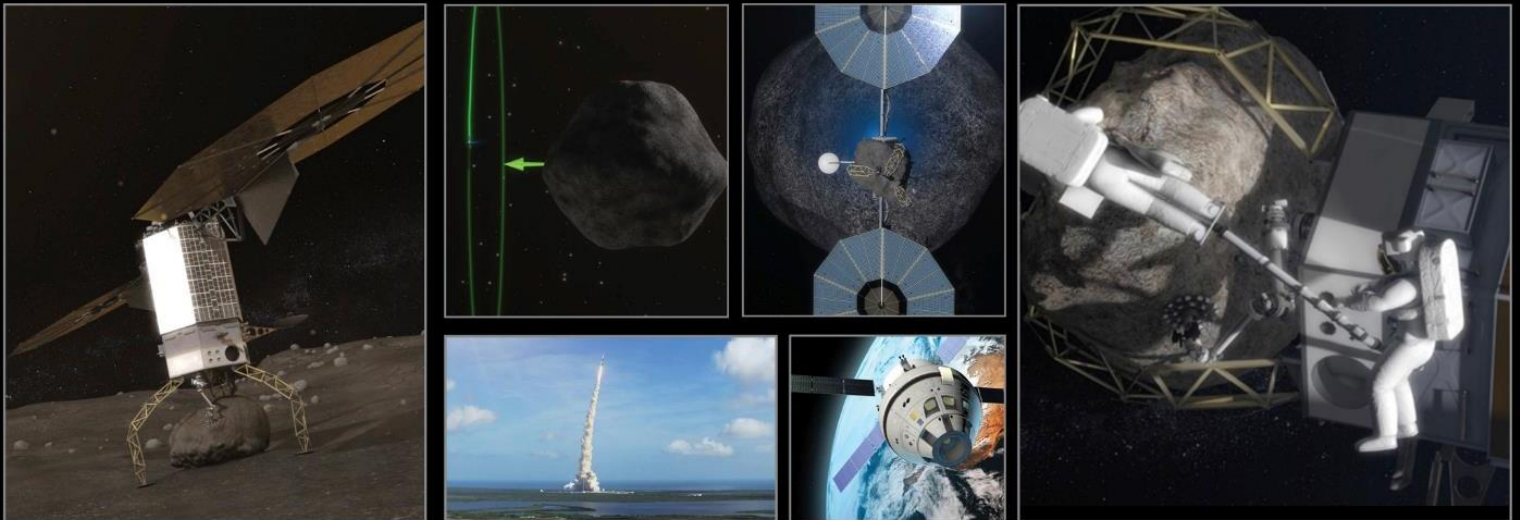


This document is a NASA working document and is subject to further revision. This document been reviewed for release to the public and is not export controlled.

Asteroid Redirect Mission (ARM) Formulation Assessment and Support Team (FAST) Final Report Draft for Public Comment



November 23, 2015

This document is a NASA working document and is subject to further revision. This document been reviewed for release to the public and is not export controlled.

This Page left Intentionally Blank

This document is a NASA working document and is subject to further revision. This document has been reviewed for release to the public and is not export controlled.

Contents

Executive Summary	3
FAST Overview	13
<i>Purpose</i>	13
<i>Asteroid Redirect Mission Background</i>	13
<i>Study Request</i>	15
<i>Membership</i>	15
FAST Responses to ARRM Project Questions.....	16
<i>Origin of 2008 EV₅</i>	16
<i>Boulder Spatial and Size Distributions</i>	20
<i>Surface Geotechnical Properties</i>	29
<i>Boulder Physical Properties</i>	35
<i>Post Collection Boulder Handling</i>	43
<i>Pre-ARCM Boulder Assessments for Crew Safety</i>	46
<i>Containment Considerations</i>	47
Potential Investigations	50
<i>Potential Investigation Descriptions</i>	50
<i>Proposed Investigations Categorization Table</i>	58
Summary of Public Inputs	63
Additional Findings	65
Closing Remarks	66
Appendices.....	67
<i>Appendix A1: Full Response on the Origin of 2008 EV₅</i>	67
<i>Appendix A2: Phase Function Analysis</i>	73
<i>Appendix A3: Asteroid 2008 EV₅ – spectral analysis</i>	77
<i>Appendix A4: Disk-integrated Photometric Models of the ARM Mission Asteroid Target 2008 EV₅</i>	81
<i>Appendix B1: Full Response on the Boulder Spatial and Size Distributions</i>	85
<i>Appendix B2: Input form Michael Busch concerning Boulders on 2008 EV₅</i>	102
<i>Appendix C: Full Surface Geotechnical Properties Response</i>	105
<i>Appendix D: Additional Boulder Physical Property Information</i>	116
Acronym List	117

This document is a NASA working document and is subject to further revision. This document has been reviewed for release to the public and is not export controlled.

Executive Summary

The Formulation Assessment and Support Team (FAST) for Asteroid Redirect Mission (ARM) was a two-month effort that was chartered by NASA to provide timely inputs for mission requirement formulation in support of the Asteroid Redirect Robotic Mission (ARRM) Requirements Closure Technical Interchange Meeting (TIM) in mid-December of 2015, to assist in developing an initial list of potential mission investigations, and to provide input on potential hosted payloads and partnerships. Participation in the FAST by non-civil service personnel was limited to providing non-consensus, non-voting input. To ensure preparedness for the start of formal formulation and development of the ARM, the FAST focused their inputs on scientific return and knowledge gain from ARM in the areas of science, planetary defense, asteroidal resources and in-situ resource utilization (ISRU), and capability and technology demonstrations. This report represents the FAST's final product for the ARM.

The ARM consists of two mission segments: 1.) the ARRM, the first robotic mission to visit a large (greater than ~100 m diameter) near-Earth asteroid (NEA), collect a multi-ton boulder from its surface along with regolith samples, and return the asteroidal material to a stable orbit around the Moon; and 2.) the Asteroid Redirect Crewed Mission (ARCM), in which astronauts will explore the boulder and return to Earth with samples. NASA originally proposed a robotic mission concept to capture an entire small asteroid (4–10 m in size) that would leverage several key ongoing activities in human exploration, space technology, and planetary defense. Subsequently, an alternate approach to collect a boulder from a large asteroid was also proposed. NASA evaluated both mission approaches, to determine their feasibility, identify the important differences between them, and evaluate the key risks and figures of merit for each concept. On March 25, 2015, NASA announced the selection of the boulder capture option for the robotic segment of ARM. The ARRM is planned launch at the end of 2020 and the ARCM is planned for late 2025.

To achieve its long-term goal of sending humans to Mars, NASA plans to proceed in a series of incrementally more complex human spaceflight missions. Today, human flight experience extends only to Low Earth Orbit (LEO), and should problems arise during a mission, the crew can return to Earth in a matter of minutes to hours. The next logical step for human spaceflight is to gain flight experience in the vicinity of the Moon. These cis-lunar missions provide a “proving ground” for the testing of systems and operations while still accommodating an emergency return path to the Earth that would last only several days. Cis-lunar mission experience will be essential for more ambitious human missions beyond the Earth-Moon neighborhood, which will require weeks, months, or even years of transit time. A principle objective of the ARM is the development of a high-power Solar Electric Propulsion (SEP) vehicle, and the demonstration that it can operate for many years in interplanetary space, which is critical for deep-space exploration missions. A second prime objective of ARM is to conduct a human spaceflight mission involving in-space interaction with a natural object, in order to provide the systems and operational experience that will be required for eventual human exploration of Mars, including the Martian moons Phobos and Deimos. The ARCM provides a compelling focus for the early flights of the Orion program, which will take place before the infrastructure for more ambitious flights will be available. Astronauts will participate in the scientific in-space investigation of nearly pristine asteroid material, at most only minimally altered by the capture process. The ARCM will provide the opportunity for human explorers to work in space with asteroid material, testing the activities that would be performed and tools that would be needed for later exploration of primitive body surfaces in deep space. The operational experience would be gained close to our home planet, making it a significantly more affordable approach to obtaining this experience.

This document is a NASA working document and is subject to further revision. This document has been reviewed for release to the public and is not export controlled.

NASA has identified the NEA 2008 EV₅ as the reference target for the ARRM (radar-based shape model shown in Figure 1). Final target selection will be made approximately a year before launch. 2008 EV₅ is a carbonaceous (C-type) asteroid that has been remotely characterized (radar, visual, and infrared wavelengths), is believed to be hydrated, and provide significant ARV return mass (boulders greater than 20 metric tonne) within the current baseline of 5-years between the ARRM and the ARCM. 2008 EV₅ provides a valid target that can be used to help with formulation and development efforts, and is the reason for it being the main NEA around which the FAST focused its attention.

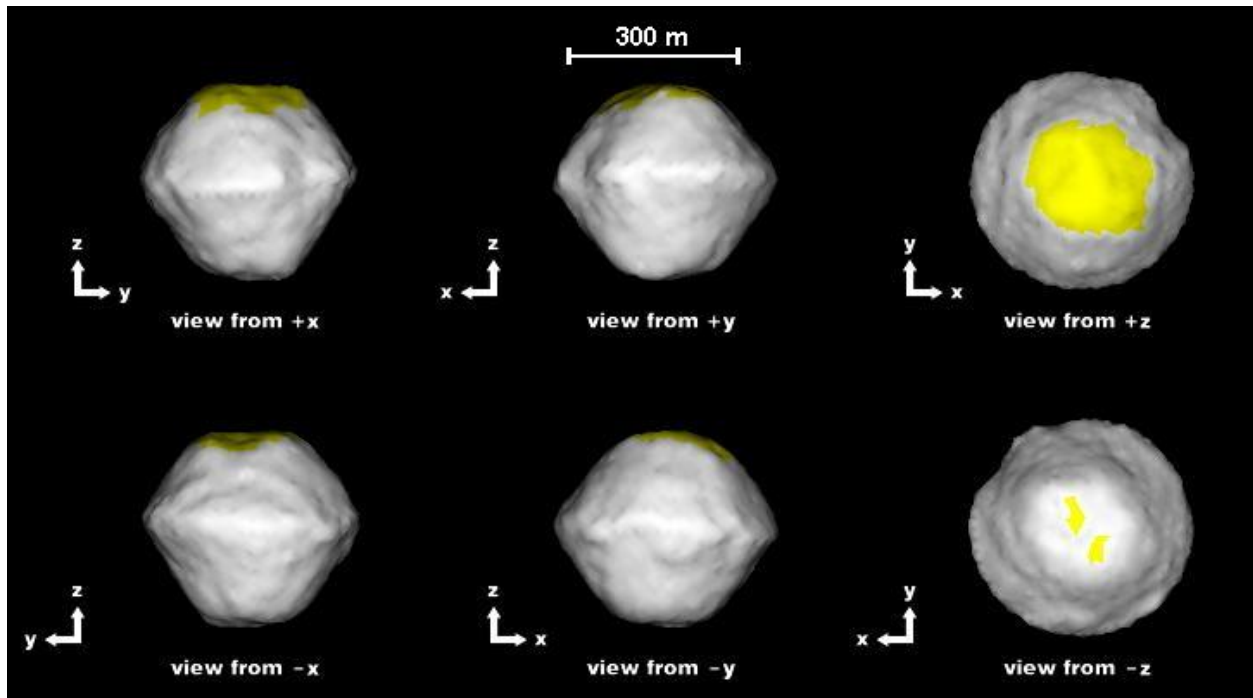


Figure 1: 2008 EV₅ shape model from radar observations [Busch et al., 2011].

The first section of this report provides details including the purpose of the FAST, an overview of ARRM, a summary of the study request, and information about the FAST selection process and membership. Eighteen participants were selected from the 100 applications received from highly-qualified individuals representing academia, industry, NASA, non-profit research institutes, and other organizations (see Table 1 for a list of the FAST members).

The second section of this report includes responses to a set of high-priority questions that were derived from the ARRM engineering team's risk analysis and were needed to help design and develop the ARRM mission, spacecraft and capture system. The responses were formulated to support the ARRM Requirements Closure Technical Interchange Meeting (TIM) planned to be held in mid-December of 2015. The questions have been grouped into seven topics and the major findings for each question are summarized below. For additional details, please see the "FAST Responses to ARRM Project Questions" section and associated appendices and references for each topic.

1. Origin of 2008 EV₅

What is the orbital history of 2008 EV₅ and has that history affected the properties of the asteroid and candidate boulders? (Where has it been in the Solar System and for how long? Has it been

This document is a NASA working document and is subject to further revision. This document has been reviewed for release to the public and is not export controlled.

closer/farther from the Sun than it is now?) Initial dynamical modeling indicates that 2008 EV₅ started its existence as part of a much larger body in the asteroid belt (likely diameter greater 100 km) and migrated inward across the inner main belt over many millions of years until it reached a planetary gravitational resonance that drove it into the NEA population. After escaping the asteroid belt, en route to its current orbit, 2008 EV₅ spent considerable time with perihelion values less than 1 AU, with estimates of 2%, 14%, 24%, 44%, 60%, 80%, and 100% probability that it reached 0.1, 0.2, 0.3, 0.4, 0.5, 0.6, and 0.9 AU, respectively. These values indicate surface temperatures may have been greater than 1,030 K, 730 K, 600 K, 510 K, 460 K, 420 K, and 340 K, respectively. These temperature estimates are not only a function of 2008 EV₅'s proximity to the Sun but also its physical parameters (e.g., shape, size, albedo, etc.), which are modestly uncertain. The interiors of the boulders on 2008 EV₅'s surface would have experienced modestly lower temperatures. These results lead to high and low probability scenarios. For the former case, 2008 EV₅'s boulders and subsurface likely did not experience temperatures greater than 500 K and thus common organic and hydrated compounds may be present, but are likely depleted in the top ~5 cm of both the surface layers of the boulders and 2008 EV₅ itself. Similarly, boulder organics may have also been depleted via exposure to ionization radiation (e.g., cosmic rays), whose penetration depth is on the order of a meter. For the latter case, boulders residing near or on the surface may have been thermally processed. 2008 EV₅ has an estimated geometric albedo that is higher than many carbonaceous chondrite meteorites. If EV₅'s estimated albedo remains above 8%, the best match to 2008 EV₅'s characteristics is likely a CR carbonaceous chondrite, (Renazzo-type meteorite), however, CI (Ivuna-type), CM (Mighei-type), and CK (Karoonda-type) carbonaceous chondrites are also possible.

2. Boulder Spatial and Size Distributions

What is the expected size-frequency distribution for boulders on 2008 EV₅? Approximately half of 2008 EV₅'s surface was observed by radar. Six distinct candidate 10-m-scale boulders have been identified in these images, corresponding to the existence of at least 10 such boulders over the asteroid's entire surface. Based on 2008 EV₅'s radar scattering properties and the highest-resolution images of asteroid surfaces (Eros and Itokawa) from spacecraft, there are millions of 10-cm scale cobbles on 2008 EV₅. Assuming a power-law distribution of boulders on 2008 EV₅ that follows that of the Eros global dataset, ~16,000 1–5 m boulders and ~1,300 2–3 m boulders are expected on the surface of 2008 EV₅. If it is assumed that there is a power-law distribution of boulders on 2008 EV₅ that connects the radar 10-m data to the radar 10-cm data, ~3,000 1–5 m boulders and ~360 2–3 m boulders would be expected on the surface of 2008 EV₅. Hayabusa2 will arrive at the C-type asteroid Ryugu (formerly 1999 JU₃) in June of 2018. NASA's Origins, Spectral Interpretation, Resource Identification, Security-Regolith Explorer (OSIRIS-REx) will arrive at the B-type asteroid Bennu in August of the same year. These will be the first primitive asteroids for which high-resolution images will be obtained, and they are roughly similar in size to 2008 EV₅. Power-law fits can be made to boulder fits for bodies where sufficient data are available and a power-law distribution would also be expected for fragments produced by fracturing.

What is the expected distribution of boulder shapes for boulders on 2008 EV₅? Most boulders found on Itokawa greater than 6 m in diameter are elongated with b/a ratios of approximately 0.7 (width/length). The third, vertical dimension of boulders (height) is not visible in most of the Hayabusa images. Several past laboratory impact experiments have been conducted and show that the fragments produced are irregular in shape and not regular 3-axis ellipsoids. An open question is whether the aspect ratio would be different for weaker rocks subject to thermal degradation, like those expected on 2008 EV₅. This question will be addressed by OSIRIS-REx and Hayabusa2.

What is the expected spatial distribution of ~1–5 meter boulders on 2008 EV₅? Based on the number of observed boulders (6 distinct candidate 10-m-scale), cobbles inferred from radar roughness, and

This document is a NASA working document and is subject to further revision. This document has been reviewed for release to the public and is not export controlled.

assuming a power-law relationship between boulder diameter and cumulative size-frequency distribution, the number of boulders of a given size per area can be calculated assuming a roughly uniform distribution across the surface. This information alone cannot tell us further information about the actual distribution. It is expected that the boulders would preferentially settle in the equatorial or near-equatorial regions, however.

What is the expected distribution in safe landing areas around ~1–5 m boulders on 2008 EV₅? The number boulders of a given size in a 10-m diameter circle can be estimated assuming a uniform distribution of boulders across the surface. Multiplying this value by the area will yield the total number of boulders greater than or equal to a given diameter in a 10-m diameter circle. Generally speaking, relatively flat, boulder-populated areas are predicted on 2008 EV₅; however the nature of these flat areas at the spatial scale of the landing pads (~1 m) requires careful consideration. Additionally, other characteristics of safe landing zones need to be considered (e.g., crushing stress of the particulate regolith surface).

What is the expected distribution in depth of burial for ~1–5 m boulders on 2008 EV₅? Due to the nature of spacecraft images of Eros and Itokawa, there is minimal information with regard to the burial of boulders on their surfaces. Regolith does migrate on asteroids, either from potential highs to lows (e.g., Itokawa) or via crater ejecta (probably less important on smaller objects, as a lot of ejecta is likely to exceed escape velocity). Boulders formed in fragmentation events have an average aspect ratio a:b:c of 1:0.7:0.5 (2:1.4:1). Assuming these shapes, burial estimates could be made based on three-dimensional images taken by the Asteroid Redirect Vehicle (ARV). If the boulder's maximum dimension parallel to the ground does not coincide with the intersection with the regolith, a symmetric shape to the boulder could be assumed and a depth of burial estimated. Three-dimensional images of the boulder will be essential for this characterization. Observations of the distribution of regolith and surface slopes could help to inform whether regolith has moved into/out of the area and may have buried boulders.

3. Surface Geotechnical Properties

What are the expected surface regolith geotechnical properties of the parent asteroid? The asteroid surface is more likely to be a pebble-rich lag depleted of fines and as such the surface porosity should be higher and compaction lower than asteroid's bulk compaction and porosity. This is an effect of the low surface acceleration and solar radiation pressure, which will tend to strip off fine particles and leave lags of larger, harder to move materials. Whatever the porosity and compaction, it is likely that the same processes apply all around the target area, so it should be fairly uniform. In turn, this should be applicable to all ARRM targets. The exceptions are "low" areas observed for example on Eros and Itokawa that were filled with relatively fine material. Coefficient of friction is a function of the magnitude of cohesive forces between regolith and the Contact and Restraint Subsystem (CRS) pads. The main sources of cohesive forces are van der Waals and electrostatic forces, but van der Waals forces should dominate. A very rough analytical estimate of the expected range of bearing strength of the surface regolith is 185-15,600 Pa, however, numerical models such as Discrete Element Method (DEM) should be used to provide better estimates and sensitivities.

What is the expected distribution in cohesion between ~1-5 meter boulders and the surface of 2008 EV₅? Cohesion is a function of particle sizes as well as particle shape, compaction history, and other material properties. Fines have higher cohesion per unit volume than coarse material. Modeling predicts that fine grains will preferentially attach to larger grains, and thus larger grains embedded in a matrix of fine grains could be held in place by the strength of the matrix itself. Hence the cohesion between large boulders and regolith will be driven by cohesion between fine particles and is estimated at 25 – 250 Pa. A high-resolution camera (mm/pixel or better) would be needed to provide good estimates for regolith size distribution. Particle size distribution could be used together with numerical

This document is a NASA working document and is subject to further revision. This document has been reviewed for release to the public and is not export controlled.

models (e.g., DEM) to assess regolith cohesion. However, if the models have not been calibrated, the regolith strength values could have significant uncertainty. The models can be calibrated through in-situ testing of regolith properties by deploying geotechnical instruments. The geotechnical data could then be used analytically or with an aid of numerical models to estimate cohesion between the surface and the boulder.

4. Boulder Physical Properties

What is the expected distribution in densities for ~1-5 meter boulders on 2008 EV₅? 2008 EV₅ appears to be composed of material similar to CM or CR chondrite meteorites. For these two carbonaceous chondrite groups, the bulk densities range from 1.88-3.94 g/cm³ and porosities are between 35% for CM chondrites and 9% for CR chondrites. If the composition of the asteroidal targets can be identified, the data on asteroid bulk density for the major carbonaceous chondrite groups can be used to derive the upper bound on meteorite bulk density and mass. Some combination of the following direct measurements are needed to bound identification and characterization of the mineralogy of the boulder:

- Multi-wavelength Spectroscopy (e.g., ultra-violet (UV), visible, near-infrared, thermal etc.)
- Alpha particle X-ray spectrometry (APXS) and/or laser-induced breakdown spectroscopy (LIBS) for elemental abundances
- Neutron and Gamma-ray spectroscopy for volatiles and elemental abundances
- Mössbauer spectroscopy for Fe mineralogy
- X-Ray diffraction (XRD) for general mineralogy

What is the expected distribution in the coefficient of thermal expansion of ~1-5 meter boulders from 2008 EV₅? The coefficient of thermal expansion of CM and CR chondrites are not well studied. However, some informed estimates based on analogs to terrestrial materials can be made. The expected distribution of the coefficient of thermal expansion is expected to be small. Direct measurements of the coefficient of thermal expansion for CM chondrites are in the works and results should be available soon. In the meantime the FAST suggests that the coefficient of thermal expansion in the range of 5-15 x 10⁻⁶/K, similar to that of terrestrial sandstones, dolomites, and concretes, should be assumed.

What is the expected distribution in minimum shear, compressive, and tensile strengths for ~1-5 meter boulders on 2008 EV₅? It is difficult to confidently predict boulder strength on 2008 EV₅ because we have no direct measurements that can be applied without uncertainty in interpretation. Hard data on asteroid material strength comes from two sources: laboratory measurements of small meteorites and data from bolide entry events, from which we derive the aerodynamic ram pressure at breakup. Other insights into the strength question come from experience with terrestrial materials and their variation with scale; experience with materials from other bodies such as the Moon and Mars; and analytical models. The difficulty with meteorite strength data is that it is measured from small samples and its applicability to large boulders requires an extrapolation which is uncertain. Likewise, bolide data clearly shows a range of breakup altitudes associated with material properties correlated with a range of component sizes. However, the nature of those components and the body's reaction to entry are subject to interpretation. A key question, is whether the bolides themselves (asteroid materials at meter-scale) are representative of meter-size boulders on asteroids.

Meteorite strength fundamentally depends on composition, texture, and structure. In general, meteorites are bi-modal in their strength with most meteorite types including ordinary chondrites, anhydrous carbonaceous chondrites, and most CMs being quite strong with compressive strengths greater than 40 MPa. The other major strength grouping includes CI and some petrologic type 2

This document is a NASA working document and is subject to further revision. This document has been reviewed for release to the public and is not export controlled.

carbonaceous chondrites (C2), such as Tagish Lake, which are quite weak with compressive strengths less than a few MPa. Caveats include that there are notable exceptions to this generalization (i.e., weak ordinary chondrites) and that the meteorite strength data is sparse on a number of important types (i.e., CMs, CIs and CRs having few or no measurements). Estimation of the overall strength of a boulder could be based on the “weakest link” approach that will likely be at least an order of magnitude weaker than data from individual meteorites.

Given these caveats, along with the uncertainty in 2008 EV₅'s classification, it is the judgment of the ARM FAST team members that boulders on 2008 EV₅ could exhibit strength characteristics that fall within the following ranges:

- Shear strength: 0.1-5 MPa
- compressive strength: 0.5-50 MPa
- tensile strength: 0.05-3 MPa

Of these parameters, the one that is most uncertain is tensile strength, and the possibility that tensile strength at large scale may be below the range in the table cannot be ruled out without further investigation. It should also be noted that there is dispute within the scientific community regarding the compressive strength, with some members of the FAST team suggesting that boulder compressive strength may be as low as 0.1 MPa, derived from the assumed aerodynamic stresses during bolide breakup in the atmosphere. More experimental data on the relevant meteorite types and experiments with large-scale simulants are needed to refine these estimates.

Note: If 2008 EV₅'s actual albedo is near or higher than the mean albedo values presented in the “Origin of 2008 EV₅” section, 2008 EV₅ is arguably a CR chondrite (though other compositions cannot be definitively ruled out, such as CK, CM, etc.). As a starting point for discussion and new work, it is probably reasonable to assume this composition when making estimates of likely boulder strengths. If 2008 EV₅'s actually has a low albedo, however, it is arguably more likely to be a CI or CM chondrite, which show a wide range of meteorite strengths and probably boulder strengths as well. This possibility is more problematic for engineering work, but it cannot be ruled out until additional information on the nature of 2008 EV₅ becomes available.

All other things being equal (i.e., similar mineralogy, albedo, exposure history, and shock history), just as with bulk density and other physical properties, a narrow distribution of shear, compressive, and tensile strength of boulder on an individual asteroid should be expected. Because of thermal shock and erosion, angularity and visible fractures may be a measure of relative boulder strength. Stronger boulders may be more angular and weaker boulders more rounded. The physical properties of homogeneous, isotropic rock are typically normally or lognormally distributed; it can reasonably be expected that boulders on 2008 EV₅ will exhibit a normal or lognormal distribution in strength. Given the uncertainties and caveats in the above discussion, it would seem prudent to work aggressively to refine estimates of boulder strength while exploring capture mechanisms that minimize the needed mechanical strength of the boulder. In addition, a broader investigation of the issue of boulder breakup is advisable including consideration of boulder thermal properties, toughness or brittleness, and ductility. Finally, given that other targets besides 2008 EV₅ are candidates for ARM, including those of interest to ISRU, and that the most desirable targets from an ISRU perspective are the hydrated CIs and CMs, some of those materials may be much weaker than 2008 EV₅ boulders.

5. Post Collection Boulder Handling

How should the boulder be handled after collection to minimize impacts to science and to the structural integrity of the object? In order to avoid fragmentation of the boulder after collection,

This document is a NASA working document and is subject to further revision. This document has been reviewed for release to the public and is not export controlled.

minimizing physical handling of the boulder until it is in a stable cis-lunar orbit could be helpful. However, additional physical contact of the boulder after collection (e.g., drilling, brushing, or scraping the surface of the boulder) could provide valuable engineering data to aid in safe transportation and the design of tools for future robotic or human sampling of the boulder. The ARRM team must reach a balance between these constraints. Monitoring the boulder during the anchoring process (e.g., as adding cameras to the ends of the robotic arms) would be highly beneficial. Imaging the effects of the microspine grippers scraping over the surface or the dispersion of the drilling chips for the anchor could provide considerable insight about the overall integrity of the boulder. Monitoring the performance of the drill anchors may also prove useful. Passive direct monitoring of the boulder during anchoring, return, and in cis-lunar space is highly desirable. Cameras could also be used to inspect the boulder surface to identify any particle shedding or cracking prior to the crewed mission.

6. Pre-ARCM Boulder Assessments for Crew Safety

Besides the existing capabilities of the ARV (i.e., cameras and CRS feedback loads), are there other ways to assess the condition of the boulder prior to crew access to determine if it's safe to approach and sample? A variety of high-heritage and/or flight-proven measurements and techniques could be employed during cruise or after Lunar Distant Retrograde Orbit (LDRO) insertion and prior to crew interaction to ensure crew safety. Assessing the fragility, hardness, sharpness, and volatile release potential of samples and the presence of fractures or textures that might suggest spallation or breakage would be most critical to astronaut safety. The following measurements would be relevant to astronaut safety and/or science/knowledge but not as critical: 1.) assessing any physical movement or dramatic temperature changes of the samples during the return transit; 2.) characterizing and determining of any abundance of any dust, volatiles, and/or organics in the samples; 3.) characterizing the chemistry and mineralogy of the samples prior to astronauts, to make eventual EVAs most efficient, and; 4.) assessing swatches of space suit material and other relevant witness samples during the robotic mission to influence ultimate choice of ARCM materials, coatings, etc. Finally, the following were of primarily relevant to science/knowledge: 1.) assess electrostatic potential in the plasma environment around the boulder; 2.) use mass determination and volume of the boulder to estimate its density; 3.) estimate the ages of the samples.

7. Containment Considerations

Given the uncertainties in the properties of the boulders, potential for contamination, possible thermal effects, and potential for particulate release that could affect spacecraft or crew safety, should some form of containment of the boulder be considered and, if so, what type of containment and materials should be considered? There is a high likelihood that particulates and possibly fragments will evolve from an unprotected boulder while it is attached to the spacecraft. These particles are likely to be small, have a very low relative velocity to the spacecraft, and are not expected to remain in the vicinity of the boulder due to spacecraft motion and solar radiation pressure. As such, these particles do not present a hazard to crew operations. Thermal effects are a primary factor in contamination and alteration of the boulder, and thus contamination and alteration can be reduced with a containment designed to reduce thermal shock and peak temperature. Monitoring the boulder throughout the period between initial collection by ARRM and sampling operations during ARCM to assess debris generation, contamination, and alteration is a prudent approach. A hermetically sealed containment mechanism for the boulder is not desirable, but a sunshade-like "containment" should be considered among the possible options. Specific requirements for physical containment of the boulder should be supported with further analyses. Since physical containment of the boulder is not necessarily suggested unless further analyses deem it necessary, a better term for this consideration is the "protection" of the boulder rather than "containment".

This document is a NASA working document and is subject to further revision. This document has been reviewed for release to the public and is not export controlled.

The third section of this report includes an initial list of potential investigations that could be performed by ARM (ARRM and ARCM) resulting from brainstorming activities by the FAST. Many of the identified investigations require additional sensors, subsystems, or operations, which are beyond the scope of the current program. These could be performed with additions and modifications as identified in Table 10 in the “Potential Investigations” section of the report. These inputs are not intended to be inclusive of all possibilities, but were meant to aid formulation and development of the ARRM, and reflect the FAST members’ experience and expertise in small bodies missions and knowledge related to science, planetary defense, asteroidal resources and in-situ resource utilization (ISRU), and relevant capabilities and technologies. In order to present these potential investigations in this report, the 63 areas identified have been sorted and grouped based on their likely benefit to ARM and relevance to NASA’s science, ISRU, planetary defense, and exploration goals by the FAST leadership (Mazanek, Abell, and Reeves) incorporating input from the rest of the FAST. Within each grouping, the investigations are listed below in the order they were proposed by the FAST with no priority or significance implied by the order. Further descriptions of the investigations are presented in the “Potential Investigations” section of the report.

High Benefit to ARM and High Relevance to NASA Goals: Asteroid Surface Interaction; Dust/Particulate Mitigation Techniques; Sample Thermal Control; Thermal Imaging of Asteroid Surface; Collect Regolith Samples; Surface Contact Science Package; Collect Samples From Boulder; and Characterize Boulder and Geotechnical Properties.

High Benefit to ARM and Medium Relevance to NASA Goals: Low Velocity Penetrator; Mineralogy and Composition; Multi-Spectral Imaging of Asteroid; Global Mapping of Asteroid; High-Power Radar; Global Boulder Imaging; LDRO Free-flying Observer; and Asteroid Free-Flyer for Observation.

High Benefit to ARM and Low Relevance to NASA Goals: None identified.

Medium Benefit to ARM and High Relevance to NASA Goals: Optical Communications Demo; Small Body Seismic Network on Asteroid; Ultrasonic Investigation of Boulder; Anchoring Techniques; Long-term Orbit Determination; Contamination Environment Monitoring; and Boulder Organics and Volatiles Characterization.

Medium Benefit to ARM and Medium Relevance to NASA Goals: Surface & Subsurface Composition.

Medium Benefit to ARM and Low Relevance to NASA Goals: None identified.

Low Benefit to ARM and High Relevance to NASA Goals: Demo of Mining Techniques; Micro-g Mobility Demo (Robotic & Crewed); ISRU Radiation Protection; Planetary Protection (“Break the Chain”); Tether Demo with Boulder Counterweight; High Velocity Asteroid Impactor; Radiation Environment Characterization; Collect Boulder Core Sample; Large Sample Return; Cold Trap Volatile Collection Demo; and ISRU Product Characterization.

Low Benefit to ARM and Medium Relevance to NASA Goals: Small Body GPS; Remote Stand-off Interaction Demo; Future Planned Instrument Demo; Space Weathering Measurements; Plasma Environment Characterization; Magnetic Environment Characterization; Deploy Science Package; Occultation Exosphere Observations; Dust Mobility Characterization; Characterize Boulder Porosity; Rubble Aggregation Experiment; Observe Kinetic Impact on Asteroid; Deploy Explosive Penetrator on Asteroid; Additional Planetary Defense Demo(s); Plume Generation and Observation; Ablation and/or

This document is a NASA working document and is subject to further revision. This document has been reviewed for release to the public and is not export controlled.

Spalling Test; In-Space Printing with Asteroid Materials; Asteroid Material Manipulation Demo; Instrumented Drill on Asteroid and/or Boulder; Boulder Composition Characterization; Deliver Samples to International Space Station (ISS); Encapsulate the Boulder for Volatile Collection; Characterize Boulder Permeability; Soil Simulation with Asteroidal Material; Microwave Volatile Extraction Test; Use of Robotic Arms for Strength Tests; and Full ISRU Demo.

Low Benefit to ARM and Low Relevance to NASA Goals: None identified.

The fourth section of this report includes a listed of additional findings by the FAST in combination with public input and are repeated in their entirety. No prioritization is implied by the ordering of these findings.

- **Unique Knowledge Gain from ARM:** ARM provides a unique opportunity that can provide a wide range of valuable knowledge gain beyond other asteroid missions or what is available in the current meteorite collection. For example:
 - Investigating pristine sub-surface material, preserved with stratigraphic context (boulder core sample) that have not been significantly altered by the space weathering and ionizing radiation environment (e.g., how organics, hydration, volatile content, etc. varies with depth).
 - Return of a multi-ton boulder, along with regolith samples for context that would provide value information about the surface of asteroids and allow for measurements and investigations that requiring large mass/samples.
 - Returning multiple kg's of sample to Earth will allow for sensitive laboratory measurements and experiments that aren't possible with the limited meteorite collection.
 - Creating an "orbital laboratory" that can be used to demonstrate asteroidal ISRU and other technologies and instruments in an operational environment.
 - Opportunity to correlate observed spectrum to the sampled asteroid surface (ground truth), asteroid interior (through boulder investigations), as well as known meteorite classes.
- **NASA Goal Traceability:** Although the FAST did not specifically address traceability to the current planetary decal survey and other NASA exploration roadmaps, there are many NASA goals that could be addressed using the results and opportunities provided by this mission.
- **Pre-launch 2008 EV₅ Characterization:** All existing data should be analyzed to provide physical characterization of the 2008 EV₅ to understand mission risks. This includes the ESA MarcoPolo-R team investigations (e.g., observations and modeling) and telescopic data sets. Opportunities for acquiring new data sets should also be investigated (e.g., Spitzer).
- **Meteorite Analog Work:** More wide-ranging laboratory studies of appropriate candidate meteorites is warranted (e.g., spectral, strength, density, etc.). Investigating the effects of grain size, packing density, and powders-on-slabs would provide stronger insights into the possible physical and chemical composition of 2008 EV₅.
- **Characterization Precursor:** A precursor to the ARRM target body in order scout for boulders and provide surface and boulder physical characteristics would effectively increase the characterization phase duration and should be further investigated. This precursor could be a dedicated mission or be co-manifested with the ARV, arriving at the target earlier.

This document is a NASA working document and is subject to further revision. This document has been reviewed for release to the public and is not export controlled.

Additional benefits would be gained if the precursor had some means of interacting with the surface to provide geotechnical data.

- **Characterization Phase:** Characterization of the target asteroid, candidate boulders, and associated collection areas are critically important. Increasing, to the greatest extent possible, the time allocated for characterization will maximize the knowledge return from the ARRM and probability of mission success.
- **Geotechnical Property Estimation:** A mechanical interaction with regolith representative of the boulder collection area is the only way to provide an accurate estimate of the geotechnical properties (e.g., cohesion, friction angle, porosity, etc.) that are critical for boulder collection. Before and after images of the interaction area at sub-cm/pixel would provide context to inform cohesion mapping around target boulders.
- **Boulder and Regolith Characterization:** On a best-effort basis, sufficient camera resolution is required to characterize:
 - the morphological relationship of the boulder to the surrounding terrain. Sub-cm/pixel resolution of a representative area of boulder/regolith interface with more of the image devoted to the regolith than the boulder.
 - the physical integrity of the boulder (e.g. cracks, fissures, etc.). Sub-cm/pixel resolution over as much of the boulder surface as possible is desired.
- **Thermal Imaging:** The thermal inertia of boulders, and the entire asteroid surface, is indicative of their near-surface characteristics (e.g., porous vs. solid), and can be measured relatively easily with a thermal detector. Ideally this detector would have two or more wavelengths (e.g., 5 and 10 microns) and a spatial resolution greater than several pixels per boulder (a minimum of about 0.5 meters per pixel). Over an asteroid's rotation period these observations can distinguish between the thermal inertia of low density, porous aggregates and higher density, potentially stronger, monolithic material, which would aid in boulder and site selection and in determining the homogeneity of boulder and surface properties.
- **Previously Visited Target:** While selecting a target that has not been visited before (i.e. not Bennu or Ryugu) is compelling, there is value in returning to a previously visited asteroid and there would be interest in returning a boulder to cis-lunar space for subsequent study and sampling. (See SBAG ARM Special Action Team Full Report http://www.lpi.usra.edu/sbag/documents/SBAG_ARM_SAT_Full_Report.pdf).

The fifth section of this report provides a summary of relevant public inputs and comments received to date by the FAST. All public inputs directly relevant to ARM, including any additional comments received in response to the posting of this draft version, will be summarized in the final version of the report and will be posted in their entirety on the FAST website: <http://www.nasa.gov/feature/arm-fast>. The public inputs for area of investigation and potential payloads are listed below and summarized in the "Summary of Public Inputs" section of the report: Yarkovsky–O'Keefe–Radzievskii–Paddack (YORP) Torque and Rotation State; Cause of Surface Restructuring; Granular Physics and Cohesion; Contextual Sampling of the Target Asteroid; Electrostatic Levitation; Comparison with Ground Based Observations; Planetary Defense Data; Geodetic Control During Enhanced Gravity Tractor (EGT); Laser Retroreflectors; Presence of Water; Deep Space Atomic Clock (DSAC); Small Spacecraft; and Bi-Static Radar Reflections.

Finally, more detailed responses to each the Project questions are provided in the Appendices. These full responses are intended to provide additional information that can be utilized by the Project Team and are not summarized in this Executive Summary.

This document is a NASA working document and is subject to further revision. This document has been reviewed for release to the public and is not export controlled.

FAST Overview

Purpose

The Formulation Assessment and Support Team (FAST) for the Asteroid Redirect Mission (ARM) was chartered by NASA to provide timely inputs for mission requirement formulation in support of the Asteroid Redirect Robotic Mission (ARRM) Requirements Closure Technical Interchange Meeting (TIM) planned for mid-December of 2015, to assist in developing an initial list of potential mission investigations, and to provide input on potential hosted payloads and partnerships. To aid formulation and development of the ARRM, the FAST focused their inputs on knowledge gain from ARM in the areas of science, planetary defense, asteroidal resources and in-situ resource utilization (ISRU), and capability and technology demonstrations, as well as provide inputs that could increase probability of mission success. This report represents the FAST's final product for the ARM.

Asteroid Redirect Mission Background

ARM is part of NASA's plan to advance the new technologies and spaceflight capabilities needed for a human mission to the Martian system in the 2030s, as well as other future human and robotic missions. ARM includes ARRM and the Asteroid Redirect Crewed Mission (ARCM), along with leveraging the global asteroid-observation community's efforts to detect, track, and characterize candidate asteroids. NASA originally proposed a robotic mission concept to capture an entire small asteroid (4–10 m in size) that would leverage several key ongoing activities in human exploration, space technology, and planetary defense. Subsequently, an alternate approach to collect a boulder from a large asteroid was also proposed. NASA evaluated both mission approaches, to determine their feasibility, identify the important differences between them, and evaluate the key risks and figures of merit for each concept. On March 25, 2015, NASA announced the selection of the boulder capture option for the robotic segment of ARM.

ARRM will be the first robotic mission to visit a large (greater than ~100 m diameter) near-Earth asteroid (NEA) and collect a multi-ton boulder from its surface, along with regolith samples. The spacecraft will use the multi-ton boulder to perform an enhanced gravity tractor asteroid deflection demonstration and then return the boulder to a stable orbit around the Moon, where astronauts will explore the boulder and return with samples in the mid-2020s as a part of the ARCM. Subsequent human and robotic missions to the returned material could also be facilitated by its availability in cis-lunar space and would benefit scientific and partnership interests (domestic and international), expanding our knowledge of small celestial bodies and enabling the demonstration of mining asteroid resources for commercial and exploration needs.

To achieve its long-term goal of sending humans to Mars, NASA plans to proceed in a series of incrementally more complex human spaceflight missions. Today, human flight experience extends only to LEO, and should problems arise during a mission, the crew can return to Earth in a matter of minutes to hours. The next logical step for human spaceflight is to gain flight experience in the vicinity of the Moon. These cis-lunar missions provide a "proving ground" for the testing of systems and operations while still accommodating an emergency return path to the Earth that would last only several days. Cis-lunar mission experience will be essential for more ambitious human missions beyond the Earth-Moon neighborhood, which will require weeks, months, or even years of transit time. A principle objective of the ARM is the development of a high-power Solar Electric Propulsion (SEP) vehicle, and the demonstration that it can

This document is a NASA working document and is subject to further revision. This document has been reviewed for release to the public and is not export controlled.

operate for many years in interplanetary space, which is critical for deep-space exploration missions. A second prime objective of ARM is to conduct a human spaceflight mission involving in-space interaction with a natural object, in order to provide the systems and operational experience that will be required for eventual human exploration of Mars, including the Martian moons Phobos and Deimos. The ARCM provides a compelling science focus for the early flights of the Orion program, which will take place before the infrastructure for more ambitious flights will be available. Astronauts will participate in the scientific in-space investigation of nearly pristine asteroid material, at most only minimally altered by the capture process. The ARCM will provide the opportunity for human explorers to work in space with unaltered asteroid material, testing the activities that would be performed and tools that would be needed for later exploration of primitive body surfaces in deep space. The operational experience would be gained close to our home planet, with a relatively quick return to Earth if problems should arise.

The ARRM will utilize an advanced 50 kW-class Solar Electric Propulsion (SEP) spacecraft along with sensors and a robotic Capture Module (CapM) to characterize the parent NEA, identify and select candidate boulders, allow contact with the parent NEA, and collect the selected boulder from the surface. Following final restraint of the boulder, the ARV will transfer into a halo orbit around the parent NEA and demonstrate the Enhanced Gravity Tractor (EGT) technique, with the collected boulder augmenting the spacecraft mass and thereby significantly increasing the gravitational force between the spacecraft and the NEA. The instrumentation currently planned includes a sensor suite for high-resolution mapping and characterization during asteroid flybys and extended horizon views for onboard navigation during the descent and planetary defense demonstration phases. The ARV is also planned to provide images of the boulder through descent and capture. Limited accommodations for science/payload instrumentation (mass, power, and volume) are planned. After the ARV returns to a lunar distant retrograde orbit (LDRO) in the mid 2020s, initial astronaut exploration and sampling of the returned material will be performed during the ARCM. The capabilities, systems, and operational experience developed and implemented by ARM and subsequent missions to the returned asteroidal material will advance NASA's goal of sending humans to deep-space destinations and eventually to surface of Mars. Currently, the ARRM is planned to be launched at the end of 2020 and the ARCM is planned for late 2025.

NASA has identified the asteroid 2008 EV₅ as the reference target for the ARRM. 2008 EV₅ has been well characterized by ground-based radar and in the infrared wavelengths, and has orbital and physical characteristics that are compatible with the planned ARM timeline and operations. Specifically, significant mass return (greater than 20 t) is possible with launch of the ARRM at the end of 2020 and the ARCM in late 2025. Ground-based measurements of 2008 EV₅ show that it is a carbonaceous chondrite asteroid (C-type) that is believed to be water/volatile-rich and possibly may contain significant amounts of organic materials. NASA has additional candidate targets (Ryugu, Bennu, and Itokawa) and will continue the search for additional asteroids and make a final target selection approximately one year prior to launch. However, 2008 EV₅ provides a valid target that can be used to help with the formulation and development of the mission, which is the rationale for it being the NEA around which the FAST focused its attention.

The ARM and Asteroid Grand Challenge (AGC) together make up NASA's Asteroid Initiative, by which the agency seeks to enhance its ongoing work in the identification and characterization of near-Earth objects for further scientific investigation. The AGC complements ARM and other asteroid-related activities at NASA in a way that allows the agency to engage the public and leverage interested citizens for science, technology, and planetary defense efforts in support of the challenge to “find all asteroid threats to human populations and know what to do about them.” This work includes locating potentially

This document is a NASA working document and is subject to further revision. This document has been reviewed for release to the public and is not export controlled.

hazardous asteroids and identifying those in viable orbits that allow for collection and redirection of a multi-ton boulder into a stable lunar orbit for future exploration by astronauts.

Please visit <http://www.nasa.gov/asteroidinitiative> for further details about the ARM and the AGC.

Study Request

The FAST was requested to work in collaboration with ARM management and technical personnel at the participating field centers to provide input during the requirements definition phase of the ARRM, which includes spacecraft interfaces, requirements, and design considerations as they relate to the ARCM. Additionally, the FAST assisted in developing an initial list of potential mission investigations focused on the following four main areas as they support the robotic and crewed segment objectives: science, planetary defense, asteroidal resources and in-situ resource utilization (ISRU), and capability and technology demonstrations. All ARM investigations will be required to operate within ARRM and ARCM capabilities, as well as programmatic constraints. Finally, the FAST provided input to NASA on potential hosted payloads and partnerships in coordination with NASA Headquarters and Ames Research Center, which is leading these areas of external cooperation. Payloads could include hosted instruments, demonstrations, deployable assets, and experiments related to these four main investigation areas.

Membership

FAST membership consisted of openly solicited NASA and non-NASA participants (U.S. citizens and permanent residents) that were selected by a committee that included key NASA Headquarters stakeholders, ARM leadership, and other NASA leadership. The selected members had demonstrated expertise and knowledge in areas highly relevant to the ARM primary areas of interest. One hundred applications were received from highly-qualified individuals representing academia, industry, NASA, non-profit research institutes, and other organizations. The applications were reviewed by the ARM Mission Investigator, Deputy Investigator, Analysis and Integration Lead, ARRM Project Manager, the HEOMD Chief Exploration Scientist, NASA's NEO Programs Executive, HEOMD Program Executive, and ARM Program Director. Eighteen participants were selected by the above committee and were approved by NASA's Associate Administrator on August 19, 2015. Participation in the FAST by non-civil service personnel was limited to providing non-consensus, non-voting input. The selected participants and their affiliations, along with the FAST leadership, are provided in Table 1.

This document is a NASA working document and is subject to further revision. This document has been reviewed for release to the public and is not export controlled.

Table 1: ARM FAST Membership

Last Name	First Name	Roll	Organization
Mazanek	Dan	ARM Mission Investigator	NASA Langley Research Center
Abell	Paul	ARM Deputy Investigator	NASA Johnson Space Center
Reeves	David	Analysis and Integration Lead	NASA Langley Research Center
Asphaug	Erik	Member	Arizona State University
Abreu	Neyda	Member	Penn State University - DuBois
Bell	Jim	Member	Arizona State University
Bottke	Bill	Member	Southwest Research Institute
Britt	Dan	Member	University of Central Florida
Campins	Humberto	Member	University of Central Florida
Chodas	Paul	Member	Jet Propulsion Laboratory
Ernst	Carolyn	Member	Johns Hopkins University-Applied Physics Laboratory
Fries	Marc	Member	NASA Johnson Space Center
Gertsch	Leslie	Member	Missouri University of Science and Technology
Glavin	Dan	Member	NASA Goddard Space Flight Center
Hartzell	Christine	Member	University of Maryland
Hendrix	Amanda	Member	Planetary Science Institute
Nuth	Joe	Member	NASA Goddard Space Flight Center
Scheeres	Dan	Member	University of Colorado
Sercel	Joel	Member	TransAstra
Takir	Driss	Member	United States Geological Survey
Zacny	Kris	Member	Honeybee Robotics

References

Busch, M.W. et al. 2011. Radar Observations and the Shape of Near-Earth Asteroid 2008 EV₅. *Icarus* 212, 649-660.

FAST Responses to ARRM Project Questions

The following are answers to questions that were put forth by the ARRM Project specifically seeking input from the FAST. The questions were given priority and addressed by FAST sub-teams. The sub-team findings are provided below. The information provided by the FAST will be incorporated into the ARRM design parameter database and/or engineering trade studies. These data will aid in the design and development of systems and help to make the mission robust to the uncertainties in the mission environment within the constraints and risk posture of the ARRM Project. For readability, the questions have been grouped into seven topics with references for each question set self-contained in that section. The following are summaries of the answers with additional details found in the appendices to this document.

Origin of 2008 EV₅

Response Lead: Bill Bottke

Sub-team Members: Jim Bell, Humberto Campins, Paul Chodas, Carolyn Ernst, Driss Takir, Amanda Hendrix

This document is a NASA working document and is subject to further revision. This document been reviewed for release to the public and is not export controlled.

What is the orbital history of 2008 EV₅ and has that history affected the properties of the asteroid and candidate boulders? (Where has it been in the Solar System and for how long? Has it been closer/farther from the Sun than it is now?)

- **What are the leading theories on the origin of 2008 EV₅? What is the prime source region for this object? From what type of object and where did it most likely originate? What is known of its formation and/or history?**

2008 EV₅ (hereafter referred to as EV₅) started its existence as part of a much larger body in the asteroid belt, with a likely diameter greater than 100 km; [Morbidelli et al., 2009]) (See Appendix A1 for a more lengthy discussion of all issues in this section). Given its size, EV₅'s parent body possibly experienced early thermal evolution from the decay of radiogenic nuclides [e.g., McSween et al., 2002], while its surface was battered by impacts for billions of years of cratering events [e.g., Bottke et al., 2005a,b]. EV₅'s immediate history likely started when its parent body experienced a large cratering event or, more likely, a catastrophic disruption event that resulted in a highly fractured or shattered object (rubble pile). From there, the newly-liberated EV₅ began to undergo dynamical evolution via non-gravitational torques; the Yarkovsky effect caused it to slowly drift in semimajor axis, while the Yarkovsky–O'Keefe–Radzievskii–Paddack (YORP) effect steadily modified its spin vector [e.g., Bottke et al., 2006; 2015]. In fact, YORP torques probably produced sufficient mass movement/mass shedding for EV₅ to take on a top-like appearance [Walsh et al., 2009; Busch et al., 2012]. EV₅'s rotation period has probably been highly variable over its lifetime.

Dynamical models indicate EV₅ migrated inward across the inner main belt over long timescales (i.e., the order of ~0.01-1 Gyr) until it reached a main belt “escape hatch”, or planetary gravitational resonance, that drove it into the near-Earth asteroid (NEA) population over a timescale of the order of ~1 Myr. From there, gravitational interactions with both the planets and resonances allowed it reach its current orbit within a few Myr to a few tens of Myr [e.g., Gladman et al., 1997]. While EV₅ was in transit, boulders exposed on the surface would be subject to comminution from impacts onto EV₅, though the same events might also allow new boulders to be created/exposed. Thermally induced cracking and erosion are also possible sources of boulder comminution [e.g., Delbo et al., 2014].

EV₅'s likely parent body, the context of other EV₅-like fragments both inside and outside of the main belt, and where precisely EV₅ departed the main belt need to be identified in order to better determine EV₅'s collisional, dynamical, and thermal history. This requires a much more extensive modeling and remote observational campaign than has yet been performed. The information provided below is the best that can be done within the timescale, capabilities, and charter of the FAST team.

Remote observation and modeling work indicates EV₅ is ~400 m in diameter [Busch et al., 2011; Ali Lagoa et al., 2013]. It has a reflectance spectrum consistent with carbonaceous chondrite meteorites; it is blue-sloped at wavelengths longer than 0.75 microns, with a possible absorption band in the 1 micron region [Reddy et al., 2012]. The estimated geometric albedo was obtained three ways: (i) by correcting the absolute magnitude for bias using Pravec et al., [2014], a geometric albedo of 9-10% ± 3% was obtained; (ii) an analysis of the EV₅ phase function by C. Hergenrother yielded 9% (+5%, -3%); (iii) applying an empirical photometric model by D. Takir yielded 13% (+1%, -8%) [see Appendix A1, A2, A4]. These values are higher than many carbonaceous chondrites. According to an analysis by E. Cloutis, if EV₅'s estimated albedo remains above 8%, the best match to EV₅'s characteristics indicate is likely a CR-type

This document is a NASA working document and is subject to further revision. This document has been reviewed for release to the public and is not export controlled.

carbonaceous chondrite [Appendix A3]. Note that with the uncertainty in the albedo and absorptions, EV₅ could also be a CI, CM, or possibly a CK. If the albedo is at the low end of this range, it would imply a CI/CM chondrite composition [Reddy et al., 2012; see also Appendix A1].

Given that CR chondrites appear to be the best match to EV₅'s mean albedo, it is useful to briefly describe them here. They are a mix of reduced, oxidized, anhydrous, hydrated, organic, and pre-solar components. They have highly variable, but on average roughly equal, amounts of hydrated fine-grained matrix and chondrules (forsteritic olivine + enstatite + feldspathic glass). Their petrographic types range from 1 (anhydrous silicates rare) to 3 (hydrated silicates rare); most CRs are type 2. All but one CR1 chondrite has substantial metallic Fe blebs (10-16 wt.%) and hydrated crystalline and amorphous silicates (~ 5.7 wt.% water).

E. Cloutis's analysis of EV₅'s spectroscopic signature indicates it is an assemblage consisting of both hydrated and anhydrous silicates, specifically a ferric iron-free phyllosilicate and iron-bearing olivine [Appendix A3]. This places it in the realm of petrologic type 2-3 carbonaceous chondrites, but could include mildly to moderately thermally metamorphosed members (e.g., possible matches to CR-type meteorites that were heated to about 600°C).

Using EV₅'s current orbit combined with numerical modeling work [Bottke et al., 2002; 2015], it can be argued that EV₅ departed the inner main belt between 2.2 - 2.3 AU with inclinations $i < 8^\circ$ (Appendix A1). Particular similarities were found for modeled asteroids having $i \sim 2 - 3^\circ$ and 5° . This may suggest a link to large low albedo carbonaceous chondrite-like "asteroid families" (i.e., swarms of fragments produced by a disrupted asteroid) such as the Erigone, Eulalia, and New Polana families [Campins et al., 2010; Walsh et al., 2014; Bottke et al., 2015]. These potential matches, however, are contingent upon whether some members of these families have albedos like EV₅. Another intriguing source for EV₅ would be the diffuse population of higher albedo carbonaceous chondrite-like asteroids residing in the innermost main belt region between $8^\circ < i < 15^\circ$. These bodies have yet to be investigated in detail.

After escaping the asteroid belt, en route to its current orbit, EV₅ spent considerable time with perihelion values $q < 1$ AU. By tracking modeled asteroids from the main belt all the way to EV₅'s observed orbit and then estimating the temperatures experienced by these bodies at their subsolar points along the way [Marchi et al., 2009; Delbo and Michel 2011; Ali Lagoa et al., 2013; see Appendix A1], the following results were found.

The median time spent by the EV₅-like test asteroids with $q < 0.5$, 0.7, and 1.0 AU was ~0.1, 1.4, and 7 Myr, respectively. Fewer than 50% of the test asteroids spent any time at $q < 0.5$ AU.

Using these model runs, it was found that a 2%, 14%, 24%, 44%, 60%, 80%, and 100% probability that the surface of EV₅ reached temperatures greater than 1,030 K, 730 K, 600 K, 510 K, 460 K, 420 K, and 340 K, respectively. It was assumed that these values correspond to q greater than 0.1, 0.2, 0.3, 0.4, 0.5, 0.6, and 0.9 AU, respectively. The interiors of the boulders on or near EV₅'s surface would have experienced modestly lower temperatures. These results lead to high and low probability scenarios.

Overall, we argue the greatest likelihood is that EV₅'s boulders and subsurface did not experience temperatures greater than 500 K. Here common organic and hydrated compounds that break up at relatively moderate temperatures (e.g., 300–670 K) may still be depleted in both the surface layers of the boulders and EV₅ itself (i.e., possibly down to 5 cm depth; [Delbo and Michel 2011]). Similarly, boulder

This document is a NASA working document and is subject to further revision. This document has been reviewed for release to the public and is not export controlled.

organics may have also been depleted via exposure to ionization radiation (e.g., cosmic rays), whose penetration depth is on the order of a meter. In the lower probability case, EV₅ spent enough time near the Sun that boulders currently located on its surface were thermally modified. Additional thermal modeling work will be needed to better quantify these probabilities, with the temperatures reached by EV₅'s current population of surface boulders a function of EV₅'s past proximity to the Sun, its physical parameters, and the residence time of those boulders near the surface [Ali-Lagoa et al., 2013].

For more information on the origin of 2008 EV₅, see Appendix A.

References

- Ali-Lagoa et al. 2013. Thermophysical Properties of near-Earth Asteroid (341843) 2008 EV₅ from WISE Data. *Astronomy & Astrophysics* 561, A45.
- Bottke, W. F., et al. 2002. Debaised Orbital and Absolute Magnitude Distribution of the Near-Earth Objects. *Icarus* 156, 399-433.
- Bottke, W. F., Durda, D. D., Nesvorny, D., Jedicke, R., Morbidelli, A., Vokrouhlicky, D., Levison, H. F. 2005. Linking the collisional history of the main asteroid belt to its dynamical excitation and depletion. *Icarus* 179, 63-94.
- Bottke, W. F., Durda, D. D., Nesvorny, D., Jedicke, R., Morbidelli, A., Vokrouhlicky, D., Levison, H. 2005. The fossilized size distribution of the main asteroid belt. *Icarus* 175, 111-140.
- Bottke, W.F., D. Vokrouhlicky, D. P. Rubincam, and D. Nesvorny. 2006. The Yarkovsky and YORP Effects: Implications for asteroid dynamics. *Ann. Rev. Earth Planet. Sci.* 34, 157-191.
- Bottke, W. F., et al. 2015. In Search of the Source of Asteroid (101955) Bennu: Applications of the Stochastic YORP Model. *Icarus* 247, 191-217.
- Busch, M.W. et al. 2011. Radar Observations and the Shape of Near-Earth Asteroid 2008 EV₅. *Icarus* 212, 649-660.
- Campins, H., Morbidelli, A., Tsiganis, K., de Leon, J., Licandro, J., Lauretta, D. 2010. The Origin of Asteroid 101955 (1999 RQ36). *The Astrophysical Journal* 721, L53-L57.
- Delbo, M., et al. 2014. Thermal Fatigue as the Origin of Regolith on Small Asteroids. *Nature* 508, 233-236.
- Delbo, M., Michel, P. 2011. Temperature History and Dynamical Evolution of (101955) 1999 RQ36: A Potential Target for Sample Return from a Primitive Asteroid. *The Astrophysical Journal* 728, L42.
- Marchi, S., Delbo', M., Morbidelli, A., Paolicchi, P., Lazzarin, M. 2009. Heating of Near-Earth Objects and Meteoroids Due to Close Approaches to the Sun. *Monthly Notices of the Royal Astronomical Society* 400, 147-153.
- McSween Jr., H.Y., Ghosh, A., Grimm, R.E., Wilson, L., Young, E.D., 2002. Thermal Evolution Models of Asteroids. In *Asteroids III* (W. F. Bottke et al., eds), U. Arizona Press., pp. 559-571.
- Pravec, P., Harris, A. W., Kusnirak, P., Galad, A., Hornoch, K. 2012. Absolute Magnitudes of Asteroids and a Revision of Asteroid Albedo Estimates from WISE Thermal Observations. *Icarus* 221, 365-387.
- Reddy et al. 2012. Composition of Near-Earth Asteroid 2008 EV₅: Potential Target for Robotic and Human Exploration. *Icarus* 221, 678-681.
- Walsh, K. J., Richardson, D. C., Michel, P. 2008. Rotational Breakup as the Origin of Small Binary Asteroids. *Nature* 454, 188-191.
- Walsh, K. J., Delbo, M., Bottke, W. F., Vokrouhlicky, D., Lauretta, D. S. 2013. Introducing the Eulalia and New Polana Asteroid Families: Re-assessing Primitive Asteroid Families in the Inner Main Belt. *Icarus* 225, 283-297.

Boulder Spatial and Size Distributions

Response Lead: Carolyn Ernst

Sub-team Members: Erik Asphaug, Bill Bottke, Humberto Campins, Paul Chodas, Christine Hartzell, Dan Scheeres, Driss Takir

What is the expected size-frequency distribution for boulders on 2008 EV₅?

- Based on the current radar data, what can we tell about the size-frequency distribution for boulders on 2008 EV₅?

It is possible to identify six distinct candidate 10-m-scale boulders on 2008 EV₅'s surface by visual inspection of the radar images. At least ten such boulders likely exist over the asteroid's entire surface [See Appendix B2].

Based on 2008 EV₅'s radar scattering properties and the highest-resolution images of asteroid surfaces (Eros and Itokawa) from spacecraft, there are likely millions of 10-cm scale cobbles on 2008 EV₅. If it is assumed that there is a power-law distribution of boulders on 2008 EV₅ that follows that of the Eros global dataset, ~16,000 1 – 5 m boulders (~1,300 2 – 3 m boulders) would be expected on the surface of 2008 EV₅. If it is assumed that there is a power-law distribution of boulders on 2008 EV₅ that connects the radar 10-m data to the radar 10-cm data, ~3,000 1–5 m boulders (~360 2 – 3 m boulders) would be expected on the surface of 2008 EV₅.

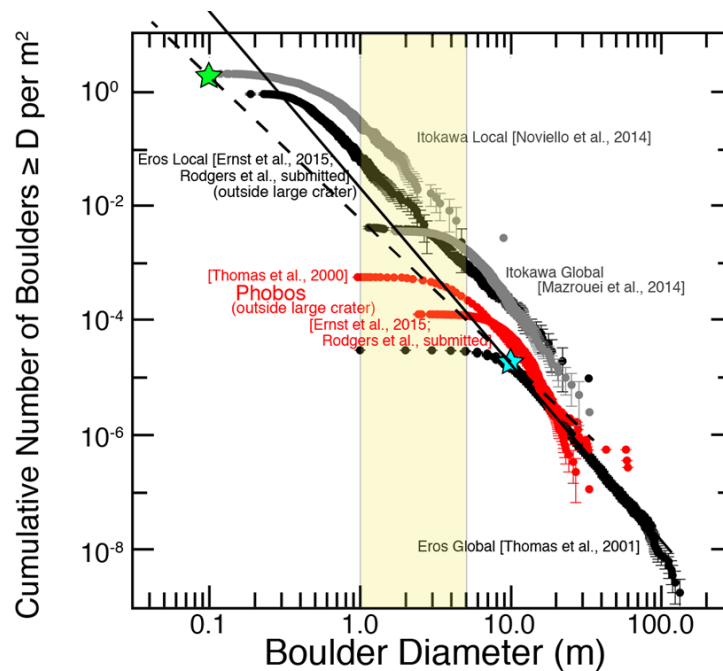


Figure 2: Measured block populations on Eros, Itokawa, and Phobos. The yellow rectangle indicates the 1–5 m boulder size range of interest for the ARRM. The cyan and green stars represent the 10-m boulder observations and the 10-cm cobble size, respectively, for 2008 EV₅ based on radar [See Appendix B2]. The surface area of 2008 EV₅, used to normalize the radar boulder counts, is taken to be 540,000 m^2 . The solid line extrapolates from the 10-m 2008 EV₅ data point using the Eros global power-law distribution (exponent of -3.2). The dashed line connects the two 2008 EV₅ data points.

This document is a NASA working document and is subject to further revision. This document has been reviewed for release to the public and is not export controlled.

- **Can any relevant information be extrapolated from existing data from other C-complex asteroids (i.e., Bennu)?**

The available data to answer this question is limited. The most appropriate data that exist today come from radar studies of 2005 YU₅₅ and 1992 UY₄, small C-complex asteroids in near-Earth space that are possibly organic-rich. Analysis suggests boulders exist on both of those bodies [Benner et al., 2015].

Available in situ asteroid data from spacecraft come from main belt asteroids Mathilde, the ~53 km C-type flyby target of the NEAR mission, and Lutetia, the ~100 km X-complex flyby target of ESA's Rosetta mission. Mathilde was only imaged at 160 m/pixel, insufficient to determine whether boulders exist [Thomas et al., 1999]. Boulders are observed on Lutetia, however Lutetia's precise composition is debated (some favor some kind of high albedo carbonaceous chondrite, while others favor an enstatite chondrite match [Barucci et al., 2015]). Boulders have been observed on bodies that could also be broadly characterized as C-complex: Phobos and Deimos, the carbonaceous chondrite-like moons of Mars, as well as comet Churyumov-Gerasimenko, the final destination of the Rosetta mission (Table 2).

Table 2: Small bodies for which boulder counts have been made from spacecraft imaging. The minimum boulder sizes measured are directly related to the best image resolution available for a given object.

Name	Mean Diameter (km)	Spectral Type	Min boulder size of global count (m)	Min boulder size of regional count (m)	Power law found	Data source	References
Eros	17	S	15	0.05	-3.2 as low as -2.3 locally	NEAR	Thomas et al., 2001; C. Ernst, personal communication
Itokawa	0.35	S	6	0.1	-3.1 -3.5 as low as -2.2 locally	Hayabusa	Michikami et al., 2010; Mazrouei et al., 2014; Noviello et al., 2014; C. Ernst, personal communication
Toutatis	3	S	n/a	10	n/a	Chang'E-2	Jiang et al., 2015
Lutetia	98	M	n/a	60	-5.0	Rosetta	Küppers et al., 2012;
Ida	31	S	n/a	45	n/a	Galileo	Lee et al., 1996
Phobos	22	D	n/a	~4	-3.3	Viking MGS MEX MRO	Thomas et al., 2000; Ernst et al., 2015; C. Ernst, personal communication
Deimos	12	D	n/a	~4	-3.2	Viking	Lee et al., 1986; C. Ernst, personal communication
Churyumov-Gerasimenko	4	comet	7	n/a	-3.6 global local ranges -2.2 to -4.0	Rosetta	Pajola et al., 2015

Hayabusa2 will arrive at the C-type asteroid Ryugu (formerly 1999 JU₃) in June of 2018. OSIRIS-REx will arrive at the B-type asteroid Bennu in August of the same year. The observations of Bennu and Ryugu will provide critical inputs to the ARRM, not only because these will be the first carbonaceous chondrite asteroids for which high-resolution images are available, but also because they are roughly similar in size and shape to 2008 EV₅. This *may* mean that they have undergone similar evolutions, but this is not definitive. Comparisons of Bennu and Ryugu to Eros and Itokawa will be vital for determining whether what is known from the extensive literature on Eros and Itokawa can reasonably be extrapolated to other near-Earth asteroids (e.g., boulder size-frequency distributions, boulder spatial distributions, etc.), or

This document is a NASA working document and is subject to further revision. This document has been reviewed for release to the public and is not export controlled.

whether they are not representative. The observations of Bennu and Ryugu will also provide important “ground-truthing” of Earth-based radar observations and have implications for detecting boulders from these types of observations.

That said, OSIRIS-REx and Hayabusa2 will not arrive at Bennu or Ryugu until mid-2018—too late to provide inputs into the mechanical designs and mission requirements, but before the currently scheduled ARRM launch date.

- **Is it expected that the size-frequency distribution of boulders on 2008 EV₅ follows a power law distribution?**

Power-law fits can be made to boulder size-frequency distributions where sufficient data are available (see The available data to answer this question is limited. The most appropriate data that exist today come from radar studies of 2005 YU₅₅ and 1992 UY₄, small C-complex asteroids in near-Earth space that are possibly organic-rich. Analysis suggests boulders exist on both of those bodies [Benner et al., 2015].

Available in situ asteroid data from spacecraft come from main belt asteroids Mathilde, the ~53 km C-type flyby target of the NEAR mission, and Lutetia, the ~100 km X-complex flyby target of ESA’s Rosetta mission. Mathilde was only imaged at 160 m/pixel, insufficient to determine whether boulders exist [Thomas et al., 1999]). Boulders are observed on Lutetia, however Lutetia’s precise composition is debated (some favor some kind of high albedo carbonaceous chondrite, while others favor an enstatite chondrite match [Barucci et al., 2015]). Boulders have been observed on bodies that could also be broadly characterized as C-complex: Phobos and Deimos, the carbonaceous chondrite-like moons of Mars, as well as comet Churyumov-Gerasimenko, the final destination of the Rosetta mission (Table 2).

Table 2: Small bodies for which boulder counts have been made from spacecraft imaging. The minimum boulder sizes measured are directly related to the best image resolution available for a given object.

Name	Mean Diameter (km)	Spectral Type	Min boulder size of global count (m)	Min boulder size of regional count (m)	Power law found	Data source	References
Eros	17	S	15	0.05	-3.2 as low as -2.3 locally	NEAR	Thomas et al., 2001; C. Ernst, personal communication
Itokawa	0.35	S	6	0.1	-3.1 -3.5 as low as -2.2 locally	Hayabusa	Michikami et al., 2010; Mazrouei et al., 2014; Noviello et al., 2014; C. Ernst, personal communication
Toutatis	3	S	n/a	10	n/a	Chang’E-2	Jiang et al., 2015
Lutetia	98	M	n/a	60	-5.0	Rosetta	Küppers et al., 2012;
Ida	31	S	n/a	45	n/a	Galileo	Lee et al., 1996
Phobos	22	D	n/a	~4	-3.3	Viking MGS MEX MRO	Thomas et al., 2000; Ernst et al., 2015; C. Ernst, personal communication
Deimos	12	D	n/a	~4	-3.2	Viking	Lee et al., 1986; C. Ernst, personal communication
Churyumov-Gerasimenko	4	comet	7	n/a	-3.6 global local ranges -2.2 to -4.0	Rosetta	Pajola et al., 2015

This document is a NASA working document and is subject to further revision. This document has been reviewed for release to the public and is not export controlled.

Hayabusa2 will arrive at the C-type asteroid Ryugu (formerly 1999 JU₃) in June of 2018. OSIRIS-REx will arrive at the B-type asteroid Bennu in August of the same year. The observations of Bennu and Ryugu will provide critical inputs to the ARRM, not only because these will be the first carbonaceous chondrite asteroids for which high-resolution images are available, but also because they are roughly similar in size and shape to 2008 EV₅. This *may* mean that they have undergone similar evolutions, but this is not definitive. Comparisons of Bennu and Ryugu to Eros and Itokawa will be vital for determining whether what is known from the extensive literature on Eros and Itokawa can reasonably be extrapolated to other near-Earth asteroids (e.g., boulder size-frequency distributions, boulder spatial distributions, etc.), or whether they are not representative. The observations of Bennu and Ryugu will also provide important “ground-truthing” of Earth-based radar observations and have implications for detecting boulders from these types of observations.

That said, OSIRIS-REx and Hayabusa2 will not arrive at Bennu or Ryugu until mid-2018—too late to provide inputs into the mechanical designs and mission requirements, but before the currently scheduled ARRM launch date.

). The boulders themselves may have been produced by more than one of the following mechanisms (e.g., collisional origin of EV₅, impact cratering, thermal fracturing of native rock, etc.). This means the power-law measured is dependent on local geological context, material strength, and possibly the sizes of the boulders that break down to produce smaller boulders. A power-law index is observed for many terrestrial fragmented objects [Turcotte 1997; see also Table 1 in Pajola et al., 2015]. Those materials listed in Pajola et al. [2015] show power law exponents ranging from -1.89 to -3.54.

In the cases of Eros, Itokawa, and Phobos, the approach of extending the SFD from large, tens-of-meter-sized boulders down to small, tens-of-centimeter-sized boulders using a power-law fit to the large population yields reasonable estimates of small block populations. It is important to note that geologic context matters for the absolute block density – if lower-resolution counts include multiple geologic settings, they will not extrapolate accurately to local areas containing only one setting [Rodgers et al., submitted; Ernst et al., 2015].

- **What is the expected distribution of boulder shapes for boulders on 2008 EV₅?**

Mazrouei et al. [2014] measured the aspect ratio for boulders greater than 6-m in diameter on Itokawa. Most boulders of this size are found to be elongated with b/a ratios of 0.7 (width/length). The third, vertical dimension of boulders (height) is not visible in most of the Hayabusa images. Michikami et al. [2010] report b/a ratios for Itokawa boulders to be 0.62–0.68. Michikami et al. [2014] measured 21 boulders on Itokawa, finding a mean c/a of 0.46.

Table 3 contains a compilation of several reports of fragment dimensions based on laboratory impact experiments. Note that the fragments are not actually 3-axis ellipsoids, they are irregular in shape. An open question is whether the aspect ratio would be different for weaker rocks (e.g., those found on a C-type asteroid like 2008 EV₅) and how much of an influence thermal degradation might have. This question will be addressed after robotic spacecraft arrive at Ryugu and Bennu in 2018.

This document is a NASA working document and is subject to further revision. This document has been reviewed for release to the public and is not export controlled.

Table 3: Compilation of fragment ratios b/a and c/a from several publications in the literature. Dimensions are defined to be $a \geq b \geq c$ for an assumed triaxial ellipsoid shape.

Reference	Target	Projectile	Impact Velocity	b/a	c/a
Fujiwara et al. 1978	Basalt	Polycarbonate cylinders	1–4 km/s	0.73	0.50
Capaccioni et al. 1986	Basalt Concrete	Aluminum spheres	9 km/s	0.7 ± 0.15	0.5 ± 0.15
Giblin et al. 1998	Porous ice	Solid ice	6 km/s	$0.56\text{--}0.71 \pm 0.1\text{--}0.2$	$0.40\text{--}0.48 \pm 0.1\text{--}0.2$
Durda et al. 2015	Basalt	Aluminum spheres	4–6 km/s	0.72 ± 0.13	0.39 ± 0.13
Michikami et al., 2014*	Basalt	Nylon spheres	1.6–7.0 km/s	0.7	0.5 (catastrophic disruption) 0.2 (impact cratering)

*Michikami et al. [2015] is a short conference abstract, so details are limited.

What is the expected spatial distribution of ~1–5 meter boulders on 2008 EV₅?

- **Where on 2008 EV₅ have boulders been detected?**

Approximately half of 2008 EV₅'s surface was observed by radar. Over this area, 6 distinct candidate 10-m-scale boulders were observed [Appendix B2]. However, due to the nature of the radar data, the exact location of the boulders cannot be determined, with the exception of one prominent boulder that is located near the asteroid's south pole.

- **Given an assumed number of certain size boulders based on a power law, is there anything that can be said about the spatial distribution of these boulders on an asteroid's surface? Specifically, does spin rate play a role in concentrating certain sized boulders at certain latitudes?**

Based on the number of observed boulders, cobbles inferred from radar roughness, and assuming a power-law relationship between boulder diameter and cumulative size-frequency distribution, the number of boulders of a given size per area (e.g., Figure 2) can be calculated assuming a roughly uniform distribution across the surface. This information alone is not enough to determine the actual distribution.

On Itokawa, potential lows are “ponds” full of cm-sized cobbles, and most of the boulders are located in other regions of the asteroid. If this is true for 2008 EV₅, concentrations of ponds at the geopotential lows with boulders at higher regions within the geopotential should be expected. Where these geopotential lows lie is a strong function of the asteroid density. For a low density of 1.5 g/cm³ the low will be at the equator and within the putative crater seen in the radar data. For a large density of 2.5 g/cm³ the geopotential low shifts off of the equator and no longer lies within the crater, but instead is at the base of the ridge.

If the boulders are sourced from the likely crater that shows up as a large concavity in the radar shape model, the distribution of the boulders would depend upon ejecta patterns around an irregularly shaped body and would require much more analysis to estimate. It is expected that the boulders would preferentially settle in the equatorial or near-equatorial regions, however.

This document is a NASA working document and is subject to further revision. This document has been reviewed for release to the public and is not export controlled.

What is the expected distribution in safe landing areas around ~1–5 m boulders on 2008 EV₅? For a 10-m diameter circle centered on the target boulder what is the expected range and likelihood over that range for the following landing site properties on C-type asteroids?

Starting with the assumption of uniform spatial distribution and a power law size-frequency distribution, the number boulders of a given size in a 10-m diameter circle can be estimated assuming a uniform distribution of boulders across the surface. Multiplying this value by the area will yield the total number of boulders greater than or equal to a given diameter in a 10-m diameter circle. If the boulders are not roughly uniformly distributed across the surface, more assumptions must be made (this will be further discussed later in this section). Likely, processes acting to move 10-m boulders would be similar to those acting to move 2 – 3-m boulders, although the responses might differ in that massive objects tend to be more easily fragmented than smaller ones, with strength decreasing with approximately the square root of size, yet require more energetic events to dislodge and accelerate.

The radar shape model of 2008 EV₅ has a range resolution of 7.5 meters [Busch et al., 2011]. Therefore, the model can provide local geometric topography to this scale. Outside of boulders and craters, local slopes generally would not be expected to change much from the 7.5-m scale down to the 1-m scale.

Local slopes will have influence over landing site safety beyond the implications for hazards to the solar arrays. Tipping hazards will be present that could seriously affect the landing operations. Eros-sized asteroids have abundant fine materials compared to smaller asteroids, which are coarser due to winnowing by solar wind and radiation effects [Hartzell and Scheeres, 2013]. The sweeping of fines ejected by electrical forces, impact vibrations, and thermal shocks leaves behind coarser material in the lag deposits on asteroid surfaces.

Steep cratered topography is not prevalent on asteroids less than ~1 km, which are of interest to the ARRM. Additionally, most small bodies seen up close and with radar appear to conform (within some reasonable angle of repose) to equilibriums of figure. On Itokawa, the smallest asteroid with good imaging, there are very few craters [Hirata et al., 2009]. On Eros, seismic shaking has acted to erase many (though not all) craters less than 100-m in diameter [Chapman et al., 2002; Thomas and Robinson, 2005], and by implication other loose topography at that scale. By implication, Eros' regolith is loose, perhaps up to 100 meters globally [Robinson et al., 2002]. A thick mobile regolith would also explain the relatively flat topography; less than 5% of the surface of Eros is steeper than 30° [Zuber et al., 2000]. Therefore, generally speaking, relatively flat, boulder-populated areas are predicted to occur on 2008 EV₅.

Another environmental concern that needs to be considered is the dust environment that could be a potential hazard for instrumentation (e.g., camera lenses, inlets, etc.) and/or systems (seals, joints, exposed bearings, solar panels, etc.). The main hazards associated with the dust environment are: 1. spacecraft sinking during landing and/or ascent, 2. high cohesion between regolith and spacecraft contactpad, 3. electrostatic motion of small dust grains 4. dust and debris liberation during the boulder capture process (e.g., thruster plume, contact pad interaction, boulder acquisition and separation). If the landing velocity exceeds the crush stress of the particulate regolith surface, the asteroid material might fluidize and slide out of the way of the lander legs, instead of holding in place to support it (discussed further in the "Surface Geotechnical Properties" section). Thus, care must be taken that the landing is done with minimal deceleration and little vibration. Additionally, the risk of the spacecraft sinking into the regolith during landing or ascent is dependent on the compaction of the regolith, which is expected to be essentially uniform about the body, except immediately next to boulders, where there may be a regolith 'apron' [Robinson et al. 2002]. The regolith apron (produced either by the migration of

This document is a NASA working document and is subject to further revision. This document has been reviewed for release to the public and is not export controlled.

dust or dust production from thermal cycling of the boulder) is unlikely to be deep enough to produce a serious sinking hazard. A regolith apron is likely to be composed of small, uncompacted regolith grains, which would form relatively strong cohesive bonds with the spacecraft. However, the fact that this apron of dust is overlaying the more densely packed surface indicates that the material is likely to fracture during separation at this striation. The plasma environment while the spacecraft is on the surface remains unknown. In order to minimize the likelihood of contamination of the spacecraft by electrostatically driven dust, the landing operation should take place close to the subsolar point and in a region with few micron-sized and smaller grains, as investigated by multispectral photometry.

What is the expected distribution in depth of burial for ~1 – 5 m boulders on 2008 EV₅?

- **Based on the theories of how asteroids and boulders form and evolve, is there anything that can be said about the likely range or distribution of burial depths?**

Due to the nature of spacecraft images of Eros and Itokawa, there is minimal information with regard to the burial of boulders on their surfaces. Regolith does migrate on asteroids, either from potential highs to lows (e.g., Itokawa) or via crater ejecta (probably less important on smaller objects, as a major fraction of the ejecta is likely to exceed escape velocity).

A minimum regolith depth of 20 – 40 m on Eros has been estimated based on the excavated volume of all large craters [Thomas et al., 2001]. Geomorphic observations indicate 50 – 100 m regolith depth, possibly globally [Robinson et al., 2002]. On Itokawa, regolith depth estimates find a minimum of ~2.3 m in the lowlands, based on roughness measurements [Barnouin-Jha et al., 2008], transitioning to a global rubble pile structure at greater depths [Fujiwara et al., 2006].

- **Is there a way to determine/estimate the depth of burial from the visual images from the characterization phase?**

Boulders formed in fragmentation events have an average aspect ratio a:b:c of 1:0.7:0.5 (2:√2:1) (see Table 3). Assuming these shapes, burial estimates could be made based on three-dimensional images taken by the Asteroid Redirect Vehicle (ARV). If the boulder's maximum dimension parallel to the ground does not coincide with the intersection with the regolith, a symmetric shape to the boulder could be assumed and a depth of burial estimated. Three-dimensional digital terrain models of the boulder will be essential for this characterization. Observations of the distribution of regolith and surface slopes/potential could help to inform whether regolith has moved into/out of the area and may have buried boulders.

- **What other ways are there to determine/estimate the depth of burial from the visual images from the characterization phase? What other ways are there to determine/estimate the depth of burial *in situ*?**

Seismic shaking can dislodge and transport boulders from depth [Asphaug et al. 2001; Miyamoto et al. 2007] as part of a convective size-sorting (Brazil-nut effect and related mechanisms). Deflation can leave behind exposed surface structures like remnants and clods. Many such apparent clasts might not be suitable for ARRM boulder retrieval (too weak). Embedded boulders emerging from the subsurface could be more difficult to extract than boulders that have been tossed downhill onto existing regolith surfaces. Identifying boulders that have survived ejection or been scattered by landslide movements, and to avoid

This document is a NASA working document and is subject to further revision. This document has been reviewed for release to the public and is not export controlled.

exclusively focusing on boulders buried in smooth sediments. Boulders found in rougher, higher-energy environments would be stronger on average than clasts found randomly in regolith, and would be subject to much lower possibility of small particulate cementation. Among these, boulders that further show evidence for meteoroid fragmentation and spallation would indicate greatest competency. A sampling approach that is able to operate in a boulder-strewn environment is likely to find very many strong, suitably sized boulders to choose from.

If a flat operational environment is required, such as a gravel-field with an isolated boulder or a wide margin, then cohesion of the regolith is more of a concern. Cementation of discrete boulders by regolith can possibly be detected by thermal imaging as, generally speaking, a boulder cohesively coupled to the regolith would also be thermally coupled. This might show up as conductive cooling on week-long timescales. In principle this rock/regolith thermal coupling can be investigated by thermal cameras before the sampling is conducted, to help in selecting among candidate boulders.

Laser altimeter data could also be used to measure the heights of boulders ('h' in Figure 3), thus enabling estimates of the short-axis ('c') dimension. This could be compared to the expected 'a' dimension, other boulders on 2008 EV₅, other boulders on Itokawa, Ryugu, and Bennu, along with expected impact fragment dimensions (see Table 3) to place estimates on burial (e.g., Figure 3).

Ground Penetrating Radar (GPR) is another approach [e.g., Hamran et al., 2014] that is a promising tool for rock and hazard avoidance. Generally the technique is capable of imaging dielectric contrasts through a few meters of loose rocky material; however the imaging technique works best for a background material with relatively uniform dielectric properties. So it would be a good choice for imaging boulders embedded in beds of dust, for instance, but not for imaging the specific configurations of boulders within blocky landslides and ejecta deposits, for which multiple scattering effects diminish the signal. Seen as an added investigation, GPR would be of good value in that it would provide essential contrast and mitigate risks in dusty environments where the temptation will be to land (because it is flat), and because it can obtain subsurface context wherever the sample is acquired. The added mass and cost of such an instrument is not insubstantial, but the most critical operational aspect is the possibly low SNR of the measurements. The radar electronics and antenna have to be isolated from the spacecraft electronics, which can become a strong source of noise, especially when motors are involved. The spacecraft itself is a strong radar reflector, and due to the relatively omnidirectional nature of GPR, it is challenging to image boulders in close proximity if they are comparable in size to the major spacecraft elements. If 2008 EV₅ is the target asteroid, and if the CR-designation holds, then the high metallic content of analogous materials would lead to a radar response that might enhance meter-scale imaging by providing strong contrasts (e.g., a metallic lag beneath silicate dust) or obscure imaging by scattering and attenuation.

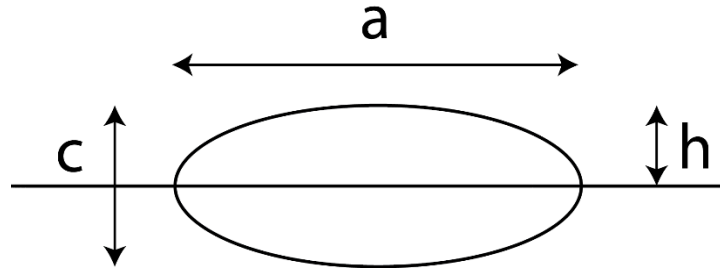


Figure 3: Example of a buried boulder. The dimension h could be measured with a laser altimeter and the dimension a could be measured with a camera. By assuming a typical $a:c$ ratio from other boulders on the body, from boulders on Itokawa, or from impact fragment experiments, the dimension c could be modeled, and the depth of burial estimated.

For more information, see Appendix B1.

References:

- Asphaug, E., King, P.J., Swift, M.R., Merrifield, M.R., 2001. Brazil nuts on Eros: Size-sorting of asteroid regolith. LPSC 32, #1708.
- Barnouin-Jha, O.S., Cheng, A.F., Mukai, T., Abe, S., Hirata, N., Nakamura, R., Gaskell, R.W., Saito, J., Clark, B.E., 2008. Small-scale topography of 25143 Itokawa from the Hayabusa laser altimeter. Icarus 198, 108–124.
- Benner, L.A.M., Busch, M.W., Giorgini, J.D., Taylor, P.A., Margot, J.-L., 2015. Radar observations of near-Earth and main-belt asteroids. In: Asteroids IV, in press. <http://echo.jpl.nasa.gov/asteroids/benner.etal.radar.chapter.20150728.pdf>
- Barucci, M.A., Fulchignoni, J., Ji, J., Marchi, S., Thomas, N., 2015. The flybys of asteroids 2867 Steins, 21 Lutetia, and 4179 Toutatis. In: Asteroids IV, in press.
- Busch, M.W., Ostro, S.J., Benner, L.A.M., Brozovic, M., Giorgini, J.D., Jao, J.S., Scheeres, D.J., Magri, C., Nolan, M.C., Howell, E.S., Taylor, P.A., Margot, J.-L., Briskin, W., 2011. Radar observations and the shape of near-Earth asteroid 2008 EV₅. Icarus 212, 649–660.
- Capaccioni, F., Cerroni, P., Coradini, M., Di Martino, M., Farinella, P., Flamini, E., Martelli, G., Paolicchi, P., Smith, P.N., Woodward, A., Zappala, V., 1986. Asteroidal catastrophic collisions simulated by hypervelocity impact experiments. Icarus 66, 487–514.
- Chapman, C.R., Merline, W.J., Thomas, P.C., Joseph, J., Cheng, A.F., Izenberg, N., 2002. Impact history of Eros: Craters and boulders. Icarus 155, 104–118.
- Durda, D.D., Bagatin, A.C., Aleman, R.A., Flynn, G.J., Strait, M.M., Clayton, A.N., Patmore, E.B., 2015. The shapes of fragments from catastrophic disruption events: Effects of target shape and impact speed. Planetary and Space Science 107, 77–83.
- Ernst, C.M., Rodgers, D.J., Barnouin, O.S., Murchie, S.L., Chabot, N.L., 2015. Evaluating small body landing hazards due to blocks. LPSC 46, #2095.
- Fujiwara, A., Kamimoto, G., Tsukamoto, A., 1978. Expected shape distribution of asteroids obtained from laboratory impact experiments. Nature 272, 602–603.
- Fujiwara, A. et al., 2006. The rubble-pile asteroid Itokawa as observed by Hayabusa. Science 312, 1330–1334.
- Giblin, I., Martelli, G., Farinella, P., Paolicchi, P., Di Martino, M., Smith, P.N., 1998. The properties of fragments from catastrophic disruption events. Icarus 134, 77–112.

This document is a NASA working document and is subject to further revision. This document has been reviewed for release to the public and is not export controlled.

- Hamran, S.E., Amundsen, H.E.F., Carter, L.M., Ghent, R.R., Kohler, J., Mellon, M.T., Paige, D.A., 2014. The RIMFAX ground penetrating radar on the Mars 2020 rover. AGU Fall Meeting, #P11A-3746.
- Hartzell, C.M., Scheeres, D.J., 2013. Dynamics of levitating dust particles near asteroids and the Moon. *Journal of Geophysical Research: Planets* 118, 116–125.
- Hirata, N., Barnouin-Jha, O.S., Honda, C., Nakamura, R., Miyamoto, H., Sasaki, S., Demura, H., Nakamura, A.M., Michikami, T., Gaskell, R.W., Saito, J., 2009. A survey of possible impact structures on 25143 Itokawa. *Icarus* 200, 486–502.
- Mazrouei, S., Daly, M.G., Barnouin, O.S., Ernst, C.M., DeSouza, I., 2014. Block distributions on Itokawa. *Icarus* 229, 181–189.
- Michikami, T., Nakamura, A.M., Hirata, N., 2010. The shape and distribution of boulders on Asteroid 25143 Itokawa: Comparison with fragments from impact experiments. *Icarus* 207, 277–284.
- Michikami, T., et al., 2015. The shapes of fragments in hypervelocity impact experiments ranging from cratering to catastrophic disruption. AGU Fall Meeting.
- Miyamoto, H. et al., 2007. Regolith migration and sorting on asteroid Itokawa. *Science* 316, 1011–1014.
- Pajola, M. et al., 2015. Size-frequency distribution of boulders ≥ 7 m on comet 67P/Churyumov-Gerasimenko. *Astronomy and Astrophysics*, <http://dx.doi.org/10.1051/0004-6361/201525975>.
- Robinson, M.S., Thomas, P.C., Veverka, J., Murchie, S.L., Wilcox, B.B., 2002. The geology of 433 Eros. *Meteoritics and Planetary Science* 37, 1651–1684.
- Rodgers, D.J., Ernst, C.M., Barnouin, O.S., Murchie, S.L., Chabot, N.L., 2015 (submitted). Methodology for finding and evaluating small body landing sites. *Planetary and Space Science*, submitted.
- Thomas, P.C., Robinson, M.S., 2005. Seismic resurfacing by a single impact on the asteroid 433 Eros. *Nature* 436, 366–369.
- Thomas, P.C., Veverka, J., Bell, J.F., Clark, B.E., Carcich, B., Joseph, J., Robinson, M., McFadden, L.A., Malin, M.C., Chapman, C.R., Merline, W., Murchie, S., 1999. Mathilde: Size, shape, and geology. *Icarus* 140, 17–27.
- Thomas, P.C., Veverka, J., Robinson, M.S., and Murchie, S., 2001. Shoemaker crater as the source of most ejecta blocks on the asteroid 433 Eros. *Nature* 413, 394–396.
- Turcotte, D.L., 1997. *Fractals and chaos in geology and geophysics*. Cambridge University Press, Cambridge, 398p.
- Zuber, M.T., et al., 2000. The shape of 433 Eros from the NEAR-Shoemaker laser rangefinder. *Science* 289, 2097–2101.

Surface Geotechnical Properties

Response Lead: Kris Zacny

Sub-team Members: Dan Britt, Leslie Gertsch, Christine Hartzell, Dan Scheeres, Joel Sercel

What are the expected surface regolith geotechnical properties of the parent asteroid? For example: What is the expected range in the coefficient of friction between the parent asteroid surface regolith and the Contact and Restraint Subsystem (CRS) contact pads? How uniform is this expected to be?

The coefficient of friction is a function of the magnitude of cohesive forces between regolith and the CRS contact pads. The main sources of cohesive forces are van der Waals and electrostatic forces, but van der Waals forces are more dominant [Scheeres, 2010]. Karafiathand and Mohr [1969] found that

This document is a NASA working document and is subject to further revision. This document been reviewed for release to the public and is not export controlled.

coefficient of friction is not affected by the ultra-high vacuum (Table 4). However, ultra-high vacuum increases the total frictional resistance by an adhesion/cohesion which is essentially constant over the range of normal loads in the experiment.

Table 4: Coefficient of friction between steel disc and crushed basalt in vacuum and at 1 g [Karafiathand and Mohr, 1969].

	Between steel disc and crushed coarse basalt (250 - 500 micron)		Between steel disc and crushed fine basalt (38 - 62 micron)		Between steel disc coated with coarse basalt and crushed basalt	
	Vacuum	Air	Vacuum	Air	Vacuum	Air
Initial Coefficient of Friction (effect of regolith dilation to allow grain displacement)	0.35	0.35	No Data	No Data	No Data	No Data
Kinetic Coefficient of Friction	0.28	0.27	0.20	0.18	0.28	0.20

- What is the expected range of surface compaction and porosity of the regolith surrounding the boulder? How uniform is this expected to be?

The asteroid surface is more likely to be a pebble-rich lag depleted of fines and as such the surface porosity should be higher and compaction lower than asteroid’s bulk compaction and porosity. Whatever the porosity and compaction, it is likely that the same processes apply all around the target area, so it should be fairly uniform. In turn, this should be applicable to all ARRM targets. Figure 4 shows macroporosities and densities for asteroids [Britt et al., 2002] and Figure 5 shows macroporosities of asteroid and comets [Consolmagno et al., 2008]. The exceptions are “low” areas observed for example on Eros and Itokawa that were filled with relatively fine material. For reference, properties of Itokawa (S-type), Bennu (B-type), and 253 Mathilde (C-type) are:

- Itokawa: bulk density of 2.0 g/cc; bulk porosity of 40.6%, or packing fraction of 0.59. [Abe et al., 2006; Gaskell et al., 2008]
- Bennu: bulk density = 1.260 ± 0.070 g/cc (1-sigma uncertainty) [Chesley, 2014]
- 253 Mathilde: 1.34 g/cc [Veveřka, 1999]

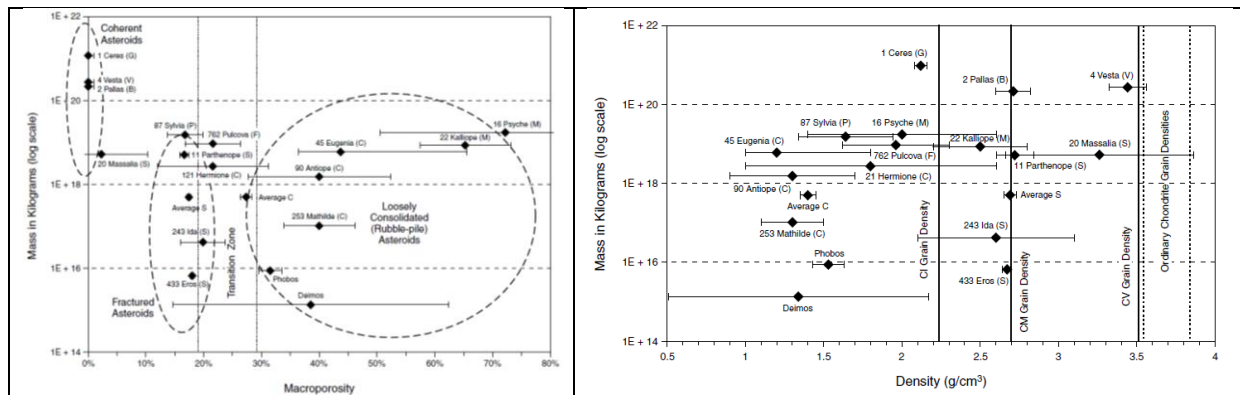


Figure 4: Macroporosities and densities of asteroids. [Britt et al., 2002]

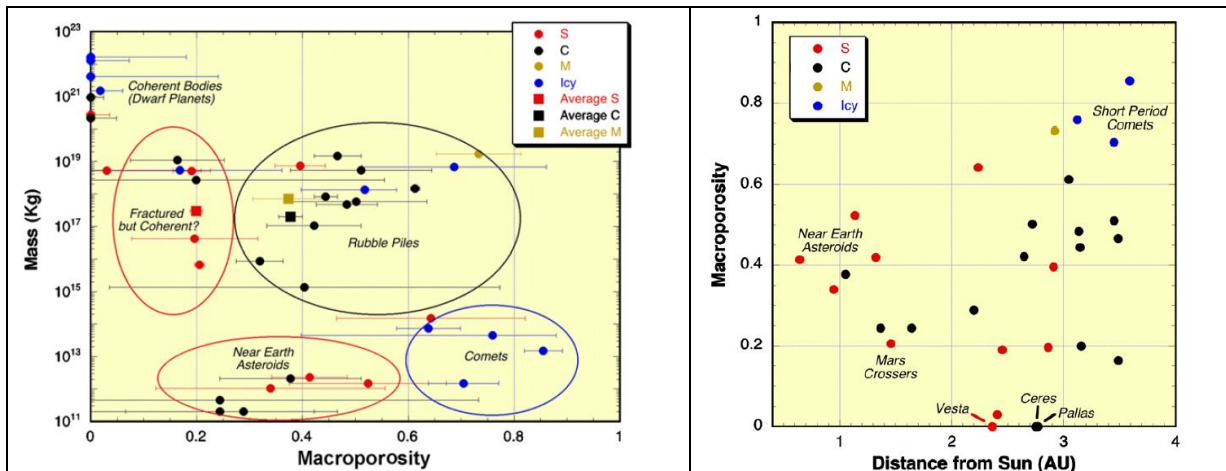


Figure 5: Macroporosities of asteroid and comets [Consolmagno et al., 2008]

- **What is the expected particle size-frequency distribution of the regolith, and how does this influence the design of the CRS contact pads and geological context samplers?**

Based on particle size-frequency distribution of rocks and boulders on Itokawa in the millimeter to tens of meters size [Michikami, 2008] and grains from less than 100 micron down to 1 micron sizes returned by Hayabusa [Tsuchiyama, 2011], the cumulative size distribution of coarse and fine regolith is expected to have a power-index of $d^{-2.8}$.

Coarse gravel (1 cm or greater) is expected to exist on the surface overlaying fine grained material with the fraction of fines increasing with depth. The combination of low surface acceleration and solar radiation pressure tend to strip off fine particles, generated by comminution processes, and leave lags of larger, harder to move materials.

Since forces during the boulder extraction will be reacted through the CRS contact pads back to the asteroid, the pads need to be designed to prevent excessive sinkage. If regolith is rich in fines, its cohesion and in turn bearing strength will be greater and thus contact pads could be made smaller. The same is true if regolith is more compact. If regolith is coarse, cohesion will be lower and in turn contact pads would need to be larger. The same is true if regolith has low density/high porosity. Contact pads also need to leave the surface when the spacecraft departs with the boulder. These two steps (boulder extraction and contact pad extraction from the surface) have competing requirements: for boulder extraction contact pad area needs to be maximized and for contact pad extraction, the area needs to be minimized. Therefore, mission risk is likely reduced if the three contact pads are oversized (with appropriate margin) to prevent excessive sinkage. The issue of departing from the surface could be eliminated by implementing 'decoupling' subsystems that would leave the pads behind. This approach requires additional study to access the ability of the capture system to perform multiple collection attempts and to retain the surface regolith samples obtained by the geological context samplers.

It is challenging to design a regolith sampler that will work with any and all particle sizes. The sampler would therefore benefit by being designed for a specific range of particle sizes.

This document is a NASA working document and is subject to further revision. This document has been reviewed for release to the public and is not export controlled.

- **What is a set of earth analog surfaces (e.g. concrete, sand) that could be used to bound the expected range of surface variability for use in validating the design of the landing system?**

From a regolith interaction standpoint, analog material should be 'designed' to match the regolith geotechnical properties. As such, parameters that are important include particle size distribution, particle shape, particle strength, magnetic moment, and particle density. All other material bulk properties, such as bulk density, porosity, shear strength (cohesion and friction angle), are directly influenced by these grain properties. Environmental parameters such as vacuum and gravity could have a much greater effect on geotechnical properties of granular material, and this needs to be taken into account.

The OSIRIS-REx team has developed several asteroid simulants, including Tagish Lake 7c (TL7c) [Hildebrand, 2015]. University of Central Florida is currently developing several asteroid simulants with a range of strengths and particle sizes. The use of asteroid simulants is the preferred analog material for validating the design of the landing system.

- **What is the expected bearing strength of surface regolith? This is needed to determine if ARV requires dampers within the three legs.**

Since asteroid gravity is negligible, Terzaghi's equation [Terzaghi, 1943] for circular or square footing could be used to obtain a first order bearing capacity of the regolith. The bearing capacity of the regolith is defined as $\sigma = 1.3 * (c+c') * N_c$, where c is the regolith cohesion due to van Der Waals forces, c' is the apparent cohesion due to particles interlocking, and N_c is the bearing capacity factor.

The low limit for bearing strength can be calculated assuming the friction angle $\phi=0^\circ$ ($N_c=5.7$), $c=25$ Pa and $c'=0$ Pa. Hence $\sigma=1.3 * (25+0) * 5.7 = 185$ Pa.

The upper limit for bearing strength can be calculated assuming $\phi=10^\circ$ ($N_c=9.6$), $c=250$ Pa and $c'=100$ Pa. Hence $\sigma=1.3 * (250+100) * 9.6 = 15,600$ Pa.

These are very rough estimates of the lower and upper limits of the bearing strength. Numerical modeling should be used to provide better estimates and sensitivities to different regolith and spacecraft parameters.

It should be noted that additional information with respect to regolith bearing strength will be available once OSIRIS-Rex- and Hayabusa2 missions performed their sampling operations.

What is the expected distribution in cohesion between ~1 - 5 meter boulders and the surface of 2008 EV₅?

Fine grains will preferentially attach to larger grains, and thus larger grains embedded in a matrix of fine grains would be held in place by the strength of the matrix itself. Hence, the cohesion between large boulders and regolith will be driven by cohesion between fine particles, estimated to be in the range of 25 – 250 Pa [Sánchez and Scheeres, 2014].

- **How does cohesion translate into the required extraction force for a given sized boulder?**

This document is a NASA working document and is subject to further revision. This document has been reviewed for release to the public and is not export controlled.

$F_{\text{extraction}}$ is a sum of two forces: cohesive force and inertial force. Cohesive force is attributed to boulder-regolith cohesion which is driven by regolith's matrix and can vary from an estimated 25 Pa to 250 Pa [Sanchez and Scheeres, 2014]. Inertial force is a function of the acceleration the boulder achieves during the process of lifting it off the surface. Hence, $F_{\text{extraction}} = \text{cohesion} * A_{\text{boulder}} + \text{Force}_{\text{inertia}}$. The extraction force could potentially be reduced by 'peeling' the boulder off the surface [Kultchitshy et al., 2015]. However, this needs to be traded against operational complexity and time.

- **Is there a way to estimate (or narrow the uncertainty in) the cohesion between the surface and boulder based on the visual images from the in situ characterization phase?**

It is not possible to estimate with great certainty the cohesion between the surface and the boulder from visual images alone. A high-resolution camera (mm per pixel or better) would be needed to provide good estimates for regolith size distribution. Particle size distribution could be used together with the numerical models (e.g. DEM) to assess regolith cohesion. However, if models have not been calibrated, the regolith strength values could have significant uncertainty. The models can be calibrated through in-situ testing of regolith properties. The regolith strength, which drives cohesion between the boulder and the surface, can be determined by deploying geotechnical instruments. The geotechnical data could then be used analytically or with an aid of numerical models, such as DEM, to estimate cohesion between the surface and the boulder.

- **How is the cohesive force expected to "break" during boulder extraction?**

The extraction of a boulder from a regolith with a size distribution ranging down to microns to 100's of microns requires the breaking of cohesive bonds within the regolith. Based on DEM simulations [Sanchez and Scheeres, 2014] this occurs in two phases, a quasi-elastic phase followed by a plastic phase when the bonds between individual grains are broken (Figure 6 **Error! Reference source not found.**). Due to the physics of cohesion, fine particles will preferentially adhere to a larger boulder, meaning that extraction occurs by breaking cohesive forces within the regolith. Figure 5 shows the results of a DEM simulation of a boulder extraction from a cohesive regolith [Sanchez and Scheeres 2014]. Note that the cohesive regolith preferentially adheres to the boulder, meaning that extraction occurs by breaking the cohesive forces within the regolith.

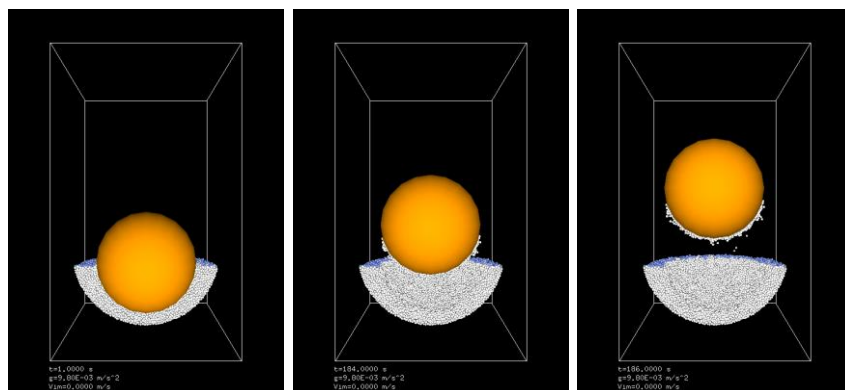


Figure 6: DEM simulation of a boulder extraction from a cohesive regolith [Sanchez and Scheeres 2014].

Figure 7 gives an example of a general shape of the Pull Force, F_p , as a function of time [Kulchitsky et al., 2015]. The exact shape will depend on the cohesive values as well as extraction methods (e.g., constant acceleration, peeling, etc.). F_c is a DEM computed force that needs to be exceeded to remove the boulder from the surface. In this example 400 N pulling force is not sufficient to separate the boulder from the regolith.

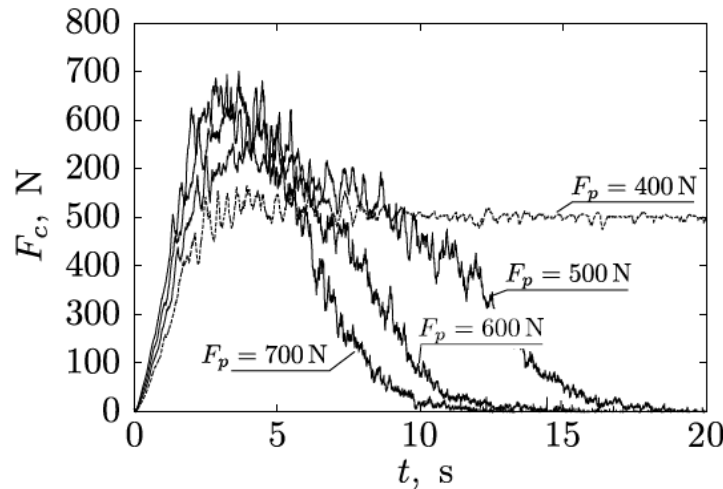


Figure 7. Resistance force profiles for different pull forces (F_p) in “peeling” test and regolith cohesive strength $c = 100$ Pa [Kulchitsky et al., 2015].

- **Are there any other likely physical properties or mechanisms that would prevent a boulder from being extracted?**

Unless boulder can be inspected underneath, there will always be a risk that another rock could be wedging the boulder in place. Additionally, the boulder could be buried in the regolith along its long axis, which would likely complicate accurately determining its depth of burial. There is also some uncertainty related to the effect that phyllosilicate minerals have on the strength of regolith and forces between the regolith and boulder. Further study is required to determine if this is a significant issue.

For more information on the entire “Surface Geotechnical Properties” section, see Appendix C.

References:

- Abe et al. (2006). Mass and local topography measurements of Itokawa by Hayabusa. *Science* 312:1344–1347.
- Britt D.T., Yoemans D., Housen K., and Consolmagno G.J. (2002) Asteroid Density, Porosity, and Structure. In *Asteroids III* (W. Bottke, A. Cellino, P. Paolicchi, and R. P. Binzel eds.), University of Arizona Press, pp. 485-500.
- Chesley et al. (2014). Orbit and bulk density of the OSIRIS-REx target asteroid (101955) Bennu. *Icarus* 235, 10-22.
- Consolmagno G.J., Britt D.T., and Macke R.J. (2008) The Significance of Meteorite Density and Porosity. *Chemie der Erde-Geochemistry* 68, 1-29 (Invited Review).
- Gaskell et al., (2008). Itokawa shape model v1. 0. NASA Planetary Data System, 92

This document is a NASA working document and is subject to further revision. This document has been reviewed for release to the public and is not export controlled.

- Hildebrand, A. R., et al. An Asteroid Regolith Simulant for Hydrated Carbonaceous Chondrite Lithologies (HCCL-1). <http://www.hou.usra.edu/meetings/metsoc2015/pdf/5368.pdf>. 78th Annual Meeting of the Meteoritical Society. 2015.
- Karafiath L., and G. Mohr, Effect of Ultrahigh Vacuum on the Friction between Metals and Granular Soils, J. Vac. Sci. Technol. 6, 198 (1969); <http://dx.doi.org/10.1116/1.1492659>
- Kulchitsky et al. (2015). Resistance forces during boulder extraction from an asteroid. Acta Astronautica AA_2015_93 (Submitted).
- MarcoPolo-R Integrated Sampling Mechanism (MPRISM). <http://us-marcopolor.jhuapl.edu/mission/docs/Potential%20NASA%20contribution.pdf>. Accessed October, 2015.
- Michikami et al. (2008). Size-frequency statistics of boulders on global surface of asteroid 25143 Itokawa. Earth, Planets and Space 60:13–20.
- Sánchez, P. and D. J. Scheeres (2014). The strength of regolith and rubble pile asteroids, Meteoritics & Planetary Science 49, Nr 5, 788–811, doi: 10.1111/maps.12293
- Scheeres, D., C. Hartzell, P. Sánchez, M. Swift (2010). “Scaling Physics to Asteroid Surfaces: The Role of Cohesion” Icarus. 2010. Vol 210, pp 968-984.
- Terzaghi, K. (1943) Theoretical Soil Mechanics, Wiley, New York.
- Tsuchiyama et al., (2011). Three-dimensional structure of Hayabusa samples: Origin and evolution of Itokawa regolith. Science 333:1125–1128.
- Veverka, J. et al. (1999). "NEAR Encounter with Asteroid 253 Mathilde: Overview". Icarus 140 (1): 3–16. Bibcode:1999Icar..140....3V. doi:10.1006/icar.1999.6120.

Boulder Physical Properties

Response Lead: Dan Britt

Sub-team Members: Neyda Abreu, Eric Asphaug, Humberto Campins, Leslie Gertsch, Joel Sercel, Kris Zacny

What is the expected distribution in densities for ~1 - 5 meter boulders on 2008 EV₅? What uncertainty in density will exist after the in situ visual imaging and characterization phase?

The bulk densities, grain densities, and porosities for the subclasses of carbonaceous chondrite meteorites are shown in Table 5. For a given meteorite analog, the upper bound of the bulk density uncertainty should be in the range cited. The major uncertainty is in the lower bound of the bulk density because of atmospheric filter bias against weak materials. Note that the ranges of density values are powerfully constrained by the physics of minerals. A mineral is an arrangement of atoms set by fundamental physics. While a mineral assemblage (rock) can be made less dense by introducing porosity, under asteroidal conditions it is physically impossible to make a given mineral denser. The uncertainty will be in the identification of the meteorite analog and the lower bound of the bulk density.

Meteorite data are inherently biased by a range of selection effects including orbital dynamics, atmospheric stresses eliminating weak materials, and a limited time series of sampling. Meteorite data should be considered upper bounds for bulk density since they are strong enough to survive entry. Boulders on the surfaces of asteroids may be weaker and less dense. There may be significant systematic differences between meteorite properties and pristine asteroid properties. In situ sensing data, including

This document is a NASA working document and is subject to further revision. This document has been reviewed for release to the public and is not export controlled.

reflectance spectroscopy and thermal inertia, can provide valuable insight into mineralogy, and the data from meteorite collections cited in this response provides an upper bound and ranges of bulk density.

Table 5: Carbonaceous Chondrite Physical Properties [Macke et al., 2011]

Meteorite Type	Average Bulk Density (g/cm ³)	Bulk Density Range (g/cm ³)	Average Grain Density (g/cm ³)	Grain Density range (g/cm ³)	Porosity (%)	Porosity Range (%)
CI	1.58	single measurement	2.43	single measurement	35	single measurement
CM	2.20	1.88 to 2.47	2.92	2.74 to 3.26	24.7	15.0 to 36.7
CV	3.03	2.59 to 3.46	3.54	3.25 to 3.68	14.6	0.6 to 27.7
CO	3.03	2.18 to 3.48	3.52	2.99 to 3.78	13.6	0 to 41.3
CK	2.90	2.54 to 3.39	3.58	3.37 to 3.66	17.8	0 to 23.4
CR	3.11	2.29 to 3.94	3.42	3.06 to 3.88	9.5	0–25.0
CB	5.25	4.90 to 5.55	5.65	5.63 to 5.66	3.9	2.0% to 5.8

An indication of the variance in the distribution of boulder densities is provided by Macke et al. [2011]. They measured bulk density and porosity for 26 stones of two major CM falls, Murchison and Murray. The physical properties of these stones are homogeneous to within a few percent. Similar measurements were carried out for major CV, CO, and ordinary chondrite falls. Again, in all cases a similar pattern of homogeneity was observed. It is therefore expected that the strength of boulders across a given asteroid would have similar homogeneity.

Some combination of remote sensing measurements prior to boulder selection and in-situ measurement prior to collection would identify the mineralogy of the boulder:

- Multi-wavelength Spectroscopy (e.g., ultra-violet (UV), visible, near-infrared, thermal etc.)
 - Alpha particle X-ray spectrometry (APXS) and/or laser-induced breakdown spectroscopy (LiBS) for elemental abundances
 - Neutron and Gamma-ray spectroscopy for volatiles and elemental abundances
 - Mössbauer spectroscopy for Fe mineralogy
 - X-Ray diffraction (XRD) for general mineralogy
- **How can a conservative mass estimate be derived from this information in order to ensure the selected boulder does not exceed the ARV return capability?**

If the composition of the asteroidal targets can be identified, the available data on meteorite bulk density for the major meteorite classes can be used to derive the upper bound on meteorite bulk density and mass.

What is the expected distribution in the coefficient of thermal expansion of ~1-5 meter boulders from 2008 EV₅?

The coefficient of thermal expansion (α) of CM and CR chondrites are not well studied. A thermal characterization of the boulder by remote sensing prior to sampling would be beneficial for studies of thermal response as described below. However, some informed estimates based on analogs to terrestrial materials can be made. Also, as with bulk density and other physical properties, the expected distribution of the coefficient of thermal expansion should be small. Direct measurements of the coefficient of thermal expansion for CM chondrites are being conducted and results should be available soon. In the meantime, it is expected that α for these materials will be in the range of $5 - 15 \times 10^{-6}/K$, similar to that of terrestrial sandstones, dolomites, and concretes.

This document is a NASA working document and is subject to further revision. This document has been reviewed for release to the public and is not export controlled.

If it is desired to determine if thermal processes are likely to break or spall the boulder, in addition to the coefficient of thermal expansion, other parameters such as Young’s Modulus and compressive strength are needed. In certain geometries involving spalling off the edges of a boulder, the thermal stress failure mode can actually be in shear. So in addition, the shear modulus or Poisson’s ratio along with thermal conductivity and specific heat will be needed. Given the same caveats as provided in regard to coefficient of thermal expansion, reasonable expected values for these parameters are provided Table 6.

Table 6: Estimated Values of Carbonaceous Chondrite Physical Properties Related to Spalling and Thermal Fracture

Parameter	Min	Typical	Max
Specific Heat (J/kg/K)	1,000	2,000	3,000
Density (kg/m ³)	1,900	2,250	3,000
Thermal Conductivity (W/K/m)	1.0	2.0	3.0
Poisson’s Ratio	0.18	0.20	0.25
Young’s Modulus (Pa)	1.0E+10	2.0E+10	3.0E+10
Tensile Strength (Pa)	3.0E+05	1.0E+06	3.0E+06
Compressive Strength (Pa)	1.0E+06	3.0E+07	5.0E+07
Shear Strength (Pa)	5.0E+05	1.0E+07	2.0E+07
Coefficient of thermal expansion (10 ⁻⁶ /K)	5	10	15

- **Homogeneity of Major Meteorite Falls:**

Heterogeneity is an important property of meteorites, and disrupted meteoroids, and presumably, the large boulders on asteroids, so meteorite falls are important to consider. According to Macke et al. [2011]: “The abundance of stones for Murchison and Murray provides an excellent opportunity to explore the homogeneity of stones from the same fall. Murchison and Murray are relatively uniform in texture, and so by comparing stones from each fall it is possible to get a sense of the homogeneity of the parent body on the scale of the size of the original meteoroid, approximately decimeters to meters. In all parameters and for both meteorites, variation among stones (determined by one standard deviation) was less than 10% from the mean value, with the greatest degree of variability in the porosities. For Murchison, grain density ranged from 2.87 to 3.05 g/cm³ (mean 2.96 g/cm³, with a variability of 0.05 g/cm³, or 1.6% of the mean value). Bulk density averaged 2.31 g/cm³, ranging from 2.15 to 2.40 g/cm³. Variability in bulk density was 0.07 g/cm³, or 3.1% of the mean. Porosity ranged from 18.7% to 24.9%, with a variability of 2.2% (10.0% of the mean 22.1% porosity). Magnetic susceptibility averaged 3.73, with a range from 3.54 to 3.90. Variability was 0.13, or 3.6% of the average. It should be noted that the mean uncertainties for the individual measurements were 0.01 g/cm³ for grain density, 0.02 g cm³ for bulk density, 0.9% for porosity, and 0.09 for magnetic susceptibility. This indicates that, while measurements did vary between stones, the differences were not many times larger than measurement uncertainty. Overall, the stones from Murchison that were included in the study are homogeneous to within a few percent. Murray produces similar results. Bulk density varied 0.05 g/cm³ (2.3% of the mean of 2.30 g/cm³), grain density varied 0.02 g/cm³ (0.7% of the mean 2.91 g/cm³), porosity 1.8% (8.6% of the mean porosity of 20.8%), and magnetic susceptibility 0.15 (4.0% of 3.66). Mean measurement uncertainties for the stones were the

same as for Murchison, but the overall variability is less. This indicates that Murray, at least for the stones in this survey, may be more homogeneous overall than Murchison.”

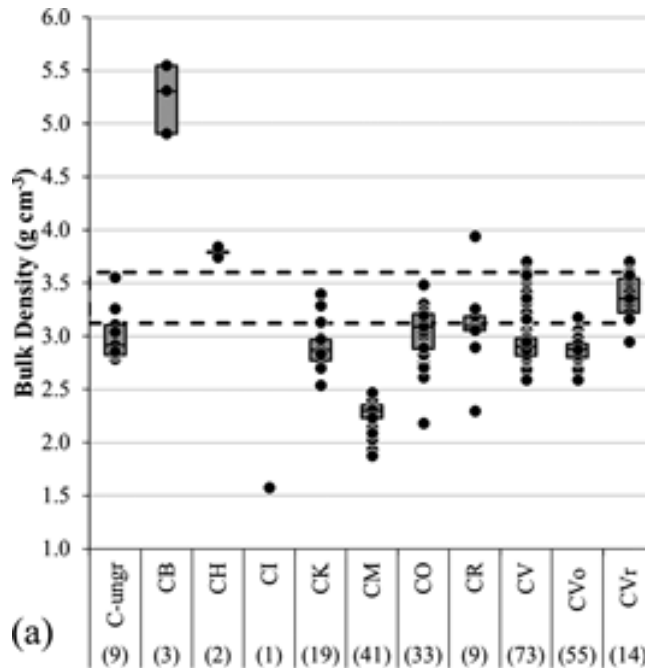


Figure 8: Bulk density ranges for C-type meteorites [Macke et al., 2011].

What is the expected distribution in minimum shear, compressive, and tensile strengths for ~1-5 meter boulders on 2008 EV₅?

It is difficult to confidently predict boulder strength on 2008 EV₅ because we have no direct measurements that can be applied without uncertainty in interpretation. Hard data on asteroid material strength comes from two sources: laboratory measurements of small meteorites and data from bolide entry events, from which we derive the aerodynamic ram pressure at breakup. Other insights into the strength question come from experience with terrestrial materials and their variation with scale; experience with materials from other bodies such as the Moon and Mars; and analytical models. The difficulty with meteorite strength data is that it is measured from small samples and its applicability to large boulders requires an extrapolation which is uncertain. Likewise, bolide data clearly shows a range of breakup altitudes associated with material properties correlated with a range of component sizes. However, the nature of those components and the body’s reaction to entry are subject to interpretation. A key question, is whether the bolides themselves (asteroid materials at meter-scale) are representative of meter-size boulders on asteroids.

Meteorite strength fundamentally depends on composition, texture, and structure. In general, meteorites are bi-modal in their strength with most meteorite types including ordinary chondrites, anhydrous carbonaceous chondrites, and most CMs being quite strong with compressive strengths greater than 40 MPa. The other major strength grouping includes CI and some petrologic type 2 carbonaceous chondrites (C2), such as Tagish Lake, which are quite weak with compressive strengths less than a few MPa. Caveats include that there are notable exceptions to this generalization (i.e., weak ordinary chondrites) and that the meteorite strength data is sparse on a number of important types (i.e.,

This document is a NASA working document and is subject to further revision. This document has been reviewed for release to the public and is not export controlled.

CMs, CIs and CRs having few or no measurements). Estimation of the overall strength of a boulder could be based on the “weakest link” approach that will likely be at least an order of magnitude weaker than data from individual meteorites.

Given these caveats, along with the uncertainty in 2008 EV₅'s classification, it is the judgment of the ARM FAST team members that boulders on 2008 EV₅ could exhibit strength characteristics that fall within the following ranges:

- Shear strength: 0.1-5 MPa
- compressive strength: 0.5-50 MPa
- tensile strength: 0.05-3 MPa

Of these parameters, the one that is most uncertain is tensile strength, and the possibility that tensile strength at large scale may be below the range in the table cannot be ruled out without further investigation. It should also be noted that there is dispute within the scientific community regarding the compressive strength, with some members of the FAST team suggesting that boulder compressive strength may be as low as 0.1 MPa, derived from the assumed aerodynamic stresses during bolide breakup in the atmosphere. More experimental data on the relevant meteorite types and experiments with large-scale simulants are needed to refine these estimates.

Note: If 2008 EV₅'s actual albedo is near or higher than the mean albedo values presented in the “Origin of 2008 EV₅” section, 2008 EV₅ is arguably a CR chondrite (though other compositions cannot be definitively ruled out, such as CK, CM, etc.). As a starting point for discussion and new work, it is probably reasonable to assume this composition when making estimates of likely boulder strengths. If 2008 EV₅'s actually has a low albedo, however, it is arguably more likely to be a CI or CM chondrite, which show a wide range of meteorite strengths and probably boulder strengths as well. This possibility is more problematic for engineering work, but it cannot be ruled out until additional information on the nature of 2008 EV₅ becomes available.

All other things being equal (i.e., similar mineralogy, albedo, exposure history, and shock history), just as with bulk density and other physical properties, a narrow distribution of shear, compressive, and tensile strength of boulder on an individual asteroid should be expected. Because of thermal shock and erosion, angularity and visible fractures may be a measure of relative boulder strength. Stronger boulders may be more angular and weaker boulders more rounded. The physical properties of homogeneous, isotropic rock are typically normally or lognormally distributed; it can reasonably be expected that boulders on 2008 EV₅ will exhibit a normal or lognormal distribution in strength.

Given the uncertainties and caveats in the above discussion, it would seem prudent to work aggressively to refine estimates of boulder strength while exploring capture mechanisms that minimize the needed mechanical strength of the boulder. In addition, a broader investigation of the issue of boulder breakup is advisable including consideration of boulder thermal properties, toughness or brittleness, and ductility. Finally, given that other targets besides 2008 EV₅ are candidates for ARM, including those of interest to ISRU, and that the most desirable targets from an ISRU perspective are the hydrated CIs and CMs, some of those materials may be much weaker than 2008 EV₅ boulders.

This document is a NASA working document and is subject to further revision. This document has been reviewed for release to the public and is not export controlled.

Table 7: Compressive and Tensile Strength of Chondrites [Kimberley, 2011, Hildebrand, 2006].

Material or Meteorite	Terrestrial Comment or Meteorite Type	Compressive Strength (MPa)	Tensile Strength (MPa)
Concrete (Unreinforced)	Typical Sidewalk	20-40	2-5
Quartz	Single Crystal	1100	55
Granite		100-140	7 – 25
Charcoal Briquette		~5	Not Measured
Medium dirt clod		0.2-0.4	Not Measured
Tagish Lake	C2	0.25-1.2	~0.3
Murchison	CM	~50	Not Measured
Holbrook, AZ	L6	6.2	Not Measured
La Lande, NM	L5	373.4	Not Measured
Tsarev	L5	160-420	16-62
Covert	H5	75.3	Not Measured
Kunashak	L5	265	49
Elenovka	L5	20	2
Krymka	LL3	160	22
Seminole	H4	173	22.5
Plutusk	H5	21.3	31
Tagish Lake	C2	0.25-1.2	~0.3
Murchison	CM	~50	Not Measured

Table 8: Bolide Breakup Data [Popova, 2011].

Meteorite (Type)	Compressive Strength Range of Meteorite Type (MPa)	Initial Mass (Metric Tons) / Diameter (Meters)	Compressive Strength at First Breakup (MPa)	Maximum Compressive Strength (Mpa)
Pribram (H5)	77-247	1.3 / 0.9	0.9	
Lost City (H5)	77-247	0.16 / 0.45	0.7	2.8
Innisfree (L5)	20-450	0.04 / 0.28	0.1	3
Tagish Lake (C2)	0.25-1.2	65 / 4.2	0.3	2.2
Moravka (H5-6)	77-327	1.5 / 0.93	<0.9	5
Neuschwanstein (EL6)	Not observed	0.3 / 0.55	3.6	9.6
Park Forest (L5)	20-450	10 / 1.8	0.03	7
Villalbeto de la Pena (L6)	63-98	0.6 / 0.7		5.1
Bunburra Rockhole (Ach)	Not observed	0.022 / 0.24	0.1	0.9
Almahata Sitta (Ure, OC)	Not observed	70 / 4	0.2-0.3	1

This document is a NASA working document and is subject to further revision. This document has been reviewed for release to the public and is not export controlled.

Jesenice (L6)	63-98	0.17 / 0.45	0.3	3.9
Grimsby (H4-6)	77-327	0.03 / 0.13	0.03	3.6

- **How homogenous are the boulder strength properties within a boulder? What is the potential, and likely, variability throughout the boulder? What is the potential for defects (fracture planes, etc.)? Is there any reason to believe the strength of boulders on an asteroid would vary with latitude or any other spatial parameter or orientation due to thermal cycling or other effects?**

Experience with the meteorites suggests that the density of fractures in asteroidal boulders will be high. However, fractures can be zones of strength as well as weakness. The shock history of meteorites does vary across the meteorite collection, but variation within a single meteorite is small. Data from the major meteorite showers are homogeneous to the first order.

The near surface material on an asteroid will probably be more space-weathered than the interior so it could be weaker and more fractured. The diurnal thermal skin depth is about 3 cm and that will be the major source of erosion from thermal shock. The extent of thermal shock will depend on the insolation distribution. Latitude variation is possible but will probably be much less important than more critical factors such as boulder strength, shock history, and albedo.

- **How can “strong” boulders be distinguished from “weak” ones in situ? What can be determined about the strength from in situ visual and other measurements? What is the uncertainty in these measurements?**

There is no definitive way to compare strengths of boulders using visual inspection alone. However, if only visual data is available, one possible method that merits further examination is to observe the boulder’s angularity. Because of thermal shock and erosion from thermal shock, angularity and visible fractures may be a measure of boulder strength. Stronger boulders may be more angular while weaker boulders become more rounded faster from the erosion driven by thermal shock. To determine the absolute strength of boulders will require some method of direct contact. As the spacecraft approaches the boulder, the following measurements could be possible: 1. From a TBD distance deploy low-speed kinetic impactors, 2. On the surface, deploy a Schmidt Hammer-like device, 3. Once anchoring process starts, use drilling telemetry.

- **What is a set of Earth analog surfaces that could be used to bound the expected range of variability for use in validating the design of the capture system?**

The Center for Lunar and Asteroid Surface Science (CLASS) and Deep Space Industries (DSI) are developing a family of simulants with correct compressive and shear strength. These should be available in quantity for capture system testing by early 2016.

- **Are smaller boulders expected to be stronger than larger ones and if so, by how much?**

All other things being equal, pre-existing fractures would be a function of volume. The relative distribution of large fractures versus small fractures typically follows a power law distribution, so smaller boulders should have a smaller chance to accumulate major fractures on average. However, the expected difference in the 1 - 4 meter range would probably be minimal. That said, the following describes the known data on strength and the factors that go into determining a boulder’s strength.

Bolide Data Explanation: The data in

Table 8 are from observed bolides that have recovered meteorites. The second column shows the compressive strength range of that meteorite type. The third column is the estimate of the pre-encounter initial mass and diameter of the asteroid as it entered the atmosphere. The fourth column is the strength

This document is a NASA working document and is subject to further revision. This document has been reviewed for release to the public and is not export controlled.

at first breakup. This is determined by the dynamic stress produced by the atmosphere at the observed altitude of first breakup and an indication of the overall cohesive strength of the asteroid as a whole. The maximum compressive strength is determined by the altitude of the major breakup event for the bolide. Note that the breakup strengths of the object as a whole are typically much less than the strength of the individual recovered meteorites, which likely indicates the presence of fracture planes or that the asteroid entered the atmosphere as a conglomerate.

Fracturing and Lag Surfaces: Asteroidal material is pervasively fractured because of strong collisional evolution over the age of the solar system. Materials in near-Earth space have experienced cycles of collisional fragmentation to arrive in this orbital space. The potential for defects such as fracture planes will be high. For example, Figure 9 is a back-scattered electron (Z-contrast) image of a polished petrographic thin section of CR2 chondrite LAP 04516. Micro-fractures crosscutting the section are shown. Note that some fractures are free of mineral deposits while veins can contain minerals that are generally terrestrial in origin (e.g., ferrihydrite, an oxyhydroxide seen in LAP 04516) are a consequence of terrestrial weathering in meteorite finds. These observations suggest that micro-fractures and cracks were probably free of mineral deposits while in the parent asteroid potentially resulting in lower strengths than seen in the population of meteorite finds. It should be noted however, that there are terrestrial mechanisms (e.g., freeze-thaw cycles) that could lower the strengths of the meteorite find samples as well.

For small asteroids, the low gravity probably results in the fine fraction of the surface material being depleted by micrometeorites and the solar wind. This will probably result in a pebble or cobble lag that builds up and armors the surface (like desert pavement).



Figure 9: Hand-sample (9cm x 9cm) specimen of CM2 fall Murchison showing numerous fractures. Notice that a fragment of the specimen appear to have been dislodged, possibly along fracture lines [Image Credit: Cari Corrigan, Smithsonian Institution, 2015].

Thermal Erosion: The weathered layer on a Bennu-like asteroid (similar size, orbit, albedo, rotation as 2008 EV₅) should be on the order of 2 - 3 cm. The annual orbital skin depth is approximately 1.5 meters. The annual orbital thermal pulse will affect any loosely bound or frozen volatiles down to about 1.5

This document is a NASA working document and is subject to further revision. This document has been reviewed for release to the public and is not export controlled.

meters, known as the annual thermal skin depth. Over long periods of time a much reduced thermal pulse will penetrate deeper into the body, but the magnitude of this effect will require modeling. The geological interpretation of these data is that outer 2-3 cm will be damaged by micrometeorites, eroded by thermal shock, and any low-temperature volatiles may be cooked-off by the diurnal thermal cycle. As suggested above, angularity of the exposed boulders may be a visual measure of relative strength. Essentially this would be a measure of the boulder's resistance to tensile stress and its extent of past fracturing. The bottom line would be that rounder boulders on a given surface would be weaker. Essentially any sharp edge would become a focus of thermal energy and would be more likely to spall off, rounding the boulder. To first order, the roundness of the boulder (for any given age of a surface) could be a measure of relative strength. Additional research and some experiments are needed to verify and calibrate the response, but this observational technique should work as an in situ measurement to determine relative strength.

Homogeneity: While it is common for small amounts of exotic material to be incorporated into meteorites, the fraction of that material in any meteorite is small. Similarly, compositional variability across boulders on a given asteroid is likely to be small (e.g., Bland et al., 2005). There is not likely to be much variation in the boulder field since a fair degree of homogeneity in composition, shock history, albedo, and thermal properties can be expected.

Suggested Additional Research:

1. As suggested above, angularity of the exposed boulders may be a visual measure of relative strength. Theoretical calculations and thermal experiments should be able to quantify this effect and provide a visual guide to relative strength.
2. Additional compressive and tensile strength measurements of targeted meteorite types.
3. Exploration of add-on mission implementations, especially: surface interaction and remote sensing.

For more information, see Appendix D.

References:

- Macke R. J., Consolmagno G. J. and Britt D. T. (2011) Density, porosity and magnetic susceptibility of carbonaceous chondrites. *Meteoritics & Planetary Science* 46, 1842-1862.
- Kimberley J. and Ramesh K.T. (2011) The dynamic strength of an ordinary chondrite. *Meteoritics & Planetary Science* 46, 1653–1669.
- Hildebrand A.R., McCausland P.J.A., Brown P.G., Longstaffe F.J., Russell S.D.J., Tagliaferri E., Wacker J.F., and Mazur M.J. (2006) The fall and recovery of the Tagish Lake meteorite. *Meteoritics & Planetary Science* 41, 407-431.
- Popova O., Borovicka J., Hartmann W.K., Spurny P., Gnos E., Nemtchinov I., and Trigo-Rodriguez J.M. (2011) Very low strengths of interplanetary meteoroids and small asteroids. *Meteoritics & Planetary Science* 46, 1525–1550.

Post Collection Boulder Handling

Response Lead: Danny Glavin

Sub-team Members: Neyda Abreu, Marc Fries, Joe Nuth, Joel Sercel, Kris Zacny

This document is a NASA working document and is subject to further revision. This document has been reviewed for release to the public and is not export controlled.

How should the boulder be handled after collection to minimize impacts to science and to the structural integrity of the object?

- **What is the suggested allowable contamination of the boulder surface prior to sample acquisition by the crew?**
- **For the tools currently planned for sampling the boulder by the crew, what is the likelihood the boulder will shed material, fracture, or break up, due to the forces applied by these tools?**
- **After collection, the boulder will experience a different thermal environment than it did on the surface of 2008 EV₅. What thermal environment constraints are reasonable for protecting the boulder?**

Assessment:

In order to avoid fragmentation of the boulder after collection, minimizing physical handling of the boulder until it is in a stable, cis-lunar orbit is suggested. However, it is recognized that additional physical contact of the boulder after collection (e.g., drilling, brushing, or scraping the surface of the boulder) could provide valuable engineering data to aid in safe transportation and the design of tools for future robotic or human sampling of the boulder.

The ARM mission team must reach a balance between these constraints. Given that CR, CM, and CI type carbonaceous chondrites, the closest analogs to C-type asteroids, contain high water content (~> 3- 20 wt%) [Kerridge, 1985; Alexander et al., 2013] mostly bound to hydrated minerals and amorphous phases (Garenne et al. 2014; LeGuillou et al. 2015) and are known to be highly friable meteorites, there is a high likelihood that the boulder will locally fragment and shed material due to the forces applied by tools (e.g. anchoring drills) if indeed the ARM target body is similar to CR, CM, and CI chondrites. CK chondrites have much lower water content (<1 wt.% in Karooda) [Kerridge, 1985].

These risks can be mitigated by conducting a full examination of the boulder including surface imaging, and some means to help identify internal cracks such as seismic measurements, could be conducted prior to any drilling or sample coring operations. Tools that exert low cutting forces include an efficient drill cuttings removal system to help contain particulate release during the coring operation can minimize the risk of particle shedding during drilling or other similar activities. The cuttings collected during the anchoring process might also make excellent samples that can be rapidly collected during the first EVA of the ARCM.

Monitoring:

Monitoring the boulder during the anchoring process, such as adding cameras to the ends of the robotic arms is highly beneficial. Imaging the effects of the microspine grippers scraping over the surface or the dispersion of the drilling chips for the anchor could provide considerable insight about the overall integrity of the boulder. Monitoring the performance of the drill anchors may also prove useful. Passive direct monitoring of the boulder during anchoring, return, and in cis-lunar space is highly desirable. Monitoring could include volatile analyses capable of monitoring compositional changes over time as the boulder experiences changes in the thermal environment. Cameras could also be used to inspect the boulder surface to identify any particle shedding or cracking prior to the ARCM.

This document is a NASA working document and is subject to further revision. This document has been reviewed for release to the public and is not export controlled.

For contamination, the OSIRIS-REx contamination control requirements for the returned boulder could be used as a starting point [Dworkin *et al.* 2015]. This would include reducing the levels of organic contamination on hardware surfaces (e.g. < 1000 ng carbon/cm², < 180 ng amino acids/cm² and < 180 ng free hydrazine/cm²) that come into direct contact with the boulder surfaces. In practice, this means cleaning sample handling hardware to 100 A/2 particulate surface cleanliness levels and avoiding recontamination of the hardware surfaces prior to launch. The OSIRIS-REx contamination plan also specifies inorganic contamination limits for other elements (e.g. K, Ni, Sn, Nd, Pb) of interest to science [Dworkin *et al.* 2015]. OSIRIS-REx developed a prohibited materials list mostly driven by the organic contamination requirements and limits on material outgassing rates. This prohibited materials list could be used as a starting point for discussion by engineers and scientists working on ARM. Instead of specifying hard limits on specific volatiles likely to contaminate the surface of the boulder (e.g., water, xenon, NH₃ and other hydrazine thruster products), a best effort approach to reduce volatile contamination of the boulder surface (e.g., keep thrusters pointed away from the boulder surface) would be reasonable. In addition, active volatile monitoring near the boulder surface and spacecraft and passive witness control materials would help document the contamination environment around the boulder surface. Witness materials that can trap volatiles such as water, ammonia, xenon and organics could also be considered.

Modeling:

Thermal models of the selected boulder on the asteroid surface and the spacecraft+boulder combination should be developed for phases of the mission ranging from the parent asteroid all the way to cis-lunar space. If possible and straightforward to do, creating a shape model of the boulder in addition to the thermal models is also suggested. Limiting the thermal shock (e.g., cooling/heating rate) of the boulder during transit to cis-lunar orbit to be no greater than the thermal cycling it experienced on the surface of the asteroid prior to capture will minimize the likelihood of any fracturing or other structural changes. Measuring mass loss of the boulder during the transit is suggested. This might be possible using an Inertial Measurement Unit (IMU) to monitor changes in the angular velocity and linear acceleration of the spacecraft-boulder system. The mass loss, coupled with the shape model taken on-route and at cis-lunar orbit could help quantify physical changes to the boulder. Contamination modeling is also needed of the spacecraft thruster exhaust products, and spacecraft outgassing to include molecular mass transport analysis. An important potential application of this modeling activity will be to inform the advisability of adding a thin film or sheet metal shield to the CRS to potentially mitigate the effects of differential solar exposure and contamination of the boulder from spacecraft effluents. The potential benefit of such a shield and determination of its design cannot be evaluated without a reasonable effort in the area of contamination and thermal modeling.

References:

Alexander, C. M. O'D. *et al.* (2013) The classification of CM and CR chondrites using bulk H, C and N abundances and isotopic compositions. *Geochim. Cosmochim. Acta* 123: 244-260.

Dworkin, J. P. *et al.* (2015) OSIRIS-REx is a pathfinder for contamination control for cost controlled missions in the 21st century. 46th Lunar and Planetary Science Conference, The Woodlands, TX. Abstract #1147 (CD-ROM).

Garenne, A. *et al.* (2014) The abundance and stability of "water" in type 1 and 2 carbonaceous chondrites (CI, CM, and CR). *Geochim. Cosmochim. Acta* 137: 93-112.

This document is a NASA working document and is subject to further revision. This document has been reviewed for release to the public and is not export controlled.

Kerridge, J. F. (1985) Carbon, hydrogen and nitrogen in carbonaceous chondrites: Abundances and isotopic compositions in bulk samples. *Geochimica et Cosmochimica Acta* 49, 1707-1714.

Le Guillou C. et al. (2015) Widespread oxidized and hydrated amorphous silicates in CR chondrites matrices: Implications for alteration conditions and H₂ degassing of asteroids. *Earth and Planetary Science Letters* 420: 162-173.

Pre-ARCM Boulder Assessments for Crew Safety

Response Lead: Jim Bell

Sub-team Members: Marc Fries, Danny Glavin, Christine Hartzell, Amanda Hendrix, Joe Nuth, Joel Sercel, Kris Zacny

Besides the existing capabilities of the ARV (i.e., cameras and CRS feedback loads), are there other ways to assess the condition of the boulder prior to crew access to determine if it's safe to approach and sample?

- **What post-capture (or post-LDRO insertion) measurements should be made prior to crew interaction to ensure crew safety?**

A variety of high-heritage and/or flight-proven measurements and techniques were identified that could be employed during cruise or after LDRO insertion and prior to crew interaction to ensure crew safety (Table 9). They have been prioritized in the first column as (A) most critical to astronaut safety; (B) relevant to astronaut safety and/or science/knowledge but not as critical; and (C) primarily relevant to science/knowledge.

- **What measurements prior to crew interaction would enhance scientific or other knowledge gain?**

All measurements that provide information relevant to crew safety could also provide important new information for science or other knowledge gain (e.g., ISRU potential, planetary defense implications). In addition, a small number of additional measurements, also listed in Table 9, would likely be most relevant only for science or other knowledge gain.

This document is a NASA working document and is subject to further revision. This document has been reviewed for release to the public and is not export controlled.

Table 9: Post-LDRO Measurements of the Boulder and/or Landing Pad Regolith Samples to Ensure Crew Safety and/or to Enhance Scientific or other Knowledge Gain.

Priority	Measurement	Possible Methods	Safety	Science/ Knowledge
A	Assess fragility, hardness, sharpness, and volatile release potential of samples	<ul style="list-style-type: none"> • Movies or time-lapse imaging of the samples while poking, pressing, drilling, brushing, scraping, hammering, and/or grinding • Use simulators of end effector tools that will actually be used later by astronauts 	✓	✓
A	Assess presence of fractures or textures that might suggest spallation or breakage	<ul style="list-style-type: none"> • Acquire stereo images of the boulder and regolith samples to construct 3-D models of their surfaces prior to any tool interactions 	✓	✓
B	Assess any physical movement or dramatic temperature changes of the samples during the transit to the Moon	<ul style="list-style-type: none"> • Use CRS feedback loads (as planned) • Thermal measurements of the samples • Acoustic sensors to assess stability/motion 	✓	✓
B	Characterize and determine abundance of any dust, volatiles, and/or organics in the samples	<ul style="list-style-type: none"> • Ion Neutral Mass Spectroscopy covering masses relevant to potential volatiles, PAHs, or other potential carcinogens • High-res imaging survey (possibly including UV imaging) to assess dust environment • Potentially active-source (e.g., laser) analysis of chemistry of released gases and/or dust/fragments 	✓	✓
B	Characterize the chemistry and mineralogy of the samples prior to astronauts, to make eventual EVAs most efficient	<ul style="list-style-type: none"> • UV, Visible, Near-IR, Mid-IR imaging spectroscopy • APXS and/or LIBS for elemental abund. • Neutron and Gamma-ray spectroscopy for volatiles and elemental abundances • Mössbauer spectroscopy for Fe mineralogy • XRD for general mineralogy 	✓	✓
B	Assess swatches of space suit material and other relevant witness samples during the robotic mission to influence ultimate choice of ARCM materials, coatings, etc.	<ul style="list-style-type: none"> • Microscope-scale UV, Visible, Near-IR, Mid-IR imaging and spectroscopy 	✓	✓
C	Assess electrostatic potential of the boulder	<ul style="list-style-type: none"> • Langmuir probe, or volt meter 	✓	✓
C	Use mass determination and volume of the boulder to estimate its density	<ul style="list-style-type: none"> • Mass determination from radio tracking • Volume from imaging-derived shape model 		✓
C	Estimate the ages of the samples	<ul style="list-style-type: none"> • Mass spectrometer for exposure age • Mini radiogenic isotope analyzer for absolute age 		✓

Containment Considerations

Response Lead: Marc Fries

Sub-team Members: Neyda Abreu, Dan Britt, Danny Glavin, Joe Nuth, Joel Sercel

Given the uncertainties in the properties of the boulders, potential for contamination, possible thermal effects, and potential for particulate release that could affect spacecraft or crew safety, should some form of containment of the boulder be considered and, if so, what type of containment and materials should be considered?

Summary

This document is a NASA working document and is subject to further revision. This document has been reviewed for release to the public and is not export controlled.

There is a high likelihood that particulates and possibly fragments will evolve from an unprotected boulder while it is attached to the spacecraft. These particles are likely to be small, have a very low relative velocity to the spacecraft, and are not expected to remain in the vicinity of the boulder due to spacecraft motion and solar radiation pressure. As such, these particles do not present a hazard to crew operations. Thermal effects are a primary factor in contamination and alteration of the boulder, and thus contamination and alteration can be reduced with a containment designed to reduce thermal shock and peak temperature. It would be beneficial to monitor the boulder throughout the period between initial collection by ARRM and sampling operations during ARCM to assess debris generation, contamination, and alteration. It was determined that a hermetically sealed containment mechanism for the boulder is not needed nor suggested. A sunshade-like “containment” should be considered among the possible options, but specific requirements for physical containment of the boulder should be supported with further analyses. Since physical containment of the boulder is not necessarily suggested unless further analyses deem it necessary, a better term for this consideration is the “protection” of the boulder rather than “containment”.

Discussion

Justification for protecting the boulder: Any need for boulder containment will arise from two fundamental needs:

- 1) Protect the spacecraft and crew from material arising from the boulder, and
- 2) Protect the boulder from contamination/alteration arising from contaminants originating on the spacecraft.

Design goals for boulder protection: Any form of physical protection offered to the boulder should be capable of preventing or significantly ameliorating two major effects:

- 1) Thermal effects in the boulder. Thermal shock (i.e., rapid changes in temperature) can drive evolution of particulates and fragments from the boulder. Thermal shock can also drive loss and/or alteration of native volatiles from the boulder. Strong, static thermal gradients on the boulder can drive alteration, migration, and/or loss of native volatiles on the boulder and degrade the native state of the boulder ahead of sample collection.
- 2) Contamination of the boulder arising from the spacecraft and crew. Volatiles released from the spacecraft and crew can contaminate the boulder and complicate analyses of native organic species, obfuscating scientific and ISRU investigations. Loss of volatiles, dehydration of native hydrated phases, mobilization of native volatiles, chemical reaction of native species with contaminant species, and other similar alteration effects can also occur while the boulder is attached to the spacecraft.

Findings

- 1) *There is a high likelihood that particulates and possibly fragments will evolve from an unprotected boulder while it is attached to the spacecraft. Thermal gradients and thermal shock (i.e., rapid heating or cooling) are primary factors in generating fragments, volatiles, and dust from the boulder, thus driving the risk of spacecraft damage from boulder-generated debris.* Studies of meteorites and meteorite analogs show that fractures and impact-derived features are common in surficial asteroidal materials, and it is reasonable to expect that the ARM boulder may spall material due to pre-existing fractures and other mechanical heterogeneities. Also, since the boulder may be composed of

This document is a NASA working document and is subject to further revision. This document has been reviewed for release to the public and is not export controlled.

relatively volatile-rich carbonaceous material, it will be innately susceptible to spallation, dust evolution, and possible ejection of fragments at low velocity via volatile loss. The worst-case scenario includes sufficient disruption of the boulder as to compromise the ARV's capability to restrain the boulder. These particles are likely to be small, have a very low relative velocity to the spacecraft, and are not expected to remain in the vicinity of the boulder due to spacecraft motion and solar radiation pressure. As such, these particles do not present a hazard to crew operations. The risk of disruption during transport may be reduced by "squeezing" it with the landing legs prior to complete retrieval and monitoring for fragmentation. If the boulder cracks, the spacecraft should drop it and go to a secondary target. Containment of the boulder should address engineering needs to protect the spacecraft against these evolved materials and to prevent significant thermal shock to the boulder. In order to protect the ARRM and ARCM spacecraft from boulder debris and volatiles, the boulder should be protected from thermal shock and excessive static heating. A suitable upper limit for imposed thermal shock may be derived from modeling the thermal history of the boulder on the asteroidal surface prior to collection. More information is needed on the thermal environment of the boulder + spacecraft combination; see #6 below.

- 2) *Thermal effects are a primary factor in contamination and alteration of the boulder, and thus contamination and alteration can be reduced with a containment designed to reduce thermal shock and peak temperature.* The spacecraft thermal environment will drive evolution of volatiles from the spacecraft, evolution and alteration of volatiles in the boulder, transport of contaminants from the spacecraft to the boulder, and migration of contaminants on the boulder. Containment strategies should consider thermal effects from this perspective and should reduce or remove extended static heating from the boulder, as well as pronounced "cold sinks" on the boulder. Materials employed on the ARV should feature low-outgassing materials where possible to diminish volatile contaminant sources, and especially in portions of the spacecraft that will experience extended or extreme heating. More information is needed on the thermal environment of the boulder + spacecraft combination; see #6 below.
- 3) *It would be beneficial to monitor the boulder throughout the period between initial collection by ARRM and sampling operations during ARCM to assess debris generation, contamination, and alteration.* Images of the boulder should be collected at intervals during the voyage so that the ARM team can monitor changes in the boulder to include mass loss, volatile migration, and changes in the mechanical stability of the boulder. Appropriate imaging would include techniques suited to observing morphological, chemical, and mechanical changes in the boulder as well as watching for evolution of volatiles. This information may also be useful to assess the mechanical state of the boulder prior to ARCM visits. Witness plates may be employed as a means to maintain "contamination knowledge"; collection of spacecraft contaminants on the boulder, and loss or alteration of volatiles in the boulder.
- 4) *A hermetically sealed containment mechanism for the boulder is not needed nor suggested.* A hermetic seal is not a significant improvement for protecting the boulder and spacecraft but it does impose significant complexity upon the ARV. Pressurization of such a container due to volatile loss would be problematic both for spacecraft operations and crewed access to the boulder, and it would not fully prevent evolution, alteration, and migration of native volatiles in the boulder. Quantification of volatile loss and other alteration effects in the boulder can be addressed without the need to contain all volatile loss, through such means as witness plate employment, collection of core sample(s) to include interior material, collection of samples from several sites, and/or other means. In addition, many potential materials for the construction of a bag around the boulder can also outgas contaminants that would complicate the monitoring of internal outgassing between boulder collection and the first crewed mission.
- 5) *A sunshade-like "containment" should be considered among the possible options.* Protection of the boulder from thermal effects, and protection of the spacecraft from evolved boulder fragments, might

This document is a NASA working document and is subject to further revision. This document has been reviewed for release to the public and is not export controlled.

be accomplished with a sunshade-type arrangement. The guiding design principles should be to maintain the boulder in a near-homogenous thermal environment, and to prevent line-of-sight transfer of boulder fragments to the spacecraft body and solar panels to protect the ARV. Design options to consider include the use of optically translucent or scattering materials and materials with moderate to high emissivity that will minimize the presence of large temporal or spatial temperature gradients. As with other spacecraft components, the “sunshade” materials should present low risk of outgassing and particulate shedding that could contaminate the boulder.

- 6) *Specific requirements for physical containment of the boulder should be supported with further analyses.* The FAST board can provide estimates based on many years of experience, but data sets that are specific to the ARRM mission and spacecraft design are necessary for finalized mission requirements. Thermal modeling of the boulder/spacecraft combination should be performed to quantify the expected range of temperatures and degree of thermal shock the boulder will experience. Modeling should also be performed with sufficient areal fidelity to predict the range of temperatures expected across the surface of the captured boulder, in order to identify areas where volatile loss (hot spots) and volatile accumulation (“cold fingers”) can be expected. These modeling results should be made available to the personnel responsible for the ARCM sampling plan to inform their planning, as well.
- 7) Since physical containment of the boulder is not necessarily suggested unless further analyses deem it necessary, a better term for this consideration is the “protection” of the boulder rather than “containment”. Protection in this case refers to the science and ISRU need to chemically and physically protect the boulder against damage, and the operational need to protect the spacecraft from damage arising from mass loss from the boulder.

Potential Investigations

The following is an initial list of potential investigations that could be performed by ARM (ARRM and ARCM) resulting from brainstorming activities by the FAST. Many of the identified investigations require additional sensors, subsystems, or operations, which are beyond the scope of the current program. These could be performed with additions and modifications as identified in Table 10. This list is not meant to be viewed as final or comprehensive, but it does indicate that there is a broad range of investigations that could be performed that would provide a benefit to the four investigation areas. This list includes only those investigations that could be carried out during the baseline ARM timeline and does not include the potential investigations that could be conducted as a part of end of mission operations. Each potential investigation has been characterized by the applicability to each of the investigation areas, potential mission phases in which the investigations could be performed, likely benefit to ARM, perceived relevance to NASA’s science, ISRU, planetary defense, and exploration goals, how well it utilizes the unique opportunities that ARM provides, and whether or not it is currently included in the baseline mission plans (see <http://www.nasa.gov/asteroidinitiative> for further details.)

Potential Investigation Descriptions

In order to present these potential investigations in this report, the 63 potential investigations have been sorted and grouped based on their likely benefit to ARM and relevance to NASA’s science and exploration goals by the FAST leadership (Mazanek, Abell, and Reeves) incorporating input from the rest

This document is a NASA working document and is subject to further revision. This document has been reviewed for release to the public and is not export controlled.

of the FAST. The investigations are numbered in the order they were proposed by the FAST with no priority or significance implied by the order or numbering. A short description of these investigations is included below with all of the full categorization performed by the FAST included in Table 10. Cost, complexity, and risk were not explicitly assessed for this preliminary list.

The descriptions of these investigations are presented in the following format:

Investigation Name (ID number that corresponds to Table 10): Investigation description

High Benefit to ARM and High Relevance to NASA Goals

Asteroid Surface Interaction (7): Use either an impact or small explosive test to gain asteroid surface property data that would be germane to future robotic and human missions, helping to understand vehicle to surface interaction. This will provide ARM with surface properties (cohesion, strength, etc.) data prior to boulder collection. At a minimum, the baseline includes the CRS pads interacting with the surface and images of this interaction could be captured by the engineering cameras.

Dust/Particulate Mitigation Techniques (8): Demonstrate cleaning and dust/particulate mitigation methods and protocols for suits and EVA systems that will be brought into the crewed volume (electrostatic, physical barriers, plasma interaction, filtration, etc.). These demonstrations could be conducted on both spacecraft and EVA suit materials (swatches) to understand the likelihood that dust will adhere to these surfaces and the effectiveness of the cleaning methods and protocols on these surfaces. This would be a feed forward to other planetary surface activities (i.e. Asteroids, Moon, Mars and Martian Moons). The complexity of this investigation depends on the specific mitigation technique. The benefit to ARM is dependent on whether or not information can be gained from ARRM in time to benefit ARCM.

Sample Thermal Control (14): Demonstrate active and passive thermal control methods for small body materials, both in-situ and after sample collection and stowage (i.e. keeping materials at ambient temperature conditions). It is desired to have a diversity of samples across the boulder as well as the return of the geological context samples following best practice contamination control. It is also desired that all samples be sealed at vacuum and ambient or colder temperatures (-80° C or lower). The benefit to ARM depends on whether or not it is determined that thermal control is needed to prevent thermal cracking of the boulder during return or in LDRO.

Thermal Imaging of Asteroid Surface (23): Thermal imaging of the entire asteroid surface over time in order to determine the thermal properties including thermal inertia and to assist characterizing the Yarkovsky and YORP effects.

Collect Regolith Samples (32): Collect regolith samples from the asteroid surface near the boulder collection in order to provide geological context. The regolith has the potential to provide a more representative sample of the asteroid as whole rather than the specific boulder composition. There are currently undefined (number and design) context sample collection devices on the CRS pads.

Surface Contact Science Package (36): Deploy a surface contact science package to investigate the surface strength and composition as well as magnetic susceptibility which could help inform the final design of EVA tools and operations.

This document is a NASA working document and is subject to further revision. This document has been reviewed for release to the public and is not export controlled.

Collect Samples from Boulder (38): Image and collect samples from the entire boulder surface. Images and samples from the side of the boulder that was in contact with the asteroid are highly desirable. Having the capability to rotate the boulder prior to restraint in order to position that side such that it is easier to image and reach with EVA would be advantageous. Having the ability to image the entire surface would also allow the development of a full shape model and assist in EVA planning to ensure the most valuable samples are collected within the EVA capabilities. The current capability cannot image the underside of the boulder with arm cameras.

Characterize Boulder Geotechnical Properties (40): Characterize the geotechnical properties of the asteroid and boulder to both inform the ISRU investigations as well as the ARCM. These properties include the permeability, tensile strength, shear strength, volatiles, and porosity, particle size, composition, etc. The benefit to ARM would be high if these properties could be identified prior to boulder collection. In the current baseline, the microspines, anchoring drill, and CRS will interact with the boulder and some data may be extracted from those interactions.

High Benefit to ARM and Medium Relevance to NASA Goals

Low Velocity Penetrator (4): Use a low velocity (not hyper-velocity) penetrator and observe regolith interaction in order to validate DEM simulations or verify minimum boulder strength. The penetrator could be controlled or uncontrolled. This could also be used as a deployment mechanism for other investigations. Cost and complexity could vary depending on specific implementation. The efficacy of a high-velocity impactor needs to be studied further.

Mineralogy and Composition (18): Imaging for mineralogy and composition mapping with well-calibrated broadband color filters and multi-wavelength sensors (UV, visual, near-IR, thermal-IR). Being able to refine the boulder density estimate and identifying potentially volatile-rich boulders would be the main benefit to ARM.

Multi-Spectral Imaging of Asteroid (21): Multi-spectral observation of the boulder collection site prior to, and as soon as possible following, boulder collection to observe the physical (e.g. thermal), geotechnical (e.g. cohesion), and compositional properties of the exposed asteroid surface. Repeated multi-spectral imaging of this area to observe any changes is also desired. Depending on the collection site, continued imaging could be performed during Enhanced Gravity Tractor operations. Being able to refine the boulder density estimate and identifying potentially volatile-rich boulders would be the main benefit to ARM.

Global Mapping of Asteroid (22): Global mapping to determine the shape, volume, and mass of the asteroid through imaging and radio science in order to determine bulk density, gravity field, center of mass, center of gravity, and gross internal structure. The use of a gravity gradiometer may improve the quality of these measurements. In the current baseline, a large majority of the asteroid will be imaged for boulder characterization and shape and gravity modeling. Higher fidelity would likely be desired for science investigations.

High-Power Radar (27): Ground penetrating radar and radar tomography to understand boulder and regolith characteristics as well as the imaging the internal structure of the asteroid.

This document is a NASA working document and is subject to further revision. This document has been reviewed for release to the public and is not export controlled.

Global Boulder Imaging (37): Investigation of the surface dust and other surface properties of the boulder through imaging of the entire surface would help interpret remote observations of both ARRM target asteroid as well as other asteroids that have been and will be imaged by other spacecraft. It would be beneficial if there were some method to image the side of the boulder that was in contact with the asteroid as well as a method to remove thin layers of the surface to understand the near sub-surface (e.g. sticky pads, grinder, abrader, etc.). This information would also benefit ARCM for EVA planning. In the current baseline, the boulder will be mapped in as much detail as possible with capability. However, there will likely be portions of the boulder that cannot be imaged based on camera placement and arm length.

LDRO Free-flying Observer (41): Deploy a free-flyer that could observe the entire boulder in LDRO as well as observe ARCM activities from multiple angles. This would benefit knowledge return in multiple areas as well as public engagement.

Asteroid Free-flyer for Observation (45): Deploy a free-flying observation platform that could provide situational awareness, observe boulder collection (for engineering and public relations purposes), observe any follow-on experiments (e.g. impactors), perform long duration orbit determination for the EGT verification, and/or perform long duration observation of the target asteroid to witness any potential evolution of the surface properties.

High Benefit to ARM and Low Relevance to NASA Goals

None identified.

Medium Benefit to ARM and High Relevance to NASA Goals

Optical Communications Demo (1): Demonstrate Deep Space Optical communications in order to raise the Technology Readiness Level (TRL) and reduce risk for future robotic and crewed missions.

Small Body Seismic Network on Asteroid (2): Deploy a seismic network on the asteroid in order to gain knowledge of the internal structure of the asteroid, demonstrate small body deployment methods, and understand energy coupling. This could be enhanced with the use of subsurface (or “down hole”) instrumentation. Complexity depends on deployment method.

Ultrasonic Investigation of Boulder (3): Deploy sensors on the collected boulder to measure the seismic velocity through the boulder and gain knowledge of the internal structure determine how energy is absorbed and how effective energy coupling and anchoring techniques would be. This could be enhanced with the use of subsurface (or down hole) instrumentation. Complexity depends on the deployment method and the benefit to ARM would be increased if knowledge of boulder strength could be gained prior to ARCM.

Anchoring Techniques (9): Demonstrate multiple anchoring techniques and tools for small-body, micro-gravity environments. Anchoring drills on microspine grippers will demonstrate one anchoring method in the current baseline.

This document is a NASA working document and is subject to further revision. This document has been reviewed for release to the public and is not export controlled.

Long-term Orbit Determination (11): Deploy an asset to allow for long-term precise orbit determination of the asteroid following the departure of the primary spacecraft. This asset could be deployed on the surface or a long-duration free-flyer. This would demonstrate the capability for future planetary defense efforts to track potentially hazardous NEOs. For certain targets, this could have a higher benefit for verifying the EGT demonstration. However, there are other methods (i.e., radar observations) by which to verify a deflection of 2008 EV₅.

Contamination Environment Monitoring (20): Contamination environment characterization, specifically any part of the spacecraft that could come in contact with the boulder or any outgassing from the spacecraft itself. This could be performed by exposing coupons (small swatches of material) or witness plates at various key times throughout the mission. Volatile monitoring for exosphere, outgassing, and plume composition to characterize not only the asteroid / boulder outgassing, but also the outgassing from the spacecraft in order to isolate the asteroid signal. Coordination and interaction with the curation team is vitally important to assess the ARRM and ARCM materials that will be used during EVA to obtain, stow, and contain samples.

Boulder Organics and Volatiles Characterization (39): Characterize the composition of the boulder and potential presence of organics and volatiles prior to EVA to help identify potential sampling locations as well as to determine a baseline prior to crew interaction. If volatiles are found, continuing to monitor volatiles through return and crew interaction for changes would also be valuable.

Medium Benefit to ARM and Medium Relevance to NASA Goals

Surface & Subsurface Composition (26): Surface and subsurface elemental composition measurements of both the boulder and asteroid obtained from remote sensing instruments such as x-ray, gamma-ray, or neutron spectrometer.

Medium Benefit to ARM and Low Relevance to NASA Goals

None identified.

Low Benefit to ARM and High Relevance to NASA Goals

Demo of Mining Techniques (5): Demonstrate various mining technique demonstrations, both optical and physical. Include demonstrations of particle segregation by density, size, composition, etc. These demonstrations could span the processing and extraction, of both feedstock and products. In the current baseline, the Capture Module will demonstrate the removal of a boulder from the surface as a potential mining technique.

This document is a NASA working document and is subject to further revision. This document has been reviewed for release to the public and is not export controlled.

Micro-g Mobility Demo (Robotic & Crewed) (6): Demonstrate robotic and/or crewed micro-g mobility techniques, both on the surface and in near-proximity of a small body. The complexity of these demonstrations depends on the specific method(s) being demonstrated. In the current baseline, the CRS will demonstrate landing and hopping, and the microspine technology is also applicable to mobility approaches (i.e., low-gravity crawlers)

ISRU Radiation Protection (15): Characterize the effectiveness of asteroidal materials for radiation reduction/ protection against both Galactic Cosmic Radiation (GCR) and Solar Particle Events (SPE) (e.g. deploying tissue-equivalent dosimeters at varying location and depths on the boulder).

Planetary Protection (“Break the Chain”) (16): Demonstrate methods and procedures for obtaining, collecting, and containing samples under Mars planetary protection protocols. These demonstrations would be focused on sample collection protocols in order to “break the chain”. This would not be a full demonstration of Mars planetary protection requirements. Examples would be testing of seals, monitoring contamination transport, but not include cleanliness requirements.

Tether Demo with Boulder Counterweight (17): Tether the boulder (or piece of boulder) to Orion and spin the system to the use of asteroidal material as a counter weight for artificial gravity systems. Other elements could be tethered to the boulder for demonstration of tether propulsion using asteroidal material as a counterweight. This would occur post ARCM, as an end-of-mission (EOM) use.

High Velocity Asteroid Impactor (29): Conduct a high/hyper-velocity impact experiment, deployed from the ARV, in order to characterize the dust, and regolith environment, impact physics, and subsurface composition. This would require imaging of the plume and/or crater over time. ARV would serve as the imager and be at safe standoff during impact. This would occur following boulder collection.

Radiation Environment Characterization (33): Use tissue-equivalent radiation sensors on the ARV to monitor GCR and SPE dosage throughout the entire mission.

Collect Boulder Core Sample (34): Collect a core sample of at least 4 cm in depth from the boulder. Deeper is better and the extreme of a segmented core all the way through the diameter of the boulder would be useful. It is desired that the core be sealed and held at external ambient temperature or colder. Deeper holes would also allow for the ability to use an instrumented bit and/or other down-hole measurements (e.g. thermal conductivity, temperature, etc.) that would allow the exploration and understanding of the internal structure.

Large Sample Return (48): Robotically return large (>100 kg) samples for large-scale ISRU laboratory demonstrations on Earth. This would be performed by a follow-on mission beyond the baseline ARCM.

Cold Trap Volatile Collection Demo (52): Demonstrate in-space, cold trap water collection with asteroidal volatiles. Use of the generated water for propulsion or other potential uses would help advance the TRL of these systems.

ISRU Product Characterization (62): Return all ISRU products for characterization on Earth in a laboratory.

This document is a NASA working document and is subject to further revision. This document has been reviewed for release to the public and is not export controlled.

Low Benefit to ARM and Medium Relevance to NASA Goals

Small Body GPS (10): Demonstrate a GPS like-system for a small body, allowing position and orientation reference for surface and orbital assets.

Remote Stand-off Interaction Demo (12): Demonstrate the capability for remote stand-off active interaction with the surface of a low gravity body (e.g. Laser-induced Breakdown Spectroscopy (LIBS), concentrated sun-light, arc-lamps, lasers, etc.).

Future Planned Instrument Demo (13): Demonstration of a planned deep space or planetary instrument in order to increase the TRL of these instruments for future space-flight mission. The benefit to ARM and complexity depends on the instrument being demonstrated.

Space Weathering Measurements (19): Space weathering environment measurements including solar wind, radiation, and micro-meteoroid impact monitoring.

Plasma Environment Characterization (24): Characterize the plasma environment, including potential and electric fields (Langmuir probe) near the surface of both the asteroid and boulder in order to understand the plasma and exosphere environment which is related to dust and small particle levitation. Complexity is increased due to the addition of activities to the surface operations for asteroid measurements.

Magnetic Environment Characterization (25): Characterize the magnetic environment of the asteroid and boulder surface to understand plasma / solar wind interaction and the remnant magnetization of the asteroid. Measurements of the Ion Propulsion System should also be taken in order to isolate the spacecraft signal from the asteroid.

Deploy Science Package (28): Deploy in-situ science packages. These could be active or passive, static or mobile. Instrumentation could include APXS, microscope, FTIR, etc.

Occultation Exosphere Observations (30): Use solar or stellar occultations to examine exosphere and dust environment.

Dust Mobility Characterization (32): Use of a dust detector on the landing pads in order to understand dust mobility due to ARV initial interaction as well as active sensor/detector on the ARV to measure dust properties and concentrations around the asteroid. This could potentially be performed at a low level with the engineering cameras.

Characterize Boulder Porosity (35): Characterize the micro- and macro-porosity of the boulder. The micro-porosity characterization would require high resolution imaging at the boulder and likely be a first order characterization while better characterization will be through examination of returned samples. Macro-porosity will be determined through mass properties determination and acoustic sounding. The benefit to ARM is low as the macro-porosity is unlikely to be determined until after collection.

Rubble Aggregation Experiment (42): Full scale rubble pile accretion and aggregation experiment and observation using asteroidal material in LDRO.

This document is a NASA working document and is subject to further revision. This document has been reviewed for release to the public and is not export controlled.

Observe Kinetic Impact on Asteroid (43): There is a potential to use the ARV as an observer of a kinetic impact experiment following the boulder collection and primary planetary defense demonstration (EGT). Additional observation platforms or instruments could be deployed during close proximity operations and/or boulder collection that could provide additional information during and after impact.

Deploy Explosive Penetrator on Asteroid (44): Deploy an explosive charge and/or an explosive penetrator that could be observed with the ARV or other deployed observing platform. The desired objective would be to observe both the ejecta and crater over a period of time.

Additional Planetary Defense Demo(s) (46): Demonstrate additional planetary defense techniques such as laser or solar ablation, altering the albedo, volatile plume generation for thrust, ion beam deflection, etc. These could be small scale experiments that would demonstrate the feasibility of the technique without altering the asteroid's trajectory such that it would interfere with the verification of the EGT deflection.

Plume Generation and Observation (47): Demonstrate volatile plume generation through the use of concentrated energy (e.g. laser, solar, arc lamp, etc.) interacting with the asteroid or boulder surface.

Ablation and/or Spalling Test (49): Conduct an ablation or thermal spalling test through the use of concentrated energy (e.g. laser, solar, arc lamp, etc.) and characterize any generated volatiles.

In-Space Printing with Asteroid Materials (50): Manipulate asteroid and/or boulder material to generate small scale structures. Demonstrate in-space printing using asteroid material. It would be desired for these materials to be brought back to Earth for analysis.

Asteroid Material Manipulation Demo (51): Conduct size distribution, particle separation, and material manipulation experiments using boulder or asteroidal material.

Instrumented Drill on Asteroid and/or Boulder (53): Use an instrumented drill to measure volatiles and how the volatiles vary with depth. This could be conducted either at the asteroid or on the boulder.

Boulder Composition Characterization (54): Through a range of sensing techniques (e.g. gamma ray spectrometer, neutron detector, etc.), characterize the elemental makeup and specifically hydrogen content in the boulder and asteroid. Benefit would be increased if this could be performed prior to collection.

Deliver Samples to ISS (55): Deliver boulder samples (either from Earth or directly from LDRO) to the International Space Station (ISS) for continued low-gravity experimentation.

Crack the Boulder to Expose New Surfaces (56): Access the interior of the boulder through cracking or other methods that would expose new surfaces as a means of accessing the potentially more volatile rich interior. Complexity is driven by the desire to maintain restraint on the boulder and eliminate debris creation.

Encapsulate the Boulder for Volatile Collection (57): Encapsulate asteroidal material to help with volatile extraction and collection (e.g. using cryotrap to capture outgassed volatiles).

This document is a NASA working document and is subject to further revision. This document has been reviewed for release to the public and is not export controlled.

Characterize Boulder Permeability (58): Introduce helium, xenon, or other noble gas into the interior the boulder and observe the diffusion through the boulder to measure permeability.

Soil Simulation with Asteroidal Material (59): Experiment with asteroidal material created soil simulants and evaluate their effectiveness. This would be performed either in an Earth laboratory or on ISS.

Microwave Volatile Extraction Test (60): Conduct microwave volatile extraction demonstrations.

Use of Robotic Arms for Strength Tests (61): Use the robotic arms with various end-effectors as a method to measure the shear and tensile strength of the boulder. In the baseline, the microspines and anchor drill will interact with the boulder and provide some data.

Full ISRU Demo (63): Conduct an end-to-end ISRU demonstration that would include rendezvous, material processing, volatile capture, and storage of products. This would likely be a follow-on mission, potentially after release of the boulder.

Low Benefit to ARM and Low Relevance to NASA Goals

None Identified.

Proposed Investigations Categorization Table

Table 10 shows the full FAST characterization of all the identified potential investigations described above. Each investigation was characterized by the FAST and are listed and numbered in the order they were proposed. There is no priority or significance implied by the order. The investigation characterization areas and a key to reading the table are below.

Investigation Area:

- X = Primary
- = Secondary

Investigation Location:

Outbound: From launch to the start of the asteroid proximity operations.

At Asteroid: Includes on the surface as well as during all proximity operations.

Inbound: Transit between asteroid vicinity and insertion into LDRO.

LDRO: All uncrewed activities in the LDRO, either before or after the ARCM.

ARCM: Crewed activities, or activities while Orion is in the vicinity of or docked to the ARV.

Earth: Investigations that will be conducted in laboratories or other locations with samples returned to Earth.

Benefit to ARM:

Low: Likely provides little to no benefit to ARM.

This document is a NASA working document and is subject to further revision. This document has been reviewed for release to the public and is not export controlled.

Mid: Will likely provide some enhancement to ARM but will not impact objectives or reduce mission risk.

High: Will likely provide a major enhancement to ARM that directly impacts objectives or reduces mission risk.

Relevance to NASA Goals:

Low: Does not likely directly align with any identified future NASA science or exploration Goals.

Med: Likely aligns with one science or exploration goal.

High: Likely aligns with multiple science and exploration goals.

Utilizes ARM:

Yes: The investigation makes use of the unique opportunities ARM provides (e.g., high-power SEP, asteroid interaction, boulder collection, etc.).

No: The investigation could be performed on another flight mission.

Included in the Baseline:

No: This investigation is not addressed with the baseline design and/or operations.

Low: This investigation is addressed with the baseline design and/or operations at a low level.

Mid: This investigation is addressed with the baseline design and/or operations at a significant level.

High: This investigation is fully addressed with the baseline design and/or operations.

Table 10: Proposed investigation characterization

#	Investigation	Investigation Area				Investigation Location						Benefit to		Utilizes ARM	Incl. in Baseline	
		Science	PD	ISRU	C & T	Outbound	At Asteroid	Inbound	LDRO	ARCM	Earth	ARM	NASA Goals			
1	Optical Communications Demo				X	X	X	X	X				Mid	High	No	No
2	Small Body Seismic Network on Asteroid	X	X	X	X		X						Mid	High	Yes	No
3	Ultrasonic Investigation of Boulder	X	X	X	X				X	X			Mid	High	Yes	No
4	Low Velocity Penetrator	X			X		X						High	Mid	Yes	No
5	Demo of Mining Techniques			X			X	X	X				Low	High	Yes	Low
6	Micro-g Mobility Demo (Robotic & Crewed)				X		X		X	X			Low	High	Yes	Low
7	Asteroid Surface Interaction	X			X		X						High	High	Yes	Low
8	Dust/Particulate Mitigation Techniques				X		X	X	X				High	High	Yes	Low
9	Anchoring Techniques				X		X		X	X			Mid	High	Yes	Mid
10	Small Body GPS				X		X						Low	Mid	Yes	No
11	Long-term Orbit Determination	X	X		X		X						Mid	High	Yes	No
12	Remote Stand-off Interaction Demo				X		X	X	X	X			Low	Mid	Yes	No
13	Future Planned Instrument Demo				X	X	X	X	X	X			Low	Mid	?	No
14	Sample Thermal Control				X		X	X	X	X	X		High	High	Yes	?
15	ISRU Radiation Protection	X			X		X	X	X	X			Low	High	Yes	No
16	Planetary Protection ("Break the Chain")				X		X		X	X			Low	High	Yes	No
17	Tether Demo with Boulder Counterweight				X				X				Low	High	Yes	No
18	Mineralogy and Composition	X			X		X		X	X			High	Mid	Yes	No
19	Space Weathering Measurements	X					X	X	X				Low	Mid	No	No
20	Contamination Environment Monitoring	X				X		X	X				Mid	High	Yes	No
21	Multi-Spectral Imaging of Asteroid	X							X				High	Mid	Yes	No

Table 10: Proposed investigation characterization (cont.)

#	Investigation	Investigation Area				Investigation Location				Benefit to		Relevance to NASA Goals	Utilizes ARM	Incl. in Baseline	
		Science	PD	ISRU	C & T	Outbound	At Asteroid	Inbound	LDRO	ARCM	Earth				ARM
22	Global Mapping of Asteroid	X	•	•			X					High	Mid	Yes	Mid
23	Thermal Imaging of Asteroid Surface	X	•				X					High	High	Yes	No
24	Plasma Environment Characterization	X					X		X			Low	Mid	Yes	No
25	Magnetic Environment Characterization	X		•			X		X			Low	Mid	Yes	No
26	Surface & Subsurface Composition	X		•			X	X	X	X		Mid	Mid	Yes	No
27	High-Power Radar	X	•	•			X		X			High	Mid	Yes	No
28	Deploy Science Package	X		•			X			X		Low	Mid	Yes	No
29	High Velocity Asteroid Impactor	X	X	X			X					Low	High	Yes	No
30	Occultation Exosphere Observations	X					X					Low	Mid	Yes	No
31	Dust Mobility Characterization	X					X		X			Low	Mid	Yes	Low
32	Collect Regolith Samples	X					X					High	High	Yes	High
33	Radiation Environment Characterization	X			X	X	X	X				Low	High	Yes	No
34	Collect Boulder Core Sample	X		•			X		X	X		Low	High	Yes	No
35	Characterize Boulder Porosity	X	•	•			X		X		X	Low	Mid	Yes	No
36	Surface Contact Science Package	X		•	•		X	X	X	X		High	High	Yes	No
37	Global Boulder Imaging	X		•			X	X	X			High	Mid	Yes	Mid
38	Collect Samples from Boulder	X	•	X			X		X	X		High	High	Yes	Mid
39	Boulder Organics and Volatiles Characterization	X		X			X		X			Mid	High	Yes	No
40	Characterize Boulder Geotechnical Properties	X		X	•	•	X		X	X		High	High	Yes	Low
41	LDRO Free-flying Observer	X			•				X	X		High	Mid	Yes	No
42	Rubble Aggregation Experiment	X	•						X			Low	Mid	Yes	No

Table 10: Proposed investigation characterization (cont.)

#	Investigation	Investigation Area				Investigation Location				Benefit to ARM	Relevance to NASA Goals	Utilizes ARM	Incl. in Baseline			
		Science	PD	ISRU	C & T	Outbound	At Asteroid	Inbound	LDRO					ARCM	Earth	
43	Observe Kinetic Impact on Asteroid	●	X						X				Low	Mid	Yes	No
44	Deploy Explosive Penetrator on Asteroid	X	X	X					X				Low	Mid	Yes	No
45	Asteroid Free-flyer for Observation	●	X						X				High	Mid	Yes	No
46	Additional Planetary Defense Demo(s)		X						X				Low	Mid	Yes	No
47	Plume Generation and Observation	X	X	X						X			Low	Mid	Yes	No
48	Large Sample Return	●	●	X	●					X	X		Low	High	Yes	No
49	Ablation and/or Spalling Test	●		X	●					X	X		Low	Mid	Yes	No
50	In-Space Printing with Asteroidal Material			X	●					X	X		Low	Mid	Yes	No
51	Asteroidal Material Manipulation Demo			X	●					X	X		Low	Mid	Yes	No
52	Cold Trap Volatile Collection Demo	●		X						X	X		Low	High	Yes	No
53	Instrumented Drill on Asteroid and/or Boulder	●	●	X	●					X	X		Low	Mid	Yes	No
54	Boulder Composition Characterization	X		X						X	X		Low	Mid	Yes	No
55	Deliver Samples to ISS	X	●	X						X	X		Low	Mid	Yes	No
56	Crack the Boulder to Expose New Surfaces	●	●	X						X	X		Low	Mid	Yes	No
57	Encapsulate the Boulder for Volatile Collection			X						X	X		Low	Mid	Yes	No
58	Characterize Boulder Permeability	●		X						X	X		Low	Mid	Yes	No
59	Soil Simulation with Asteroidal Material	●		X	X					X			Low	Mid	Yes	No
60	Microwave Volatile Extraction Test	●		X	●					X	X		Low	Mid	Yes	No
61	Use of Robotic Arms for Strength Tests	●		X	●					X	X		Low	Mid	Yes	Low
62	ISRU Product Characterization	●		X							X		Low	High	Yes	No
63	Full ISRU Demo	●		X	●					X			Low	Mid	Yes	No

This document is a NASA working document and is subject to further revision. This document has been reviewed for release to the public and is not export controlled.

Summary of Public Inputs

Below is a summary of the public inputs received to date by the FAST. All public inputs directly relevant to ARM, including any additional comments received in response to the posting of this draft version, will be summarized in the final version of the report and will be posted in their entirety on the FAST website: <http://www.nasa.gov/feature/arm-fast>. All public inputs directly relevant to ARM will be posted in their entirety on the FAST website (<http://www.nasa.gov/feature/arm-fast>) (Please note: any additional comments received in response to the posting of this draft version will also be incorporated into the final version of the report).

Input from Marshall Eubanks (Asteroid Initiatives, Inc.)

YORP Torque and Rotation State: A science goal for the ARRM should be to describe the YORP torque and rotation state of the target as accurately as possible during the initial “stand-off” phase of the mission (before the spacecraft itself can perturb the satellite’s albedo rotation). This should include:

- Characterizing the regions important to YORP and Yarkovsky radiation pressure forces.
- Determine the axial rotation and compare to previous ground-based or other observations of the same target asteroid.
- Observe and characterize any polar motion (Eulerian wobble period) of the target asteroid.
- These observations should be made both before and after boulder collection to determine if the interaction has any impact on rotation (unlikely to be large enough to detect) or albedo (more likely and could impact YORP and Yarkovsky).

Cause of Surface Restructuring: The physics of asteroid surface restructuring is unclear, and ARM may be able to provide important constraints on this process. Accurately characterizing the shape will provide information about any past mass motions and imaging the collection site both before and after the boulder collection will help identify any mass flow caused by the collection operations.

Granular Physics and Cohesion: The ARRM mission should offer numerous opportunities to investigate the source of cohesion, both during the boulder capture process and possibly during sampling or other surface operations. Among the most important regions for an in situ surface properties experiment would be any smooth “seas” or “ponds” of smooth fine material. Observations of surface restructuring during the boulder collection process itself should provide information on the cohesion between the boulder and the surrounding regolith. It is also important to observe the behavior of material shaken loose or dropped during the boulder acquisition process, and other surface motions caused by surface operations. The ARRM should also map the surface slopes and local acceleration (gravitational plus rotational) for the complete surface of the target asteroid. In addition landing pico-spacecraft with accelerometers could provide ground truth for this effort.

Contextual Sampling of the Target Asteroid: I think it is important to collect samples from the “smooth” surfaces, such as those present on Itokawa and Eros, should such surfaces be present on the ARRM target. This material is extremely unlikely to be present on a meteorite sample and would thus likely be a previously unobserved material type. It would also be beneficial to collect a core sample from these “smooth” areas in order to determine the circulation and size-sorting of the fine granular material, and also constrain the motion of this material over time and past resurfacing events.

This document is a NASA working document and is subject to further revision. This document has been reviewed for release to the public and is not export controlled.

Electrostatic Levitation: Levitated dust is thought to be important in removing very fine material from strong asteroids; the AARM mission could test this hypothesis and provide valuable observations for improved modeling of this phenomenon. At the beginning of the mission, the spacecraft could attempt to observe levitated dust through forward or reversed scattering of light. A levitated dust sample return would provide the first samples of such material from any solar system object.

Comparison with Ground Based Observations: As with any asteroid mission, an important scientific goal will be the comparison of in situ results with previous ground-based observations.

Planetary Defense Data: The description of the proportions and distribution of fine and coarse material, and of the nature of the cohesion between the various components making up the asteroid, will be very important if it is ever necessary to resort to kinetic impacts or nuclear explosions to deflect a hazardous asteroid.

Geodetic Control During EGT: During the AARM “gravity tractor” planetary defense test, it will be important to have a very tight geodetic control over the target asteroid, and the ARV itself. The ARV will not itself be a drag free platform, and it will thus be necessary to combine radiometric observations of the ARV from Earth, and LIDAR observations of the target asteroid from the ARV, to determine the asteroid’s velocity change from the gravity tractor. The use of phase-connected Very Long Baseline Interferometry (VLBI) of the ARV during the gravity tractor phase of the mission could improve the transverse accuracy of the spacecraft orbit determination.

Laser Retroreflectors: Laser retroreflectors for use over a few km distance can be very small (~ 1 mm) and lightweight and provide fiducial points which have proven to be very important in terrestrial geodesy. If boulder capture or other surface operations result in significant surface motions, it should be possible to track the actual flows, and not just surface shape changes, through LIDAR to the fiducial points.

Presence of Water: Attention should be paid to the availability of water in and around the target asteroid. The AARM should attempt to characterize the amount of water being released from the target asteroid. The AARM should attempt to immediately collect a sample from directly underneath the collected boulder, where regolith may have been hidden from the Sun for a considerable time, and thus might serve as a trap for water and other volatiles outgassed from the interior of the body. The acquisition of a core sample would also be of great interest to Asteroid Water Mining, and for mining in general.

Deep Space Atomic Clock (DSAC): The DSAC would provide adequate frequency stability to allow for one-way Doppler and Range tracking which (with differential VLBI) would substantially reduce the need for DSN tracking time during the gravity tractor phase of the mission.

Small Spacecraft: The deployment of small nano- or pico-spacecraft as engineering demonstrations which can also provide useful scientific information. They could be used on the AARM target to monitor surface changes during the boulder extraction process, and demonstrate the utility of this new technology.

Bi-Static Radar Reflections: Bi-static radar reflections using the very strong decametric emissions from electrons flowing in the Io-flux tube could be used to examine the interiors of asteroids with a single receive antenna.

This document is a NASA working document and is subject to further revision. This document has been reviewed for release to the public and is not export controlled.

Additional Findings

Beyond the specific questions from the ARM project, the FAST, in combination with public input, developed a list of observations and assessments that would provide value to ARM. Below is a list of these findings. No prioritization is implied by the ordering of these findings.

- **Unique Knowledge Gain from ARM:** ARM provides a unique opportunity that can provide a wide range of valuable knowledge gain beyond other asteroid missions or what is available in the current meteorite collection. For example:
 - Investigating pristine sub-surface material, preserved with stratigraphic context (boulder core sample) that have not been significantly altered by the space weathering and ionizing radiation environment (e.g., how organics, hydration, volatile content, etc. varies with depth).
 - Return of a multi-ton boulder, along with regolith samples for context that would provide value information about the surface of asteroids and allow for measurements and investigations that requiring large mass/samples.
 - Returning multiple kg's of sample to Earth will allow for sensitive laboratory measurements and experiments that aren't possible with the limited meteorite collection.
 - Creating an "orbital laboratory" that can be used to demonstrate asteroidal ISRU and other technologies and instruments in an operational environment.
 - Opportunity to correlate observed spectrum to the sampled asteroid surface (ground truth), asteroid interior (through boulder investigations), as well as known meteorite classes.
- **NASA Goal Traceability:** Although the FAST did not specifically address traceability to the current planetary decal survey and other NASA exploration roadmaps, there are many NASA goals that could be addressed using the results and opportunities provided by this mission.
- **Pre-launch 2008 EV₅ Characterization:** All existing data should be analyzed to provide physical characterization of the 2008 EV₅ to understand mission risks. This includes the ESA MarcoPolo-R team investigations (e.g., observations and modeling) and telescopic data sets. Opportunities for acquiring new data sets should also be investigated (e.g., Spitzer).
- **Meteorite Analog Work:** More wide-ranging laboratory studies of appropriate candidate meteorites is warranted (e.g., spectral, strength, density, etc.). Investigating the effects of grain size, packing density, and powders-on-slabs would provide stronger insights into the possible physical and chemical composition of 2008 EV₅.
- **Characterization Precursor:** A precursor to the ARRM target body in order scout for boulders and provide surface and boulder physical characteristics would effectively increase the characterization phase duration and should be further investigated. This precursor could be a dedicated mission or be co-manifested with the ARV, arriving at the target earlier. Additional benefits would be gained if the precursor had some means of interacting with the surface to provide geotechnical data.
- **Characterization Phase:** Characterization of the target asteroid, candidate boulders, and associated collection areas are critically important. Increasing, to the greatest extent possible, the time allocated for characterization will maximize the knowledge return from the ARRM and probability of mission success.

This document is a NASA working document and is subject to further revision. This document has been reviewed for release to the public and is not export controlled.

- **Geotechnical Property Estimation:** A mechanical interaction with regolith representative of the boulder collection area is the only way to provide an accurate estimate of the geotechnical properties (e.g., cohesion, friction angle, porosity, etc.) that are critical for boulder collection. Before and after images of the interaction area at sub-cm/pixel would provide context to inform cohesion mapping around target boulders.
- **Boulder and Regolith Characterization:** On a best-effort basis, sufficient camera resolution is required to characterize:
 - the morphological relationship of the boulder to the surrounding terrain. Sub-cm/pixel resolution of a representative area of boulder/regolith interface with more of the image devoted to the regolith than the boulder.
 - the physical integrity of the boulder (e.g. cracks, fissures, etc.). Sub-cm/pixel resolution over as much of the boulder surface as possible is desired.
- **Thermal Imaging:** The thermal inertia of boulders, and the entire asteroid surface, is indicative of their near-surface characteristics (e.g., porous vs. solid), and can be measured relatively easily with a thermal detector. Ideally this detector would have two or more wavelengths (e.g., 5 and 10 microns) and a spatial resolution greater than several pixels per boulder (a minimum of about 0.5 meters per pixel). Over an asteroid's rotation period these observations can distinguish between the thermal inertia of low density, porous aggregates and higher density, potentially stronger, monolithic material, which would aid in boulder and site selection and in determining the homogeneity of boulder and surface properties.
- **Previously Visited Target:** While selecting a target that has not been visited before (i.e. not Bennu or Ryugu) is compelling, there is value in returning to a previously visited asteroid and there would be interest in returning a boulder to cis-lunar space for subsequent study and sampling. (See SBAG ARM Special Action Team Full Report http://www.lpi.usra.edu/sbag/documents/SBAG_ARM_SAT_Full_Report.pdf).

Closing Remarks

This report has been developed over a two-month period to provide input during the requirements definition phase of the ARRM, which includes spacecraft interfaces, requirements, and design considerations as they relate to the ARCM. The inputs represent the FAST's best effort in the time available to assist with the formulation and design of the ARRM mission, spacecraft, and capture system. The FAST has also provided inputs relevant to the ARM in general. These inputs are not intended to represent an exhaustive effort to cover all possibilities, but provide an initial effort based on the FAST members areas of experience and expertise. All timely public inputs directly relevant to ARM have been summarized in the "Summary of Public Inputs" section of this report and will be posted in their entirety on the FAST website (<http://www.nasa.gov/feature/arm-fast>).

The ARM FAST will be formally retired following the ARRM Requirements Closure TIM, and prior to the Announcement of Opportunity for participation in any follow-on ARM-related activities. Following the completion of the FAST duties, NASA plans to fund an ARM Investigation Team (IT) which is currently planned to be formed in mid-2016 with a call for membership expected in early 2016. The multidisciplinary IT will assist with the definition and support of investigations in the same four main areas as the FAST. The

This document is a NASA working document and is subject to further revision. This document has been reviewed for release to the public and is not export controlled.

IT will support ARM program-level and project-level functions, provide technical expertise, and support NASA Headquarters interactions with the technical communities. The IT will support ARM through mission formulation, mission design and vehicle development, and mission implementation, which includes the operational phases of both the ARRM and the ARCM.

Appendices

Appendix A1: Full Response on the Origin of 2008 EV₅

Some additional background details on the response to the question on the orbital history of 2008 EV₅ are provided here, specifically on the dynamical/physical evolution of (341843) 2008 EV₅ and possible links to other main belt families.

(341843) 2008 EV₅, hereafter EV₅, is a candidate target for NASA's Asteroid Redirect Robotic Mission (ARRM). It is not only in a highly accessible Earth-like orbit, but it also appears to have characteristics similar to some type of carbonaceous chondrite meteorite. This potentially makes it highly useful to study in detail from an in situ resource utilization perspective. In order to maximize the science return from this mission, it is important to identify where EV₅ came from and what happened to it along the way to its current orbit. This is a difficult task, with the limited and, in some cases uncertain, information on EV₅. Nevertheless, using what is known of both EV₅ and the asteroid belt from remote observations and collisional/dynamical modeling work, it is possible to winnow down the possibilities.

Taking advantage of what has been learned about asteroid evolution over the past several decades, a reasonable scenario describing how EV₅ reached its current orbit can be constructed. EV₅ likely started its existence as part of a much larger body. Given the existing knowledge of planetesimal formation mechanisms, EV₅'s parent body probably had a diameter greater than 100 km (Morbidelli et al. 2009). The formation location of this body could have been the main asteroid belt, but it may also have been another region altogether (e.g., the terrestrial planet region; the giant planet region or beyond; Bottke et al. 2006b; Levison et al. 2009; Walsh et al. 2011). In the latter scenarios, dynamical processes implanted EV₅'s parent body in the main belt within the first few hundreds of Myr of solar system history.

Once formed, EV₅'s parent body would have experienced early thermal evolution by the decay of radiogenic nuclides (e.g., McSween et al. 2002), while its surface would have been battered by impacts for billions of years of cratering events (e.g., Bottke et al. 2005a,b). The location of what is now EV₅ within this parent body is unknown; if it was deep in the interior, it may have been substantially metamorphosed and potentially desiccated. If it formed near the exterior, it may still be primitive enough to have retained substantial volatiles in the form of hydrated phyllosilicates.

EV₅'s immediate history likely starts when its parent body experienced a large cratering event or, more likely, a catastrophic disruption event. This collision would have created enormous numbers of fragments near the impact site, some of which were roughly EV₅-sized. Here, the clustered semimajor axes a , eccentricities e , and inclinations i of these fragments are referred to as an "asteroid family". EV₅'s maximum potential age is therefore the same as that of the family-forming event, and dynamical methods exist that can potentially determine the latter (e.g., Bottke et al. 2006; Nesvorný et al. 2015).

From here, the newly liberated EV₅, or perhaps a somewhat larger precursor, began to undergo dynamical evolution via the non-gravitational forces referred to as the Yarkovsky and Yarkovsky-O'Keefe-

This document is a NASA working document and is subject to further revision. This document has been reviewed for release to the public and is not export controlled.

Radzievskii-Paddack (YORP) effect (e.g., Vokrouhlicky and Bottke 2012). The Yarkovsky effect describes a small force that affects the orbital motion of $D < 40$ km bodies. It is caused by sunlight; when these bodies heat up in the Sun, they eventually re-radiate the energy away as heat, which in turn creates a tiny thrust. This recoil acceleration is much weaker than solar and planetary gravitational forces, but it can produce substantial secular semimajor axis changes over timescales ranging from many millions to billions of years. The same physical phenomenon also creates a thermal torque that, complemented by a torque produced by scattered sunlight, can modify the rotation rates and obliquities of small bodies as well. The YORP effect likely modified EV₅'s obliquity (or that of its immediate precursor) to a value approaching 180°. This allowed EV₅ (or its immediate precursor) to drift inward by the Yarkovsky effect far enough to reach a dynamical resonance capable of pushing it out of the main belt and onto a terrestrial planet-crossing orbit.

The transit time for EV₅ to reach a main belt “escape hatch” is probably on the order of tens of Myr to a billion years, so this phase likely makes up most of its lifetime. From there, powerful resonances typically drive asteroids onto planet-crossing orbits over less than 1 Myr. Once on planet-crossing orbits, their lifetime is likely to be a few Myr to many tens of Myr. The most common fate for NEAs is to hit the Sun or be thrown out of the inner solar system via an encounter with Jupiter (e.g. Gladman et al. 1997; Bottke et al. 2002). Only a tiny fraction of all asteroids escaping the main belt strike a planet (i.e., roughly 0.3% across all resonances, though ~1% hit from escape routes in the innermost main belt region). If EV₅ or its precursor had a high enough eccentricity within the main belt, and the right initial orbit, it could have also escaped the main belt by drifting directly onto a Mars-crossing orbit via the Yarkovsky effect. From there, a combination of planetary close encounters and resonances would have moved it to where it is seen now, namely on a very Earth-like orbit. En route, EV₅'s precursors may have disrupted one or more times by collisions or by mass-shedding via YORP spin up, enough to take it to its current size. Alternatively, EV₅ might have always been near its current size, and it potentially avoided all meaningful collisions.

To determine more specifics about EV₅'s likely evolution, its existing physical properties need to be considered and put into context using the current understanding of solar system dynamics and physical effects produced by collisional/thermal physical processes. What is known about EV₅ that can be used to help identify its source region is summarized below.

- **Orbit.** EV₅ has an osculating (a, e, i) orbit of (0.96 AU, 0.084, 7.4°), respectively. This places it into the Aten sub-class of the NEA population.
- **Shape, Size, Spin Vector.** Radar observations suggest EV₅ has a top-like shape with an equatorial bulge reminiscent of many other NEAs (Busch et al. 2011). These components are consistent with the idea that EV₅ has been significantly modified by YORP torques over time (e.g., Walsh et al. 2008). Its radar-derived mean diameter is 400 ± 50 m (Busch et al. 2011). The spin period is $P = 3.725$ h, with an obliquity around 180° (retrograde rotation) [Ali Lagoa et al. 2013]).
- **Spectra.** Reddy et al. (2012) shows that the spectroscopic signature of EV₅ is mostly featureless with an overall blue slope. They classify it as a C-type body. See Appendix A3 for additional details. Note that the spectra of some NEAs have proven variable, so spectral comparisons may only refer a portion of a possibly heterogeneous surface composition (e.g., Binzel et al. 2015).
- **Albedo.** EV₅ has a geometric albedo of $9\text{-}10\% \pm 3\%$ or $9 (+5, -3)\%$ (see main text and Appendix A1-A2). The average albedo for C-complex NEAs, based on five objects observed by the Spitzer space telescope, is $13\% (+6\%, -5\%)$ (Thomas et al. 2011). This suggests the derived value for EV₅ is consistent with at least some other C-complex NEAs. Most C-complex families across the main

This document is a NASA working document and is subject to further revision. This document has been reviewed for release to the public and is not export controlled.

belt, however, are dominated by members whose albedos are less than 10% (Masiero et al. 2013). EV₅'s albedo may be useful for determining its source and precise nature. The implications of EV₅'s albedo will be discussed below.

Dynamical modeling of the source of EV₅

Using the debiased NEA model of Bottke et al. (2002), it is possible to determine, in a probabilistic sense, the likely source region through which EV₅ or its immediate precursor left the main belt. This model assumes that NEAs with $a < 7.4$ AU and absolute magnitude $H < 22$ were derived from one of five primary source regions: the ν_6 secular resonance along the inner edge of the main belt, the intermediate source Mars-crossing region (IMC) that is dominated by objects escaping from the inner main belt, the J3:1 mean motion resonance with Jupiter at 2.5 AU (J3:1), the outer main belt region beyond 2.8 AU, and the Jupiter Family Comet region, which is resupplied by the scattered disk in the transneptunian region. Note that high inclination sources of NEAs were not included in the model; this point will be briefly revisited below.

By comparing the (a,e,i) orbit of EV₅ with this model, it was found that it had a 48% and 52% probability of reaching its current orbit through the ν_6 resonance and IMC regions, respectively. Accordingly, this model predicts the likely departure point of EV₅ from the main belt was probably near 2.2-2.3 AU along the innermost edge of the main asteroid belt. This also means a likely source of EV₅ is the inner main belt between 2.1-2.5 AU (e.g., Bottke et al. 2015).

To gain more fidelity on this prediction, the dynamical runs described in Bottke et al. (2015) were used to explore the specific main belt objects likely to produce EV₅. Here tens of thousands of test asteroids were tracked, starting in regions adjacent to the source regions. These bodies, with assumed diameters of $D = 0.1$ and 1 km, were allowed to drift into escape routes via the Yarkovsky effect. Then, which asteroids passed very close to EV₅'s current (a,e,i) orbit were identified. A good match was arbitrarily defined as those with $\Delta a < 0.01$ AU, $\Delta e < 0.01$, and $\Delta i < 1^\circ$.

Forty test asteroids that matched the criteria were found, with roughly equal numbers coming from the ν_6 resonance and IMC regions. For both sources, it was found that nearly all of the EV₅ matches came from main belt test asteroids that had starting $a < 2.3$ AU, $0.1 < e < 0.3$, and $i < 7^\circ$. Only two test asteroids from the IMC region successfully matched EV₅'s orbit from an initial $i > 8^\circ$. Creating probability distributions from the initial orbits of the successful matches, it was found that EV₅ probably had $1^\circ < i < 5^\circ$ prior to leaving the main belt, with peaks near 2-3° and 5°. This suggests that EV₅ may have come from a sizable C-complex asteroid family residing in the inner main belt between 2.1-2.5 AU with $i < 7^\circ$ (e.g., Bottke et al. 2015).

The proxies for EV₅ were also tracked for how close they approached the Sun during the simulation. After escaping the asteroid belt, en route to its current orbit, the proxies for EV₅ spent considerable time with perihelion values $q < 1$ AU. By tracking these test asteroids from the main belt all the way to EV₅'s observed orbit, and then estimating the temperatures experienced by these bodies at their subsolar points along the way (Marchi et al. 2009; Delbo and Michel 2011; Ali Lagoa et al. 2013), the following was found:

- The median time spent by the EV₅-like test asteroids with $q < 0.5$, 0.7, and 1.0 AU was ~0.1, 1.4, and 7 Myr, respectively. Less than 50% and 25% of the test asteroids spent any time at $q < 0.5$ and 0.2 AU respectively. Thus, while close solar encounters for EV₅ cannot be ruled out, the most

This document is a NASA working document and is subject to further revision. This document has been reviewed for release to the public and is not export controlled.

probable scenario is that it probably avoided such orbits.

- Using these model runs, it was found that a 2%, 14%, 24%, 44%, 60%, 80%, and 100% probability that the surface of EV₅ reached temperatures greater than 1,030 K, 730 K, 600 K, 510 K, 460 K, 420 K, and 340 K, respectively. It was assumed that these values correspond to q greater than 0.1, 0.2, 0.3, 0.4, 0.5, 0.6, and 0.9 AU, respectively. The interiors of the boulders on or near EV₅'s surface would have experienced modestly lower temperatures. These results lead to high and low probability scenarios.
- Overall, we argue the greatest likelihood is that EV₅'s boulders and subsurface did not experience temperatures greater than 500 K. Here common organic and hydrated compounds that break up at relatively moderate temperatures (e.g., 300–670 K) may still be depleted in both the surface layers of the boulders and EV₅ itself (i.e., possibly down to 5 cm depth; [Delbo and Michel 2011]). Similarly, boulder organics may have also been depleted via exposure to ionization radiation (e.g., cosmic rays), whose penetration depth is on the order of a meter.
- In the lower probability case, EV₅ spent enough time near the Sun that boulders currently located on its surface were thermal modified.
- Additional thermal modeling work will be needed to better quantify these probabilities, with the temperatures reached by EV₅'s current population of surface boulders a function of EV₅'s past proximity to the Sun, its physical parameters, and the residence time of those boulders near the surface [Ali Lagoa et al. 2013].

Potential Links Between EV₅ and Known Asteroid Families

Using the dynamical criteria above, and assuming EV₅ most likely came from a sizeable main belt family rather than simply being a background body from the asteroid belt, the family definitions from Nesvorny et al. (2015) were used to identify candidate low inclination C-complex families in the inner main belt: Eulalia, New Polana, Erigone, Baptistina, Sulamitis, and Clarissa (Campins et al. 2010; Walsh et al. 2013; Bottke et al. 2015). Central and outer main belt families were rejected as candidate sources because neither model from Bottke et al. (2002; 2015) showed a viable pathway for them to make EV₅. (In addition, EV₅'s spectral shape is not consistent with the typically-spectrally red outer main belt asteroids.)

Of the remainder, using the criteria discussed in Bottke et al. (2015), smaller families like Sulamitis and Clarissa can be eliminated from discussion; their fragments are unlikely to transit the main belt, escape, and reach EV₅ orbits within the likely age of their families. For the remainder, considerable uncertainty exists about which one may be most likely source, and it is unlikely a definitive match can be determined without extensive modeling work that goes beyond the short timescale of the FAST effort.

In lieu of this, it is useful to consider proxies for EV₅. For example, Campins et al. (2010) identified the low-albedo component of the Nysa-Polana complex as the most likely source of NEA 101955 Benu, the $D = 0.5$ km, low albedo target of the OSIRIS-REx mission. This work was refined by Walsh et al. (2013) and Bottke et al. (2015), who identified the low albedo Eulalia and the New Polana families as the top candidate source families of Benu. Benu is a top-shaped low albedo C-complex asteroid with an orbit highly similar to EV₅. Using a range of numerical models, Bottke et al. argued that the older ages of the Eulalia and New Polana families (~830 and ~1400 Myr old, respectively) would allow many 0.5 km fragments to have reached Benu-like orbits via the ν_6 resonance and the IMC region at the present time. Given that EV₅ is modestly smaller than Benu, and that it likely traversed faster across the main belt than Benu via the Yarkovsky effect, one must consider these families as solid candidates to make EV₅ as well.

This document is a NASA working document and is subject to further revision. This document has been reviewed for release to the public and is not export controlled.

These families may also be the source of the low albedo NEA (162173) 1999 JU₃. This km-sized asteroid, now known as Ryugu, is the target of JAXA's Hayabusa2 mission. See Campins et al. (2013) and Bottke et al. (2015) for additional details.

Erigone, a sizeable low albedo family with a likely age of ~130 Myr, was deemed slightly too young to be a strong source of Bennu-like objects by Bottke et al. (2015). Essentially, insufficient $D = 0.5$ km bodies escaped the main belt within ~130 Myr to make Erigone members competitive with Eulalia and New Polana. EV₅, on the other hand, is modestly smaller than Bennu, perhaps enough that EV₅-sized objects can now escape and reach an EV₅ orbit within the age of the family. Accordingly, Erigone must also be considered a candidate family to produce EV₅. Moreover, the inclination of Erigone family members is close to 5°, a value that is modestly favored among the test asteroids above that reproduce EV₅'s orbit. More work on this family is needed.

Recent spectroscopic surveys of primitive asteroids in the inner belt, including the Polana, Eulalia and Erigone families (e.g, Pinilla-Alonso et al. 2014, de Leon et al. 2015) are consistent with the dynamical arguments presented above and may be used to refine the source region. In addition, these authors are now obtaining spectra of the low-albedo inner-belt asteroids adjacent to the ν_6 resonance at inclinations between 8 and 12 degrees (Campins et al. 2013, figure 1). Because of its position at the very edge of the ν_6 resonance, this group may also be a potential source of EV₅.

A key question for all three of these families, however, is whether EV₅'s mean albedo should be treated as a discriminant for ruling out candidate families. The distribution of albedos of known family members observed by WISE, mostly those bodies with $D >$ several km, indicate that Eulalia, New Polana, nor Erigone have very few members with albedos $> 10\%$ (Masiero et al. 2013). It should be noted that EV₅-sized bodies below WISE's detection limit may plausibly have a different albedo distribution. Moreover, the estimated albedos of EV₅, $9-10\% \pm 3\%$ or $9\% (+5\%, -3\%)$, are ambiguous enough that these families cannot be ruled out as candidate sources.

Moving to higher albedo candidate families, the Baptistina family was considered. It is an X-complex family whose members have a mean albedo of 16% (Nesvorny et al. 2015). It is located near the ν_6 resonance at relatively low inclinations, such that its members could readily reach EV₅'s orbit. The age of the family is debated, with a definitive solution depending on the bulk density of Baptistina family members (Bottke et al. 2007; Maserio et al. 2012; Nesvorny et al. 2015). If all things were equal, Baptistina would likely be the strongest candidate family based on these criteria alone. Here, however, spectral signatures need to be considered, which place the Baptistina family at a distinct disadvantage to the other candidate families (Reddy et al., 2014). The spectral signatures of several members of the Baptistina family indicate the presence of pyroxene band, which is probably enough to rule out Baptistina as a candidate source for EV₅.

A potential compelling spectral and albedo match exists between high inclination Pallas family members and EV₅. Pallas is the second largest asteroid in the main belt, and it and its family members have a B-type spectra, similar to EV₅ in many respects. Pallas family members also have a mean albedo of 16%, such that many would probably fit the EV₅'s albedo (Nesvorny et al. 2015). Moreover, many links can be found in the literature between CR chondrites and Pallas; this increases the possibility of a potential match between EV₅ and CR chondrites. The problem is that there is no known dynamical pathway for Pallas family members, which reside in the main belt with $i > 30^\circ$, to reach EV₅'s orbit (de Leon et al. 2010). Numerical simulation suggest the lowest inclination reached by Pallas family members entering onto

This document is a NASA working document and is subject to further revision. This document has been reviewed for release to the public and is not export controlled.

planet-crossing orbits is 20° , much higher than EV₅'s inclination of 7° . Other orbital constraints are missed as well. Thus, while dynamically implausible, it is suggested that this possible match is still interesting enough to warrant further study, depending on EV₅'s actual albedo.

To close this section, it should be noted that an intriguing source for a high albedo EV₅ would be the diffuse population of higher albedo CC-like asteroids residing in the innermost main belt region between $8 < i < 15^\circ$. Many of these bodies have WISE-derived albedos $> 10\%$. Dynamically, they are a less likely fit than the low albedo families discussed above, but they appear to be one of the few small body populations in the inner main belt that have the appropriate albedo to match EV₅. These bodies have yet to be investigated in detail.

Spectral and Meteorite Matches to EV₅

Given that the EV₅'s spectrum is essentially featureless throughout the visible near-infrared (VNIR) wavelengths, it is difficult to find unique matches between it and known carbonaceous chondrites; this makes it difficult to glean insights into its composition and volatile abundance. To date in the literature, the best match has been found for CI chondrites (Reddy et al. 2012), though a match to certain kinds of CM chondrites may also be possible (R. Binzel, Massachusetts Institute of Technology, personal communication). The biggest issue is whether the relatively high albedo of EV₅ for a carbonaceous chondritic asteroid should be applied when considering spectral matches. If EV₅'s albedo is substantially lower than the reported mean value of 9%, EV₅ would likely be able to match primitive CI/CM carbonaceous chondrite meteorites as well as candidate families such as Eulalia, New Polana, and Erigone. If the albedo is higher than 9%, it may be possible to reject these families and consider alternative sources for EV₅.

To glean additional insights into the high albedo case, Ed Cloutis (University of Winnipeg) was contacted and asked to search his spectra data base for carbonaceous chondrite spectra that could provide a match EV₅. His write-up, provided in Appendix A3, argues that EV₅ is most consistent with being a CR-type carbonaceous chondrites.

Conclusions

Given the available modeling work and data, one could argue that the most plausible source family candidates for EV₅ from a dynamical perspective are Eulalia, New Polana, and Erigone. This assumes that these families have numerous $D \sim 0.4$ km members with greater than 10% albedos, or that EV₅'s true albedo is considerably lower than 10%. If EV₅ does have a high albedo, a plausible source would be a population of high albedo C-complex objects in the inner main belt between $8 < i < 15^\circ$. Second tier candidate families for the high albedo case are Baptistina and Pallas. For the Baptistina family to work, it would need to be demonstrated that some family members have EV₅-like spectra. For Pallas family to match, some dynamical pathway would need to be found that would allow its members to reach EV₅'s current orbit. Also, the possibility cannot be ruled out that some smaller family or the main belt background is responsible for EV₅. Investigations into all of these possibilities are strongly needed to better understand the nature and context of EV₅.

Additional References Not Listed in the Main Text

This document is a NASA working document and is subject to further revision. This document has been reviewed for release to the public and is not export controlled.

Binzel, R. P., and 16 colleagues 2015. Spectral slope variations for OSIRIS-REx target Asteroid (101955) Bennu: Possible evidence for a fine-grained regolith equatorial ridge. *Icarus* 256, 22-29.

Bottke, W. F., D. Nesvorný, R. E. Grimm, A. Morbidelli, and D. P. O'Brien. 2006b. Iron meteorites as remnants of planetesimals formed in the terrestrial planet region. *Nature* 439, 821-824.

Bottke, W. F., D. Vokrouhlický, and D. Nesvorný. 2007. An asteroid breakup 160 My ago as the probable source of the K-T impactor. *Nature* 449, 48-53.

Campins, H., de Leon, J., Morbidelli, A., Licandro, J., Gayon-Markt, J., Delbo, M., Michel, P. 2013. The Origin of Asteroid 162173 (1999 JU₃). *The Astronomical Journal* 146, 26.

de Leon, J., Campins, H., Tsiganis, K., Morbidelli, A., Licandro, J. 2010. Origin of the near-Earth asteroid Phaethon and the Geminids meteor shower. *Astronomy and Astrophysics* 513, A26.

de Leon, J., Pinilla-Alonso, N. 2015. PRIMitive Asteroids Spectroscopic Survey - PRIMASS: First Results. AAS/Division for Planetary Sciences Meeting Abstracts 47, \#106.09.

Levison, H. F., W. F. Bottke, M. Gounelle, A. Morbidelli, D. Nesvorný, and K. Tsiganis. 2009. Contamination of the asteroid belt by primordial trans-Neptunian objects. *Nature*, 460, 364-366.

Masiero, J. R., Mainzer, A. K., Bauer, J. M., Grav, T., Nugent, C. R., Stevenson, R. 2013. Asteroid Family Identification Using the Hierarchical Clustering Method and WISE/NEOWISE Physical Properties. *The Astrophysical Journal* 770, 7.

Masiero, J. R., Mainzer, A. K., Grav, T., Bauer, J. M., Jedicke, R. 2012. Revising the Age for the Baptistina Asteroid Family Using WISE/NEOWISE Data. *The Astrophysical Journal* 759, 14.

Morbidelli, A., W. F. Bottke, D. Nesvorný, and H. Levison. 2009. Asteroids were Born Big. *Icarus* 204, 558-573

Nesvorný, D., Broz, M., Carruba, V. 2015. Identification and Dynamical Properties of Asteroid Families. In *Asteroids IV* (P. Michel, W. F. Bottke, eds), in press. Also in ArXiv e-prints arXiv:1502.01628.

Thomas, C. A., and 18 colleagues 2011. ExploreNEOs. V. Average Albedo by Taxonomic Complex in the Near-Earth Asteroid Population. *The Astronomical Journal* 142, 85.

Pinilla-Alonso, N., Campins, H., Lorenzi, V., de Leon, J., Landsman, Z., Licandro, J., Ali-Lagoa, V. 2014. Near-infrared spectroscopy of asteroids in the Polana-family region: Where are the Eulalias? *Asteroids, Comets, Meteors 2014*, 419.

Reddy, V., and 10 colleagues 2014. Chelyabinsk meteorite explains unusual spectral properties of Baptistina Asteroid Family. *Icarus* 237, 116-130.

Vokrouhlický, D. and W. F. Bottke. 2012. Yarkovsky and YORP effects. *Scholarpedia*, 7(5):10599

Appendix A2: Phase Function Analysis

Note: Input from non-FAST members have not been edited and are included as they were received.

What Does Phase Function Analysis Tells Us About the Albedo of NEA (341843) 2008 EV₅?

*Carl Hergenrother
Lunar and Planetary Laboratory
University of Arizona
Last Updated: 2015 October 27*

Abstract:

This document is a NASA working document and is subject to further revision. This document has been reviewed for release to the public and is not export controlled.

Phase function analysis can help constrain the albedo of near-Earth asteroid (341843) 2008 EV₅ in two ways. If the diameter of the object is known, which thanks to radar imaging is true for 2008 EV₅, the absolute magnitude can be used in conjunction with the diameter to derive the albedo. Indirectly, there is a relationship between the slope of the linear phase function and albedo.

The Muinonen H-G₁₂ phase function (Muinonen et al. 2012) was used to derive an absolute magnitude of $H = 20.22 \frac{+0.23}{-0.15}$, a value ~0.2 magnitudes fainter than previously found (Alí-Lagoa et al. 2014). When taken in conjunction with a radar-derived diameter of 400 ± 50 m, an albedo of $0.09 \frac{+0.05}{-0.03}$ was found. Indirect measures of taxonomy such as the value of the Muinonen G₁₂ parameter are consistent with a carbonaceous taxonomy and relatively dark albedo.

Observations:

V and R band photometry of (341843) 2008 EV₅ were obtained from the archives of the Minor Planet Center via their 'MPC Database Search' tool (http://www.minorplanetcenter.net/db_search) resulting in 568 observations made between 2008 March 4 and 2010 April 11 UT. Phase angles from 31° to 113° were observed. Observations were averaged to produce a single measurement per observer per night. A color index of V-R = +0.4 was used to transform R band photometry to V band. This color index is consistent with the spectrum of 2008 EV₅ obtained by Reddy et al. (2012).

Imaging radar observations made with Arecibo and Goldstone found an equivalent diameter of 400 ± 50 m (Busch et al. 2012). An independent diameter of 370 ± 6 m was derived from WISE photometry (Alí-Lagoa et al. 2014).

Phase Function Analysis:

Three different phase function methods were used to estimate the absolute magnitude of 2008 EV₅.

Linear Fit – A linear fit yielded absolute magnitude (H) = 20.41 ± 0.19 and slope (β) = 0.031 ± 0.004 magnitudes per degree of phase angle (Figure 10). The fit was restricted to photometry obtained on the linear portion of the asteroid's phase function (phase angles between 15° and 70°). This constraint limits the fit to the linear portion of EV₅'s phase function.

IAU H-G – The IAU H-G phase function as described in Bowell et al. (1989) yielded $H = 19.91 \frac{+0.42}{-0.30}$ and $G = +0.04 \frac{+0.10}{-0.18}$ (Figure 11). The 2008 EV₅ asteroid and dataset provide problems for the H-G function due to the object's dark(ish) albedo and lack of photometry at small phase angles (Shevchenko et al. 2008, Muinonen et al. 2012).

Muinonen H-G₁₂ – The Muinonen H-G₁₂ phase function as described in Muinonen et al. (2010) yielded $H = 20.22 \frac{+0.23}{-0.15}$ and $G_{12} = 0.55 \frac{+0.31}{-0.42}$ (Figure 12).

Conclusions:

The lack of observations at phase angles less than 31° increases the uncertainty of H. This is

This document is a NASA working document and is subject to further revision. This document been reviewed for release to the public and is not export controlled.

evident from nearly one magnitude spread in possible H values (19.61 to 20.60) produced by the three different phase functions. The linear fit is overly simplistic and does not model the non-linearity of phase functions at low phase angles. The H-G function is prone to produce an opposition effect that is much larger than those observed for dark objects (Shevchenko and Belskaya, 2010). An analysis of Pan-STARRS photometry found that the Muinonen phase function provides better results than the IAU H-G phase function (Veres et al. 2015).

A range of possible albedos produced for the minimum, mean and maximum H values produced by each of the three phase functions and the range of radar derived equivalent diameters is shown in Table 11.

Table 11: Albedos for a range of absolute magnitudes and diameters for 2008 EV₅.

	H	Radar Dimensions			Albedo
		0.35 km	0.40 km	0.45 km	
H-G₁₂	20.07	0.135	0.103	0.082	0.09 $\frac{+0.05}{-0.03}$
	20.22	0.118	0.090	0.071	
	20.46	0.094	0.072	0.057	
H-G	19.61	0.206	0.158	0.125	0.12 $\frac{+0.08}{-0.06}$
	19.91	0.157	0.120	0.095	
	20.33	0.106	0.081	0.064	
Linear	20.22	0.118	0.090	0.071	0.08 $\frac{+0.04}{-0.03}$
	20.41	0.099	0.076	0.060	
	20.60	0.083	0.064	0.050	

The IAU H-G solution finds an albedo that is consistent with the results of Alí-Lagoa et al. (2014). This is not surprising since the H used by Alí-Lagoa et al. (2014) was based on the same data sets and H-G function as calculated by the Minor Planet Center via the JPL Small-Body Database. The Linear function assumes no non-linearity and ignores any opposition effect at small phase angles so its H values trend towards fainter.

The Muinonen H-G₁₂ function produces albedos in between the IAU H-G and Linear functions. It found an absolute magnitude of $H = 20.22 \frac{+0.23}{-0.15}$. When taken in conjunction with a radar-derived diameter of 400 ± 50 m, an albedo of $0.09 \frac{+0.05}{-0.03}$ was found. The $G_{12} = 0.55 \frac{+0.31}{-0.42}$ is consistent with both carbonaceous and non-carbonaceous taxonomic types but asteroids with a similar G_{12} are predominately C and X complex types.

The albedo of 2008 EV₅ is still relatively uncertain and spans a range that is safely within the expected values for a carbonaceous object to a little bit higher than expected for the same. This work did find that the absolute magnitude used by previous studies was ~ 0.2 magnitudes too bright resulting in a mean albedo of $0.09 \frac{+0.05}{-0.03}$ rather than 0.13 ± 0.05 .

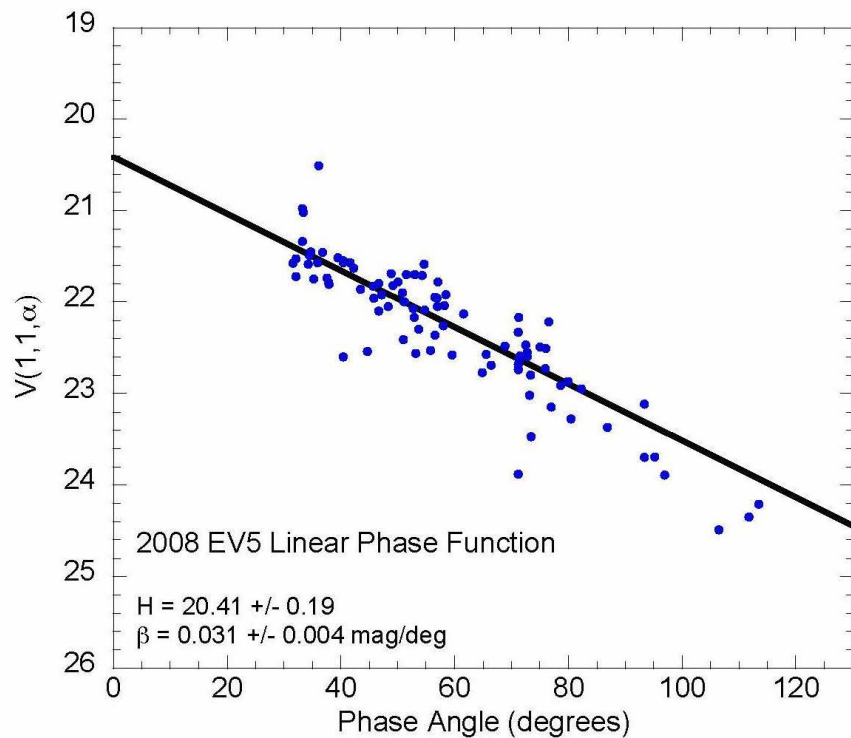


Figure 10: Linear phase function fit to the 2008 EV₅ MPC data.

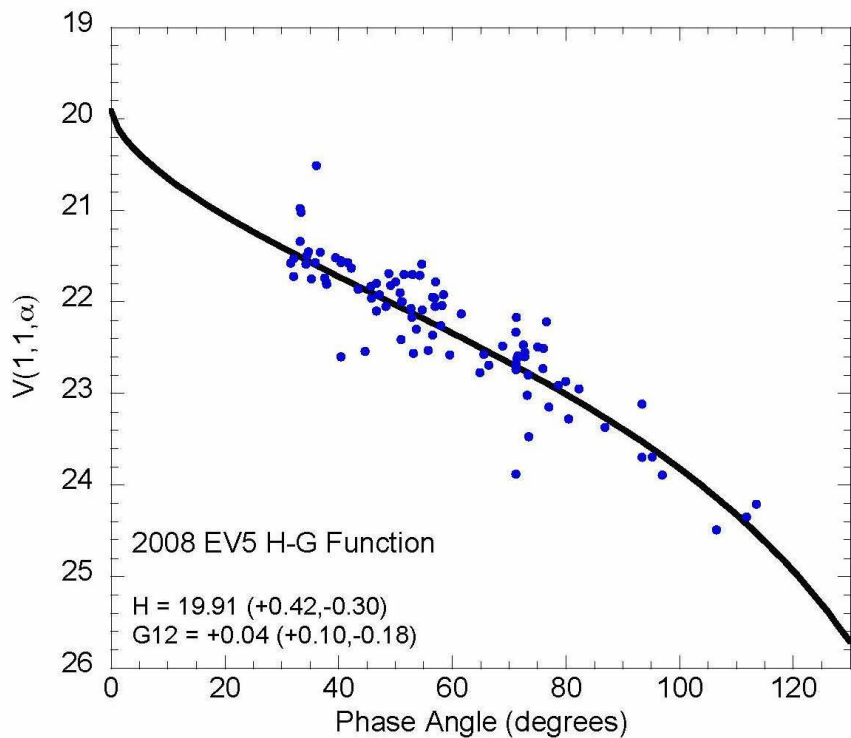


Figure 11: IAU H-G phase function fit to the 2008 EV₅ MPC data (Bowell et al. 1989).

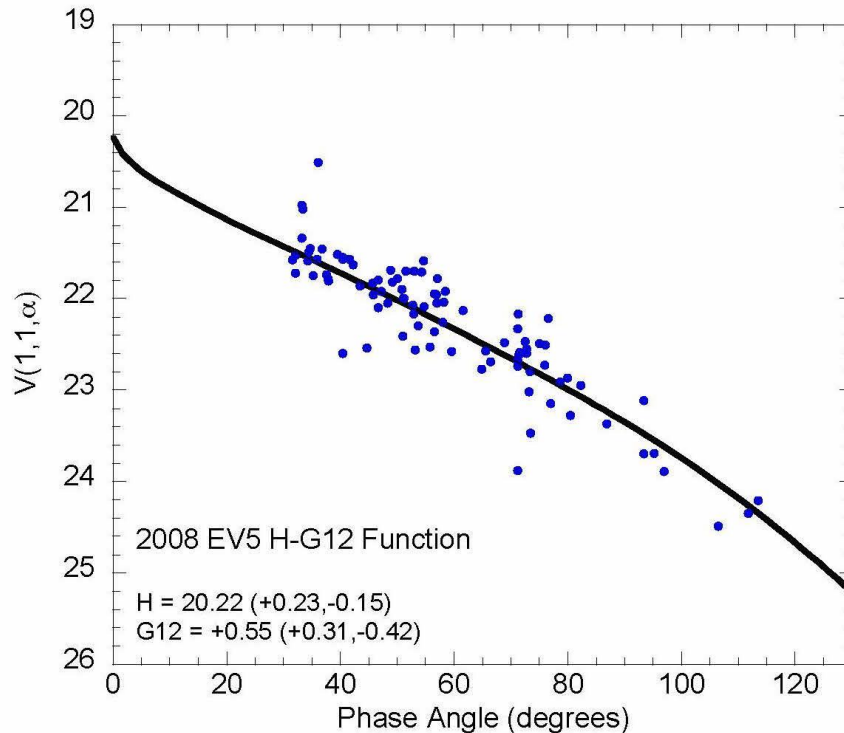


Figure 12: Muinonen H-G12 phase function fit to the 2008 EV₅ MPC data (Muinonen et al. 2010).

References:

- Alí-Lagoa et al. 2014. Thermophysical Properties of near-Earth Asteroid (341843) 2008 EV₅ from WISE Data. *Astronomy & Astrophysics* 561, A45.
- Busch, M.W. et al. 2011. Radar Observations and the Shape of near-Earth Asteroid 2008 EV₅. *Icarus* 212, 649-660.
- Muinonen et al. 2010. A Three-parameter Magnitude Phase Function for Asteroids. *Icarus* 209, 542-555.
- Oszkiewicz, D.A. et al. 2012. Asteroid Taxonomic Signatures from Photometric Phase Curves. *Icarus* 219, 283-296.
- Reddy et al. 2012. Composition of near-Earth Asteroid 2008 EV₅: Potential Target for Robotic and Human Exploration. *Icarus* 221, 678-681.
- Shevchenko, V.G. and Belskaya, I.N. 2010. Opposition Effect of Dark Asteroids: Diversity and Albedo Dependence. In: EPSC 2010, p. 738.
- Veres, P. et al. 2015. Absolute Magnitudes and Slope Parameters for 250,000 Asteroids Observed by Pan-STARRS PS1 – Preliminary Results. arXiv:1506.00762v3.

Appendix A3: Asteroid 2008 EV₅ – spectral analysis

Note: Input from non-FAST members have not been edited and are included as they were received.

This document is a NASA working document and is subject to further revision. This document has been reviewed for release to the public and is not export controlled.

Ed Cloutis (University of Winnipeg)

October 21, 2015

Characteristics:

Diameter: 400 +/- 50 meters

Albedo: between ~7 and 15%

Reflectance spectrum of EV₅:

The 0.3-2.5 micron spectrum of 2008 EV₅ is red sloped from ~0.3 to 0.75 microns, and blue sloped out to 2.5 microns. The visible region spectrum (0.3-0.98 microns) shows no strong evidence of any absorption bands (Figure 13). There may be weak absorption bands near 0.41 and 0.43 microns; they could plausibly be attributed, respectively, to aromatic organics and some ferric iron-bearing phase, such as a sulfate or serpentine. The spectrum beyond 0.7 microns suggests the possible presence of an absorption feature in the 1 micron region. This is suggested by continuum removal which has been applied to carbonaceous chondrites, where a straight line continuum is fit from the 0.7 micron region peak to the neighborhood of 1.35 microns.

The continuum removed spectrum is somewhat noisy, but there appears to be a broad absorption feature over the 0.75-1.35 micron interval (Figure 14). In carbonaceous chondrite spectra, individual absorption bands are often seen depending on the nature of the major silicates:

- Two bands, near 0.9 and 1.1 microns attributable to ferrous iron-bearing phyllosilicates
- A band near 1.05 microns accompanied by a shoulder near 1.25 microns when olivine is present
- A broad band near 1 micron when magnetite is present

Any or all of these features may be present in carbonaceous chondrite spectra depending on relative phase abundances.

The continuum removed absorption feature suggests the presence of both ferrous iron-bearing phyllosilicates (absorption features in the ~0.9 and 1.1 micron regions), and olivine (absorption features near 1.05 microns and 1.25 microns).

Comparison to carbonaceous chondrites:

The combination of relatively high albedo (7-15%), blue-sloped spectrum beyond 0.75 microns, and likely absorption band in the 1 micron region, allows us to place constraints on possible analogues. The focus here is on carbonaceous chondrites, not necessarily only because they are the best candidate, but because the spectral properties of other possible candidates, such as enstatite chondrites, are less well known.

Spectral comparisons are generally more robust in terms of which meteorite classes 2008 EV₅ is inconsistent with rather than which classes it could be.

Of the carbonaceous chondrite classes compared to 2008 EV₅, the following **DO NOT** provide good matches:

This document is a NASA working document and is subject to further revision. This document has been reviewed for release to the public and is not export controlled.

1. **CI chondrites:** their albedos are generally too low, most do not show an absorption feature in the 1 micron region, those that are blue sloped are much darker than the asteroid, the 1 micron region absorption feature, when present, is more similar to phyllosilicates rather than phyllosilicates + olivine.
2. **CM chondrites:** their spectra are generally flat to red sloped, those that are blue sloped are usually quite dark (a few percent albedo) and are depleted in the finest fraction, a 0.7 micron absorption band is nearly ubiquitous (attributable to ferrous+ferric iron-bearing clays).
3. **CO chondrites:** many are blue sloped and with the right albedo (e.g., Ornans, <150 μm ; Felix, <150 μm ; Kainsaz, <150 μm). The lowest petrologic grade COs are closest to EV₅ in this regard. However, they all have a broad 2 micron region absorption feature attributable to CAIs, and this is not evident in the EV₅ spectrum (although its spectrum are too noisy to make a definitive identification). Most of them also have a 1 micron region absorption band that is more olivine-like than EV₅.
4. **CV chondrites:** Some powder CV spectra can be blue-sloped and of the right albedo (e.g., ALHA 81003, <125 μm , Grosnaja, <45 μm). However, the continuum-removed spectra show a well-defined absorption band with a minimum near 1.05 μm , attributable to olivine only, unlike EV₅. Also, the peak reflectance of these meteorites occurs shortward of 0.75 μm , also unlike EV₅.
5. **CK chondrites:** Powdered CK spectra are blue-sloped, some with reflectance peaks near 0.75 μm and usually of the right albedo. However, they all show a clear and deep olivine absorption band near 1.05 μm , unlike EV₅.
6. **“Other” carbonaceous chondrites:** of the various “other” carbonaceous chondrites (Cloutis et al., 2012 – Icarus, v. 221 p984), none match more than one or two of the salient features of EV₅.
7. **Naturally thermally metamorphosed carbonaceous chondrites:** Of the various naturally thermally metamorphosed carbonaceous chondrite spectra that are available, no one spectrum matches EV₅ simultaneously in terms of peak reflectance position, albedo, and shape of the 1 micron region absorption band. Some are blue sloped, but too dark or have their peak at the wrong position.
8. **Laboratory thermally metamorphosed CI/CM chondrites:** While lab heating of an Ivuna CI chondrite powder (<125 μm) can produce blue-sloped spectra (for 100, 300 and 700C), and a 1 micron region absorption feature with some similarities to EV₅ (bands at 0.9 and 1.1 μm), the spectra are darker than EV₅ (<5%).

The following **ARE** possible matches:

1. CR chondrites: some uncertainties because CR spectra seem susceptible to the presence of terrestrial alteration products. However, some CR powder spectra are (almost certainly) blue sloped, in the right albedo range, and with a peak near 0.75 microns (e.g., A881595). Its spectrum also shows a broad 1 micron region absorption band with individual bands near 0.9 and 1.2 microns (like EV₅), but it also has a band near 1 micron (unlike EV₅).

Other spectral characteristics:

There are also suggestions of an absorption band in the 1.6-1.7 micron region. Such a feature is most consistent with aliphatic organics. However, such a feature would be accompanied by a stronger absorption feature beginning at 2.31 microns, and such a feature is not evident (given the noise in the spectrum).

Summary

This document is a NASA working document and is subject to further revision. This document has been reviewed for release to the public and is not export controlled.

One of the difficulties facing spectral matching is the relative importance of the various spectral parameters used in this comparison. For instance, spectral slope can vary from blue to red for subsamples of a single carbonaceous chondrite (e.g., Ivuna, Orgueil). Similarly, subsamples of a single carbonaceous chondrite can also show no or no readily apparent absorption features in the 1 micron region. The shape of the 1 micron region is potentially diagnostic of the presence of specific minerals, and the data for EV₅ suggest ferrous iron-bearing phyllosilicates and olivine, not unlike CR2 chondrites, which should have a mix of hydrous and anhydrous silicates. Many groups are almost certainly non-starters because of albedo and absorption band characteristics.

Blue spectral slopes are generally most characteristic of coarse powders where the finest grain size fraction has been removed, or solid slabs. These spectra are darker than fine-grained powders, so if a fine-grained powder is already dark, then the finest fraction-removed or slab spectra would be even darker. Also, whether an asteroid surface would be essentially devoid of only the finest grains or exist as a clean slab appears unlikely.

At present, EV₅ appears most consistent with an assemblage consisting of both hydrous and anhydrous silicates, specifically a ferric iron-free phyllosilicate and iron-bearing olivine. This places it in the realm of petrologic grade 2-3 carbonaceous chondrites (most similar to CR2) but could include mildly to moderately thermally metamorphosed members (e.g., EET 90043 – heated to about 600C).

Suggestions:

A more wide-ranging laboratory spectral study of the “best” candidate meteorites is warranted. Looking more closely at the effects of grain size, packing density, and powders-on-slabs would provide stronger insights into the possible physical and chemical composition of EV₅.

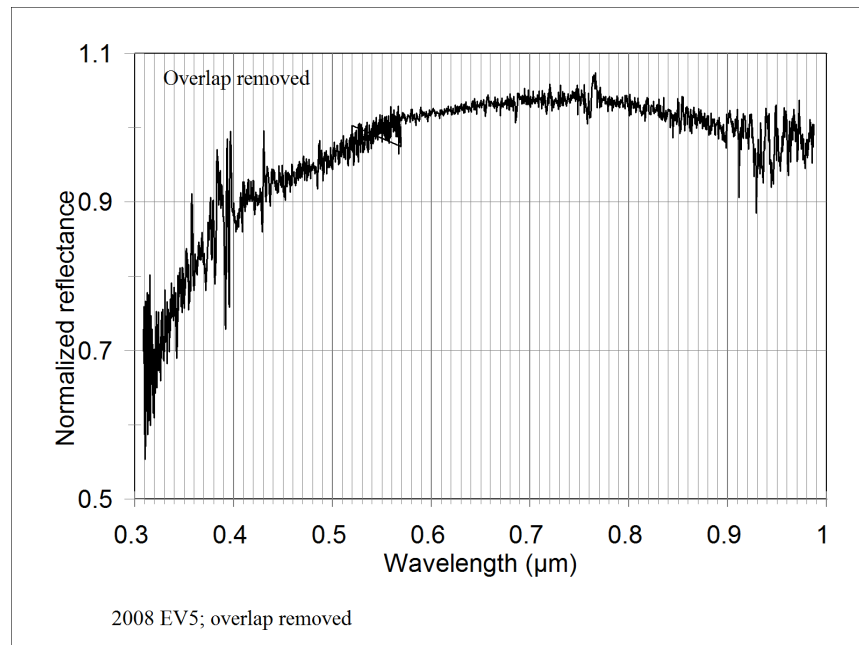


Figure 13: Visible region spectrum of 2008 EV₅

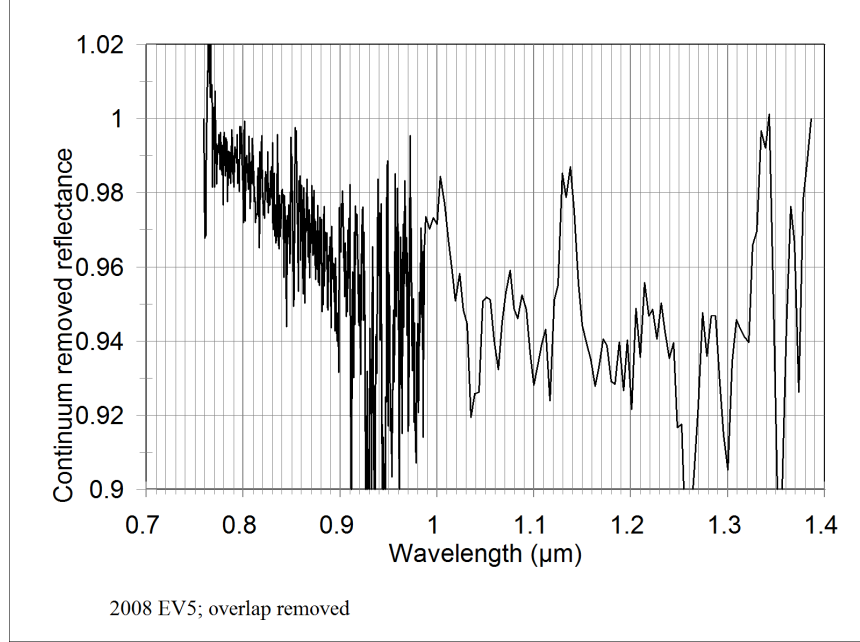


Figure 14: Reflectance spectrum of 2008 EV₅ with straight line continuum removed from ~0.78 to 1.38 microns.

Appendix A4: Disk-integrated Photometric Models of the ARM Mission Asteroid Target 2008 EV₅

The reflectance and albedo quantities, relevant to the ARM mission asteroid target 2008 EV₅, and how viewing conditions [incidence (i), emission (e), and phase angles (α)] vary for each quantity will be reviewed in this appendix. Disk-integrated ground-based photometric data of 2008 EV₅ will be used to constrain the average disk-resolved brightness across EV₅'s surface by fitting phase curve data, compiled by C. Hergenrother archived at the Minor Planet Center (MPC).

The Radiance Factor ($RADF$) is the ratio of the bidirectional reflectance of a surface to that of a perfectly diffuse surface illuminated at $i = 0$ [Hapke, 2012]. The Bidirectional Reflectance Distribution Function ($BRDF$) is the ratio of the radiance scattered by a surface into a given direction to the collimated power incident on a unit area of the surface [Hapke, 2012]. Reflectance, $r(i, e, \alpha)$, is directly related to $BRDF(i, e, \alpha)$ $RADF(i, e, \alpha)$ (or $[I/F](i, e, \alpha)$) as described in the following Lommel-Seeliger $RADF$ function:

$$\begin{aligned}
 [I/F](i, e, \alpha) &= RADF(i, e, \alpha) = BRDF(i, e, \alpha)[\mu_o\pi] = \pi r(i, e, \alpha) \\
 &= \frac{\varpi_o}{4} \frac{\mu_o f(\alpha)}{\mu_o + \mu} \quad (1),
 \end{aligned}$$

where $\mu_o = \cos(i)$, $\mu = \cos(e)$, i is the incidence angle (degrees), e is the emission angle (degrees). $A_{LS} = \frac{\varpi_o}{4\pi}$ is the Lommel-Seeliger albedo, $f(\alpha) = e^{\beta\alpha + \gamma\alpha^2 + \delta\alpha^3}$ is the phase function, and ϖ_o is the average particle single scattering albedo. I is the radiance and has units of W/m²/nm/sr. $J = \pi F$ is the

This document is a NASA working document and is subject to further revision. This document been reviewed for release to the public and is not export controlled.

collimated (sun) light (irradiance) and has units of $W/m^2/nm$. Strictly speaking I/\mathcal{F} is a dimensionless quantity (\mathcal{F} has units of $W/m^2/nm/steradian$ and π here has units of steradian).

1. Model BRDFs for 2008 EV₅

The quantities $BRDF$ and $RADF$ (or $[I/\mathcal{F}]$) of EV₅ would be of particular interest to the ARRM instrument guidance & navigation control teams when selecting a multi-ton boulder from the

surface. In what follows is the empirical Lommel-Seeliger model for use in predicting the $[I/\mathcal{F}]$ (i, e, α) of EV₅, using the methodology adopted for OSIRIS-REx target asteroid (101955) Bennu [Takir et al., 2015]. The model inputs and their errors are shown in Table 12. Table 13 shows the Lommel-Seeliger model for nominal, maximum, and minimum predicted brightness of EV₅ at 550 nm. Table 12 shows the model fits to the data. The Lommel-Seeliger model is also useful for predicting flux and brightness quantities for EV₅ at a wide range of view geometries, which can provide important information to engineers designing ARM instruments (Table 13).

Table 12: Description of inputs used to reproduce nominal, maximum, and minimum models.

	Maximum Brightness	Nominal Brightness	Minimum Brightness
	Reduced Magnitude (Vmag-error)*	Reduced Magnitude (Vmag)*	Reduced Magnitude (Vmag+error)*
Diameter (km)**	0.357	0.385	0.413

*The Vmag values are from the Minor Planet Center with uncertainties of ± 0.5 .

**EV₅'s average diameter computed by Busch et al. 2011 and Ali Lagoa et al. 2013.

For the nominal model, the Reduced Vmag values also include NEAR spacecraft data of Mathilde (as the best available proxy data) at the lowest and highest phase angles (Clark et al. 1999). The Minimum and Maximum models capture the scatter in the moderate phase angle ground-based observations of EV₅, and the uncertainties in the size and the low and high phase-angle behavior.

Table 13: Lommel-Seeliger functions that predict $[I/\mathcal{F}](i,e,\alpha)$ of EV₅ at 550 nm.

	A_{LS}	β^{**}	γ^{**}	δ^{**}
Nominal	0.085	-4.37×10^{-2}	4.19×10^4	-2.02×10^{-6}
Maximum	0.091	-1.61×10^{-2}	-0.05×10^8	-0.13×10^8
Minimum	0.032	-2.39×10^{-2}	1.16×10^4	-5.97×10^7

** $f(\alpha) = e^{\beta\alpha + \gamma\alpha^2 + \delta\alpha^3}$. The values given in this table for β , γ , and δ were derived for phase angle values in units of degrees.

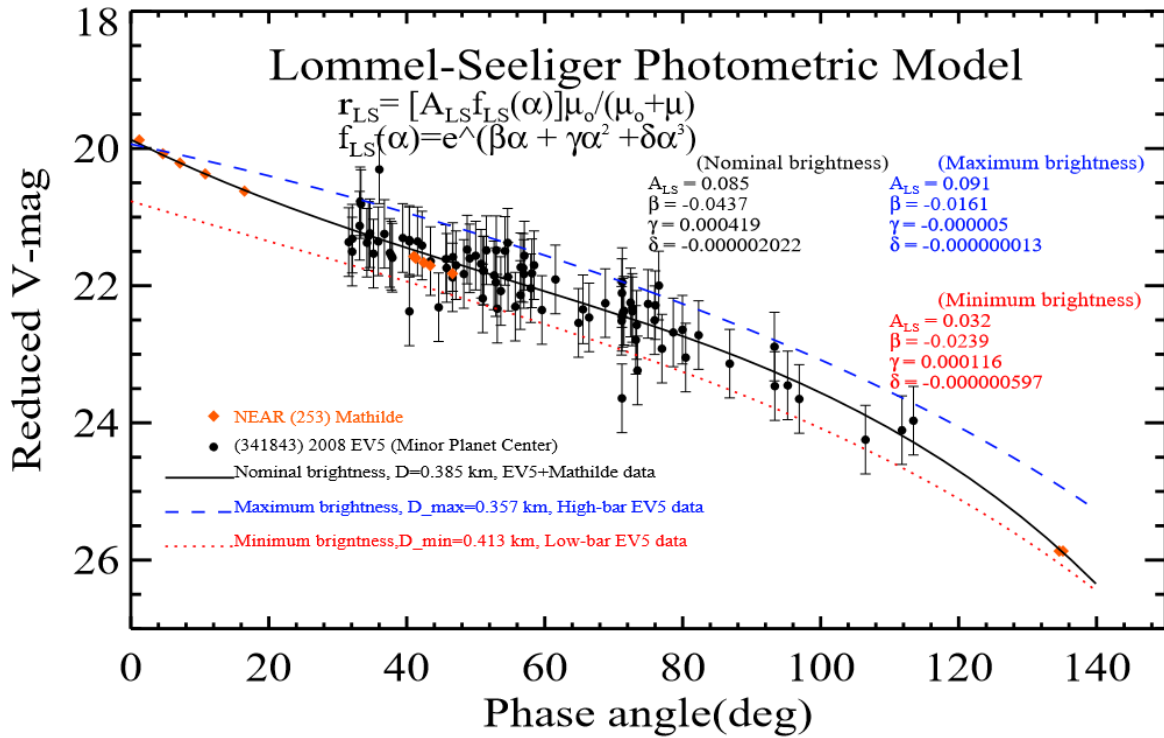


Figure 15: The Reduced V magnitude of EV₅ as a function of phase angle predicted by the Lommel-Seeliger model is shown compared with the ground-based measurements. Shown are the minimum (red dots), maximum (blue dashes), and nominal (black solid line) models. Our minimum and maximum models do not include the Mathilde data, however our nominal model does). Reflectance r_{LS} is in units of sr^{-1} .

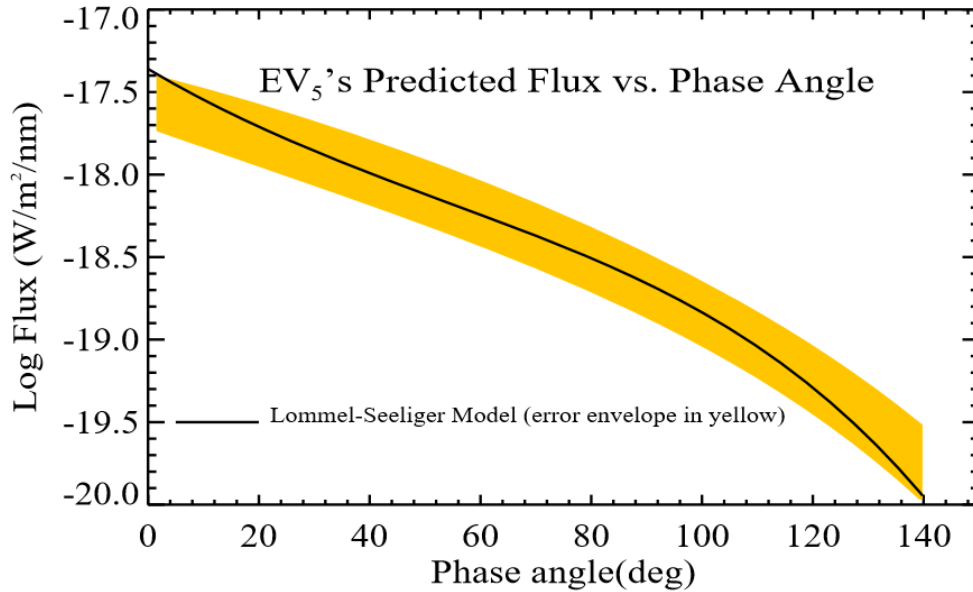


Figure 16: The logarithm of flux in W/m²/nm as a function of phase angle predicted by the Lommel-Seeliger model (black solid fit with a yellow error envelope) at 550 nm.

2. Geometric Albedo, Phase Integral, and Spherical Albedo for EV₅

The minimum and maximum models capture the uncertainties in the size of EV₅, its low and high phase-angle behavior, and the scatter in the moderate phase angle ground-based observations of EV₅. Using the Lommel-Seeliger model minimum, maximum, and nominal geometric albedo (A_{geo}), phase integral (q), and spherical albedo (A_{sph}) for EV₅ are computed, using the methodologies described in Takir et al. [2015] (Table 14). The spherical albedo and phase integral are important quantities to compute the bolometric Bond albedo map, used for making temperature predictions across the surface of EV₅ during the boulder acquisition events, as well as for thermal inertia calculations.

Table 14: EV₅'s geometric albedo, phase integral, and spherical albedo.

	Geometric Albedo (A_{geo})	Phase Integral (q)	Spherical Albedo (A_{sph})
Lommel-Seeliger Model	$0.133^{+0.010}_{-0.083}$	$0.39^{+0.16}_{+0.15}$	$0.052^{+0.027}_{-0.021}$

References

- Alí-Lagoa et al. 2013. Thermophysical Properties of near-Earth Asteroid (341843) 2008 EV₅ from WISE Data. *Astronomy & Astrophysics* 561, A45.
- Busch, M.W. et al. 2011. Radar Observations and the Shape of Near-Earth Asteroid 2008 EV₅. *Icarus* 212, 649-660.
- Clark, B.E., Veverka, J., Helfenstein, P., Thomas, P. C.; Bell, J. F., Harch, A.,

This document is a NASA working document and is subject to further revision. This document has been reviewed for release to the public and is not export controlled.

- Robinson, M. S., Murchie, S. L., McFadden, L. A., Chapman, C. R. 1999. NEAR Photometry of Asteroid 253 Mathilde. *Icarus* 140, 53-65.
- Hapke, B. 2012. *Theory of Reflectance and Emittance Spectroscopy*. Cambridge University Press.
- Takir, D. et al. 2015. Photometric models of disk-integrated observations of the OSIRIS-REx target Asteroid (101955) Bennu. *Icarus* 252, 393-399.

Appendix B1: Full Response on the Boulder Spatial and Size Distributions

What is the expected size-frequency distribution for boulders on 2008 EV₅?

- **Based on the current radar data, what can be said about the size-frequency distribution for boulders on 2008 EV₅?**

Wordsmithed excerpts from write-up provided by Michael Busch [See Appendix B2]:

Boulders of a wide range of sizes, from ~100 m to sub-meter cobbles, are present in large numbers on the surfaces of all three NEAs so far visited by spacecraft (Eros, Itokawa, and Toutatis). This is consistent with NEAs being derived from products of the collisional cascade in the main asteroid belt: NEAs larger than 100–200 m in diameter are predominately rubble pile aggregates.

Boulders are evident in radar images of a large number of NEAs. They appear as single or small clumps of radar-bright pixels that track with a target asteroid's rotation, indicating features on the asteroid's surface, and that are offset from the rest of the radar echo, indicating that they are high-standing relative to the surface around them. The interpretation of such radar-bright features as boulders is verified by comparison between 2012 radar images of Toutatis and optical images of Toutatis from the Chang'E-2 spacecraft (Figure 17 and Figure 18).

This document is a NASA working document and is subject to further revision. This document been reviewed for release to the public and is not export controlled.

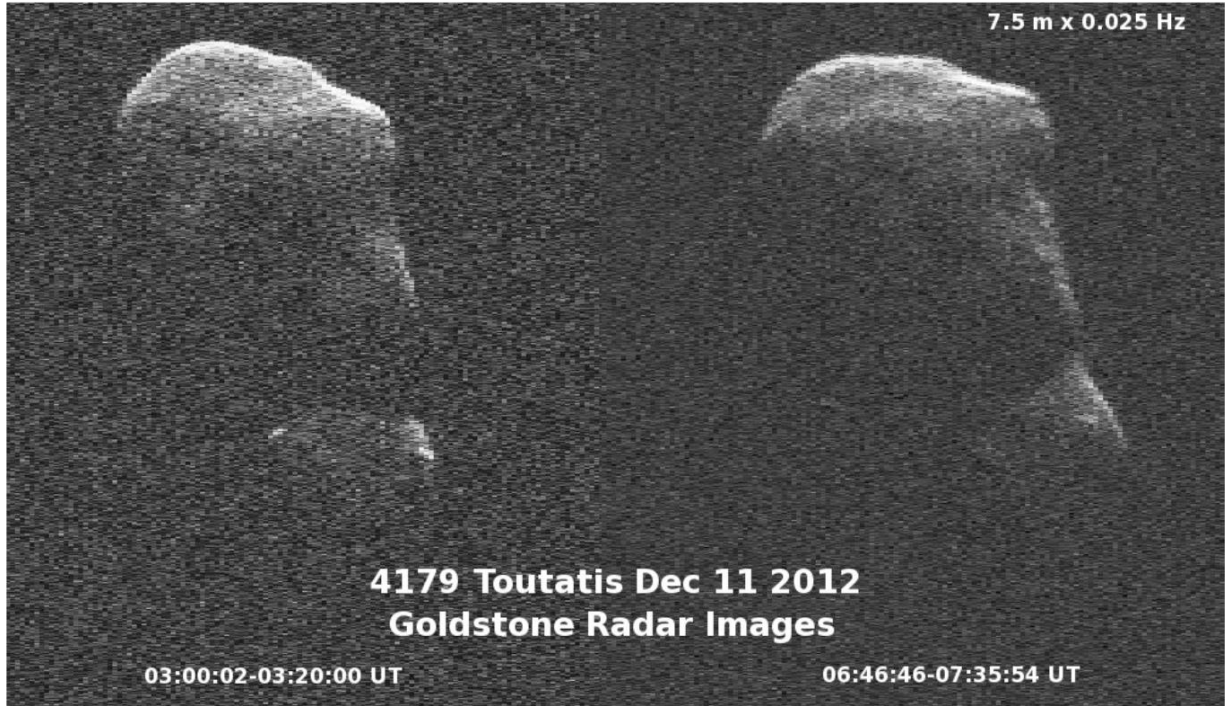


Figure 17: Radar images of Toutatis showing the bright features that are interpreted as boulders [JPL, 2015].



Figure 18: Optical image of Toutatis taken from the Chang'E-2 spacecraft [Zou, 2014].

Boulders have been seen on more asteroids as the resolution of radar images has improved. For a review of radar images of boulders on NEAs, see Benner et al. [2015].

Radar observations also provide very approximate information on the presence of cobbles on the scale of the radar wavelength, 0.035 m for the Goldstone Solar System Radar and 0.126 m for the Arecibo Radar, by measuring the radar scattering properties of the surface. See Nolan et al. [2013] for discussion.

This document is a NASA working document and is subject to further revision. This document has been reviewed for release to the public and is not export controlled.

2008 EV₅ made an 8.4 lunar distance (0.022 AU, 3.2 million km) flyby of Earth on 2008 December 23, and was observed with ground-based astronomical radars over 2008 December 16–27. The highest-resolution radar images were obtained with Arecibo during 2008 December 23–27 and have resolution of 7.5 m in range from Earth. Details of the radar observing campaign and discussion of 2008 EV₅'s trajectory, spin state, and shape are given in Busch et al. [2011].

The candidate boulders visible in the radar images from 2008 December 23, 26, and 27 appear as unresolved single bright pixels or as two adjacent bright pixels (Fig. 1). Given a range resolution of 7.5 m, an unresolved boulder is less than 15 m in diameter – only the Earthward side of each boulder was illuminated by the radar. Some boulders are visible more than 50 m behind the trailing limb of 2008 EV₅, implying that they are at least 7 m higher than their surroundings. These boulders are described as “10 m scale”.

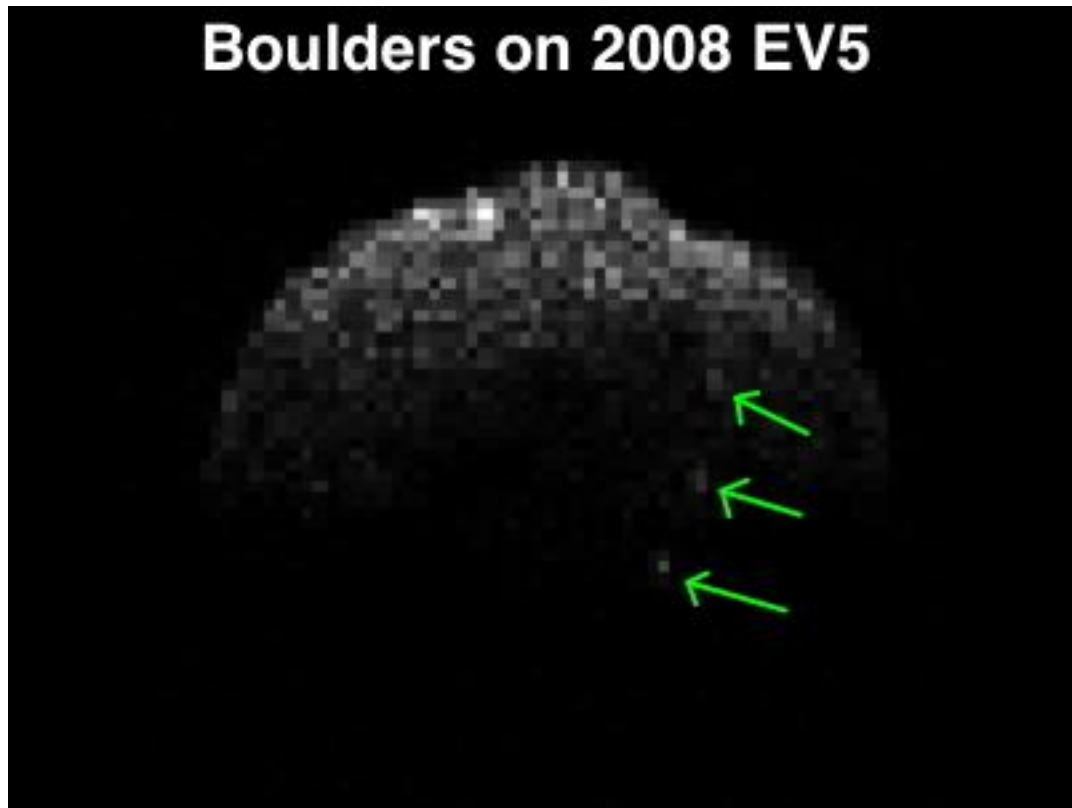


Figure 19: Range-Doppler radar image of 2008 EV₅, obtained at Arecibo Observatory at 2008 December 23 07:41 UT. Range from Earth increases from top to bottom. Image resolution is 7.5 m/pixel in range. The large concavity at 2008 EV₅'s equator is visible at upper right. Green arrows denote three candidate 10-m-scale boulders.

The radar images from 2008 December were all obtained with the subradar point just south of 2008 EV₅'s equator. This means that candidate boulders cannot be identified near the asteroid's north pole or at equatorial latitudes. Near the equator, larger areas of the 2008 EV₅'s surface fall within a given range-Doppler radar pixel and small boulders are lost to confusion with the surface around them. At present, 10-m-scale boulders can be identified over about half of 2008 EV₅'s surface. Finally, the range-Doppler projection has a north-south ambiguity. For most of the candidate boulders identified, there is ambiguity about the hemisphere where they reside. The exception is a prominent

This document is a NASA working document and is subject to further revision. This document has been reviewed for release to the public and is not export controlled.

boulder near the asteroid's south pole (lowest arrow in Figure 19).

With these caveats, it is possible to identify 6 distinct candidate 10-m-scale boulders on 2008 EV₅'s surface by visual inspection of the radar images. At least 10 such boulders likely exist over the asteroid's entire surface.

Based on 2008 EV₅'s radar scattering properties and the highest-resolution images of asteroid surfaces from spacecraft (Eros and Itokawa), there are millions of 10-cm scale cobbles on 2008 EV₅.

If there is a power-law distribution between the two size ranges sampled by the available radar data, as seen on Itokawa and Eros, there are probably a few hundred 3-m scale boulders on 2008 EV₅'s surface. There should be an abundant number of choices for the ARV.

End excerpts

Figure 20 is a plot of the cumulative number of boulders greater than or equal to a given diameter normalized by the count area versus boulder diameter. Data for global and local counts of Eros and Itokawa are shown, in addition to local counts of Phobos. The equivalent data points for 10-m and 10-cm boulders on 2008 EV₅ based on radar observations are also plotted. The 10-m 2008 EV₅ data point lies on top of the Eros global dataset. If it is assumed that there is a power-law distribution of boulders on 2008 EV₅ that follows that of the Eros global dataset, ~16,000 1–5 m boulders (~1,300 2–3 m boulders) on the surface of 2008 EV₅ would be expected. If it is assumed that there is a power-law distribution of boulders on 2008 EV₅ that connects the radar 10-m data to the radar 10-cm data, ~3,000 1–5 m boulders (~360 2–3 m boulders) on the surface of 2008 EV₅ would be expected. Please note that there are major assumptions made to derive these estimates. The following equations can be used to calculate the cumulative number of boulders per m² on 2008 EV₅ (to calculate the number for the whole asteroid, multiply by the surface area, 540,000 m²; to calculate the number of boulders in a given range, subtract the total from the larger diameter from the total from the smaller diameter):

Lower line (connecting 2008 EV₅ 10-m radar boulders to 10-cm roughness):

$$(\text{Cumulative \# boulders } \geq D)/\text{m}^2 = (5.8438\text{e-}3)*D^{-2.5}$$

Upper line (connecting 2008 EV₅ 10-m radar boulders to Eros global count):

$$(\text{Cumulative \# boulders } \geq D)/\text{m}^2 = (2.9293\text{e-}2)*D^{-3.2}$$

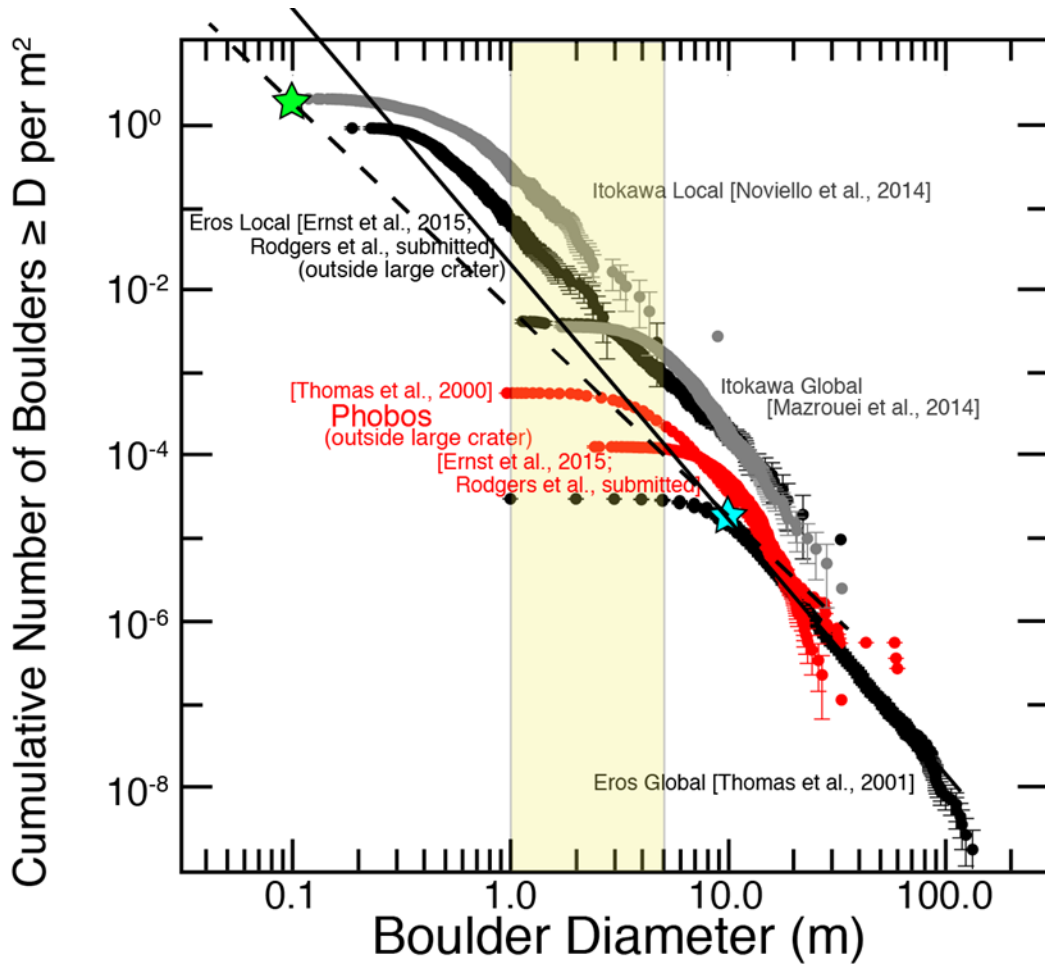


Figure 20: Measured block populations on Eros, Itokawa, and Phobos. The yellow rectangle indicates the 1–5 m boulder size range of interest for the ARRM. The cyan and green stars represent the 10-m boulder observations and the 10-cm cobble size, respectively, for 2008 EV₅ based on radar [Busch write-up, attached]. The surface area of 2008 EV₅, used to normalize the radar boulder counts, is taken to be 540,000 m². The solid line extrapolates from the 10-m 2008 EV₅ data point using the Eros global power-law distribution (-3.2). The dashed line connects the two 2008 EV₅ data points.

- **Can any relevant information be extrapolated from existing data from other C-complex asteroids (i.e., Bennu)?**

The available data to answer this question is limited. The most appropriate data that exist today come from radar studies of 2005 YU₅₅ and 1992 UY₄, small C-complex asteroids in near-Earth space that are possibly organic-rich. Analysis suggests boulders exist on both of those bodies [Benner et al., 2015].

Available in situ asteroid data from spacecraft come from main belt asteroids Mathilde, the ~53 km C-type flyby target of the NEAR mission, and Lutetia, the ~100 km X-complex flyby target of ESA's Rosetta mission. Mathilde was only imaged at 160 m/pixel, insufficient to determine whether boulders exist [Thomas et al., 1999]. Boulders are observed on Lutetia, however Lutetia's precise composition is debated (some favor some kind of high albedo carbonaceous chondrite, while others favor an enstatite chondrite match [Barucci et al., 2015]). Boulders have been observed on bodies that could also be broadly characterized as C-complex: Phobos

This document is a NASA working document and is subject to further revision. This document has been reviewed for release to the public and is not export controlled.

and Deimos, the carbonaceous chondrite-like moons of Mars, as well as comet Churyumov-Gerasimenko, the final destination of the Rosetta mission (Table 15).

Hayabusa2 will arrive at the C-type asteroid Ryugu (formerly 1999 JU₃) in June of 2018. OSIRIS-REx will arrive at the B-type asteroid Bennu in August of the same year. The observations of Bennu and Ryugu will provide critical inputs to the ARRM, not only because these will be the first carbonaceous chondrite asteroids for which high-resolution images are available, but also because they are roughly similar in size and shape to 2008 EV₅. This *may* mean that they have undergone similar evolutions, but this is not definitive. Comparisons of Bennu and Ryugu to Eros and Itokawa will be vital for determining whether what is known from the extensive literature on Eros and Itokawa can reasonably be extrapolated to other near-Earth asteroids (e.g., boulder size-frequency distributions, boulder spatial distributions, etc.), or whether they are not representative. The observations of Bennu and Ryugu will also provide important “ground-truthing” of Earth-based radar observations and have implications for detecting boulders from these types of observations.

That said, OSIRIS-REx and Hayabusa2 will not arrive at Bennu or Ryugu until mid-2018—too late to provide inputs into the mechanical designs and mission requirements, but before the currently scheduled ARRM launch date.

Table 15: Small bodies for which boulder counts have been made from spacecraft imaging. The minimum boulder sizes measured are directly related to the best image resolution available for a given object.

Name	Mean Diameter (km)	Spectral Type	Min boulder size of global count (m)	Min boulder size of regional count (m)	Power law found	Data source	References
Eros	17	S	15	0.05	-3.2 as low as -2.3 locally	NEAR	Thomas et al., 2001; C. Ernst, personal communication
Itokawa	0.35	S	6	0.1	-3.1 -3.5 as low as -2.2 locally	Hayabusa	Michikami et al., 2010; Mazrouei et al., 2014; Noviello et al., 2014; C. Ernst, personal communication
Toutatis	3	S	n/a	10	n/a	Chang'E-2	Jiang et al., 2015
Lutetia	98	M	n/a	60	-5.0	Rosetta	Küppers et al., 2012;
Ida	31	S	n/a	45	n/a	Galileo	Lee et al., 1996
Phobos	22	D	n/a	~4	-3.3	Viking MGS MEX MRO	Thomas et al., 2000; Ernst et al., 2015; C. Ernst, personal communication
Deimos	12	D	n/a	~4	-3.2	Viking	Lee et al., 1986; C. Ernst, personal communication
Churyumov-Gerasimenko	4	comet	7	n/a	-3.6 global local ranges -2.2 to -4.0	Rosetta	Pajola et al., 2015

The observations of Bennu and Ryugu will provide critical inputs to the ARRM, not only because these will be the first carbonaceous chondrite asteroids for which high-resolution images are available, but also because they are roughly similar in size and shape to 2008 EV₅. This *may* mean that they have undergone

This document is a NASA working document and is subject to further revision. This document has been reviewed for release to the public and is not export controlled.

similar evolutions, but this is not definitive. Comparisons of Bennu and Ryugu to Eros and Itokawa will be vital for determining whether what is known from the extensive literature on Eros and Itokawa can reasonably be extrapolated to other near-Earth asteroids (e.g., boulder size-frequency distributions, boulder spatial distributions, etc.), or whether they are not representative. The observations of Bennu and Ryugu will also provide important “ground-truthing” of Earth-based radar observations and have implications for detecting boulders from these types of observations.

That said, OSIRIS-REx and Hayabusa2 will not arrive at Bennu or Ryugu until mid-2018—too late to provide inputs into the mechanical designs and mission requirements, but before the currently scheduled ARRM launch date.

- **Is it expected that the size-frequency distribution of boulders on 2008 EV₅ follows a power law distribution?**

Power-law fits can be made to boulder fits for bodies where sufficient data are available (see The available data to answer this question is limited. The most appropriate data that exist today come from radar studies of 2005 YU₅₅ and 1992 UY₄, small C-complex asteroids in near-Earth space that are possibly organic-rich. Analysis suggests boulders exist on both of those bodies [Benner et al., 2015]).

Available in situ asteroid data from spacecraft come from main belt asteroids Mathilde, the ~53 km C-type flyby target of the NEAR mission, and Lutetia, the ~100 km X-complex flyby target of ESA's Rosetta mission. Mathilde was only imaged at 160 m/pixel, insufficient to determine whether boulders exist [Thomas et al., 1999]). Boulders are observed on Lutetia, however Lutetia's precise composition is debated (some favor some kind of high albedo carbonaceous chondrite, while others favor an enstatite chondrite match [Barucci et al., 2015]). Boulders have been observed on bodies that could also be broadly characterized as C-complex: Phobos and Deimos, the carbonaceous chondrite-like moons of Mars, as well as comet Churyumov-Gerasimenko, the final destination of the Rosetta mission (Table 15).

Hayabusa2 will arrive at the C-type asteroid Ryugu (formerly 1999 JU₃) in June of 2018. OSIRIS-REx will arrive at the B-type asteroid Bennu in August of the same year. The observations of Bennu and Ryugu will provide critical inputs to the ARRM, not only because these will be the first carbonaceous chondrite asteroids for which high-resolution images are available, but also because they are roughly similar in size and shape to 2008 EV₅. This *may* mean that they have undergone similar evolutions, but this is not definitive. Comparisons of Bennu and Ryugu to Eros and Itokawa will be vital for determining whether what is known from the extensive literature on Eros and Itokawa can reasonably be extrapolated to other near-Earth asteroids (e.g., boulder size-frequency distributions, boulder spatial distributions, etc.), or whether they are not representative. The observations of Bennu and Ryugu will also provide important “ground-truthing” of Earth-based radar observations and have implications for detecting boulders from these types of observations.

That said, OSIRIS-REx and Hayabusa2 will not arrive at Bennu or Ryugu until mid-2018—too late to provide inputs into the mechanical designs and mission requirements, but before the currently scheduled ARRM launch date.

Table 15). A power-law distribution would also be expected for fragments produced by fracturing. However, the value of this power-law is dependent on local geological context, material strength, and possibly boulder size.

This document is a NASA working document and is subject to further revision. This document has been reviewed for release to the public and is not export controlled.

A power-law index is observed for many terrestrial fragmented objects [Turcotte 1997; see also Table 1 in Pajola et al., 2015]. Those materials listed in Pajola et al. [2015] show power laws ranging from -1.89 to -3.54.

Excerpts from Rodgers et al., submitted (also see Ernst et al., 2015)

Analyses of the Surveyor [Cintala and McBride 1995], Viking 1 and 2, Mars Pathfinder, Phoenix, Spirit, Opportunity, and Curiosity landing sites [Golombek and Rapp 1997; Golombek et al. 2003; 2008; 2012; Arvidson et al. 2008] have indicated that for a reasonable difference in size (a factor of several to ten), the size-frequency distribution (SFD) of blocks can be modeled, allowing extrapolation from large-block SFDs measured from orbit to population densities of smaller blocks. By characterizing the larger size range of the block distribution from orbital imaging, the distribution of smaller blocks is estimated. From that estimate, the probability of a lander encountering hazardous blocks can be calculated for a given lander design. Such calculations are used routinely to vet candidate sites for Mars landers [Golombek et al. 2003; 2008; 2012; Arvidson et al. 2008].

Global and local block SFDs for Eros, Itokawa, and Phobos are shown in Figure 20. Remarkably, the distributions of blocks from 0.5 to 100 m in diameter are on average well fit by a power-law slope on the order of -3 regardless of block scale. Some deviations in slope are apparent regionally, and for differing block size ranges. There are also some variations in absolute block densities, but broadly the slopes remain consistent from body to body.

The Mars Orbiter Camera (MOC) on Mars Global Surveyor obtained a small number of high-resolution images of Phobos useful for measuring blocks 5 m or larger in size. These images are concentrated in the area just east of Stickney crater, in an area interpreted to contain blocky ejecta from that crater [Thomas et al. 2000]. Block counts performed by Thomas et al. [2000] and in this study both indicate a power-law slope similar to those of Eros [Thomas et al. 2001] and Itokawa global counts [Michikami et al., 2010; Mazrouei et al. 2014], with the absolute density of blocks similar to that of global Eros.

In the cases of Eros, Itokawa, and Phobos, the approach of extending the SFD from large, tens-of-meter-sized blocks down to small, tens-of-centimeter-sized blocks using a power-law fit to the large population yields reasonable estimates of small block populations. It is important to note that geologic context matters for the absolute block density – if lower-resolution counts include multiple geologic settings, they will not extrapolate accurately to local areas containing only one setting.

End Excerpts

The power law exponent for the SFD of large boulders on Lutetia is significantly higher than that for Eros, Itokawa, and Phobos (-5.0, Küppers et al., 2012). The local counts of Eros and Itokawa using very high resolution images often yield power-law exponents lower than the global count SFDs. It is unclear whether this indicates a power-law progression from the largest boulder sizes observed (100–300 m) down to the smallest boulder sizes observed (10s of cm).

- **What is the expected distribution of boulder shapes for boulders on 2008 EV₅?**

Mazrouei et al. [2014] measured the aspect ratio for boulders greater than 6-m in diameter on Itokawa (see figure 5 of that paper). Most boulders of this size are found to be elongated with b/a ratios of 0.7 (width/length). The third, vertical dimension of boulders (height) is not visible in most of the

This document is a NASA working document and is subject to further revision. This document has been reviewed for release to the public and is not export controlled.

Hayabusa images. Michikami et al. [2010] report b/a ratios for Itokawa boulders to be 0.62–0.68. Michikami et al. [2014] measured 21 boulders on Itokawa, finding a mean c/a of 0.46.

Table 16 contains a compilation of several reports of fragment dimensions based on laboratory impact experiments. Note that the fragments are not actually 3-axis ellipsoids, they are irregular in shape (see Figure 21).

An open question is whether the aspect ratio would be different for weaker rocks (e.g., those found on a C-type asteroid like 2008 EV₅) and how much of an influence thermal degradation might have.

Table 16: Compilation of fragment ratios b/a and c/a from several publications in the literature. Dimensions are defined to be a ≥ b ≥ c.

Reference	Target	Projectile	Impact Velocity	b/a	c/a
Fujiwara et al. 1978	Basalt	Polycarbonate cylinders	1–4 km/s	0.73	0.50
Capaccioni et al. 1986	Basalt Concrete	Aluminum spheres	9 km/s	0.7 ± 0.15	0.5 ± 0.15
Giblin et al. 1998	Porous ice	Solid ice	6 km/s	0.56–0.71 ± 0.1–0.2	0.40–0.48 ± 0.1–0.2
Durda et al. 2015	Basalt	Aluminum spheres	4–6 km/s	0.72 ± 0.13	0.39 ± 0.13
Michikami et al., 2014*	Basalt	Nylon spheres	1.6–7.0 km/s	0.7	0.5 (catastrophic disruption) 0.2 (impact cratering)

*Michikami et al. [2015] is a short conference abstract, so details are limited.

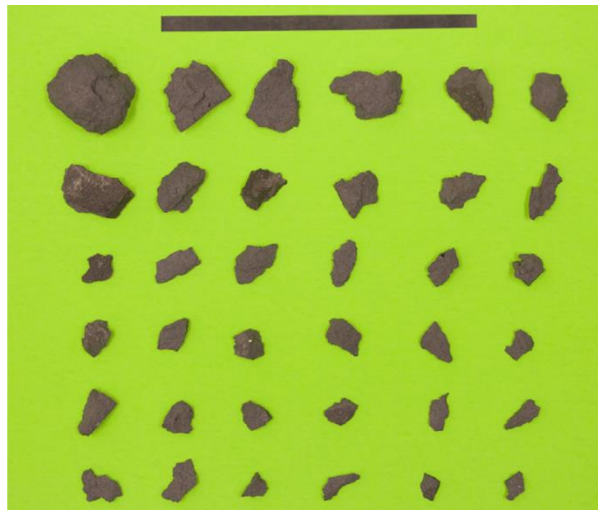


Figure 21: Example of fragment shapes from impact experiments. (This is Durda et al., 2015 figure 4.)

What is the expected spatial distribution of ~1–5 meter boulders on 2008 EV₅?

- **Where on 2008 EV₅ have boulders been detected?**

Approximately half of 2008 EV₅'s surface was observed by radar. Over this area, 6 distinct candidate

This document is a NASA working document and is subject to further revision. This document has been reviewed for release to the public and is not export controlled.

10-m-scale boulders were observed [Busch write-up, attached]. However, due to the nature of the radar data (see also response concerning size-frequency distribution above and the Appendix B2), the location of the boulders cannot be determined, with the exception of one prominent boulder that is located near the asteroid's south pole.

- **Given an assumed number of certain size boulder based on a power law, is there anything that can be said about the spatial distribution of these boulders on an asteroid's surface? (e.g., does spin rate play a role in concentrating certain sized boulders at certain latitudes?)**

Based on the number of observed boulders, cobbles inferred from radar roughness, and assuming a power-law relationship between boulder diameter and cumulative size-frequency distribution, the number of boulders of a given size per area (e.g., Figure 20) can be calculated assuming a roughly uniform distribution across the surface. This information alone does not provide further information about the actual distribution.

On Itokawa, potential lows are "ponds" full of cm-sized cobbles, and most of the boulders are located in other regions of the asteroid. If this is true for 2008 EV₅, concentrations of ponds at the geopotential lows with boulders at higher regions within the geopotential should be expected. The location of these geopotential lows is a strong function of the asteroid density (see Figure 22). For a low density of 1.5 g/cm³, the low will be at the equator and within the putative crater seen in the radar data. For a large density of 2.5 g/cm³, the geopotential low shifts off of the equator and no longer lies within the crater, but instead is at the base of the ridge.

If the boulders are sourced from the likely crater that shows up as a large concavity in the radar shape model, the distribution of the boulders would depend upon ejecta patterns around an irregularly shaped body and would require much more analysis to estimate. However, it is expected that the boulders would preferentially settle in the equatorial or near-equatorial regions.

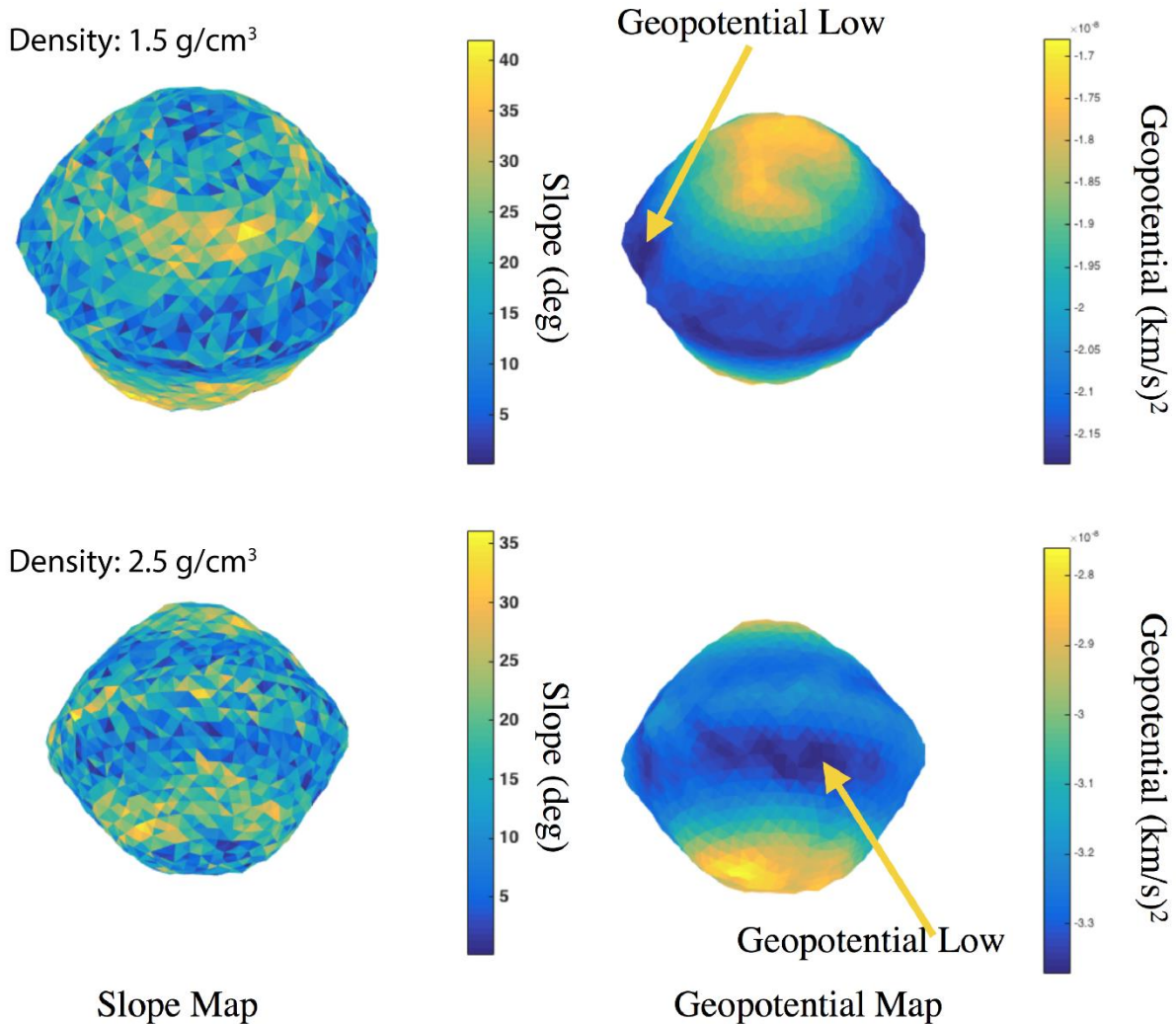


Figure 22: Maps of slope and geopotential for 2008 EV₅ assuming a bulk density of 1.5 g/cm³ (top row) and 2.5 g/cm³ (bottom row). The “lowest point” on the body shifts with the density of the body. At low densities the low is at the equator and in the crater. At higher densities the low is off of the equator and not in the crater. [Scheeres, personal communication]

What is the expected distribution in safe landing areas around ~1–5 m boulders on 2008 EV₅? For a 10-m diameter circle centered on the target boulder what is the expected range and likelihood over that range for the following landing site properties on C-type asteroids?

- **Spatial and size distribution of boulders**

As before, an assumption of the boulder population on 2008 EV₅ using a power law would be needed as a starting point (keep in mind that the “correct” power law to use is not known). Estimates of the number of boulders of a given size in a 10-m diameter circle (area = 78.5 m²) assuming a uniform distribution of boulders across the surface can be made. Reading the numbers off of the y-axis of the plot in Figure 20 will give the number of boulders greater than or equal to a given diameter in a 1-m² area. Multiplying this value by the 78.5 m² area of interest will yield the total number of boulders greater than or equal to a given diameter in a 10-m diameter circle. If the boulders are not roughly uniformly distributed across the surface, more assumptions must be made.

This document is a NASA working document and is subject to further revision. This document has been reviewed for release to the public and is not export controlled.

- **Would the distribution of small 10-cm-size and larger 2- to 3-m diameter boulders be expected to be similar?**

This cannot be known with certainty. Likely, processes acting to move 10-m boulders would be similar to those acting to move 2–3-m boulders, although the responses might differ in that massive objects tend to be more easily fragmented than smaller ones, with strength decreasing with approximately the square root of size, yet require more energetic events to dislodge and accelerate.

- **Local topography**

The radar shape model of 2008 EV₅ has a range resolution of 7.5 meters [Busch et al., 2011]. Therefore, the model can provide local geometric topography to this scale. Outside of boulders and craters, local slopes generally would not be expected to change much from the 7.5-m scale down to the 1-m scale.

- **Dust environment**

Another environmental concern that needs to be considered is the dust environment that could be a potential hazard for instrumentation (e.g., camera lenses, inlets, etc.) and/or systems (seals, joints, exposed bearings, solar panels, etc.). The main hazards associated with the dust environment are: 1. spacecraft sinking during landing and/or ascent, 2. high cohesion between regolith and spacecraft contactpad, 3. electrostatic motion of small dust grains, and 4. Dust and debris created by physical interaction during the boulder capture process (e.g., thruster plume, contact pad interaction, boulder acquisition and separation). The risk of the spacecraft sinking into the regolith during landing or ascent is dependent on the compaction of the regolith (expected packing fraction of 0.59, see discussion in Surface Geotechnical Properties). The compaction of the regolith is expected to be essentially uniform about the body, except immediately next to boulders, where there may be a regolith “apron” [Robinson et al. 2002]. The regolith apron (produced either by the migration of dust or dust production from thermal cycling of the boulder) is unlikely to be deep enough to produce a serious sinking hazard. A discussion of the cohesion between regolith and the spacecraft contactpad is given in the Surface Geotechnical Properties discussion. A regolith apron is likely to be composed of small, uncompacted regolith grains, which would form relatively strong cohesive bonds with the spacecraft. However, the fact that this apron of dust is overlaying the more densely packed surface indicates that the material is likely to fracture during ascent at this striation. The plasma environment while the spacecraft is on the surface remains unknown. In order to minimize the likelihood of contamination of the spacecraft by electrostatically controlled dust, the landing operation should take place close to the subsolar point (to reduce shadows, which can produce strong electric fields) and in a region with few micron-sized and smaller grains (which would be more likely to levitate if detached from the surface) [Hartzell and Scheeres, 2013], as investigated by multispectral photometry.

- **What other properties should ARM be concerned with?**

Local slopes will have influence over landing site safety beyond the implications for hazards to the solar arrays. Tipping hazards will be present that could seriously affect the landing operations. The highest resolution images of Eros at pixel scales of 0.014–0.027 m (Figure 23) reveal a complex geomorphology at the sub-meter scale, especially in the flat areas where sample collection would otherwise be the easiest (e.g., the idealized flat, competent area with a 3-m boulder just sitting there). Eros-sized asteroids have abundant fine materials compared to smaller asteroids, which are coarser due to winnowing by solar wind

This document is a NASA working document and is subject to further revision. This document has been reviewed for release to the public and is not export controlled.

and radiation effects [Hartzell and Scheeres, 2013]. The sweeping of fines ejected by electrostatic forces, impact vibrations, and thermal shocks leaves behind coarser material in the lag deposits of asteroids.

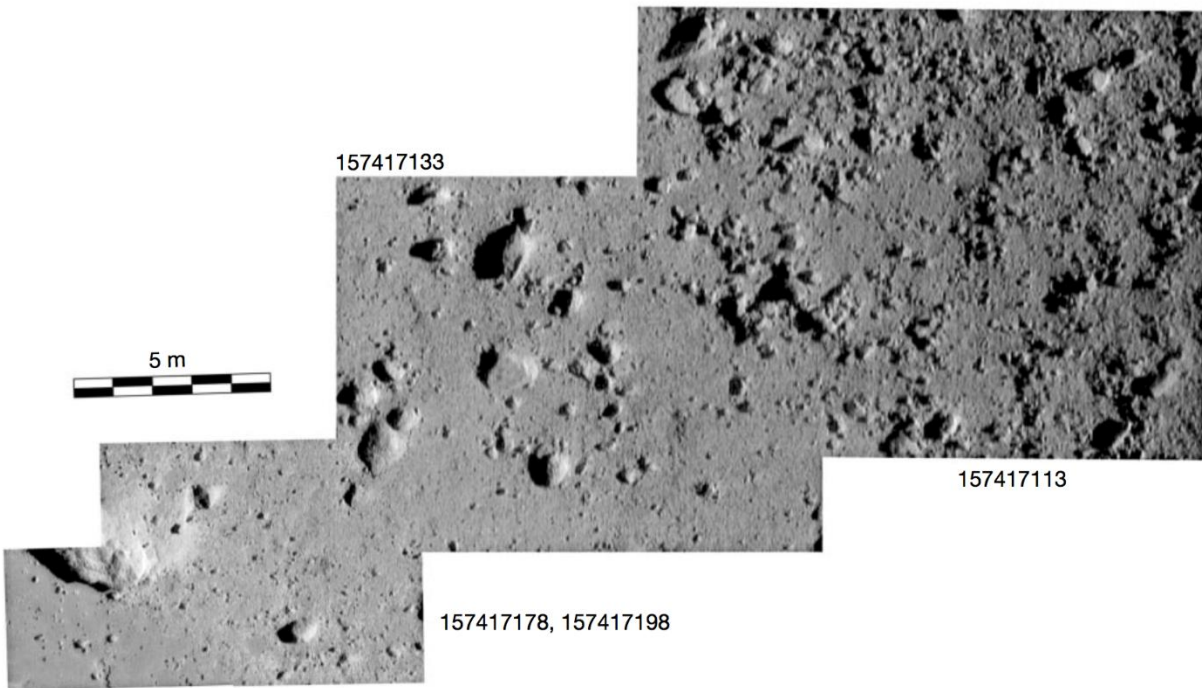


Figure 23: The last four descent-sequence NEAR images of Eros. The pixel scale of these images ranges from 0.014–0.027 m. (This is Veverka et al., 2001 figure 3.)

Steep cratered topography is not prevalent on small asteroids; most small bodies seen up close and with radar appear to conform (within some reasonable angle of repose) to equilibria of figure. On Itokawa, the smallest asteroid for which there are good images, there are very few craters [Hirata et al., 2009]. On Eros, seismic shaking has acted to erase many (though not all) craters less than 100-m in diameter [Chapman et al., 2002; Thomas and Robinson, 2005], and by implication other loose topography at that scale. By implication Eros' regolith is loose to 100 meters, perhaps globally [Robinson et al., 2002]. A thick mobile regolith would also explain the relatively flat topography; less than 5% of the surface of Eros is steeper than 30° [Zuber et al., 2000].

Therefore generally speaking, relatively flat, boulder-populated areas are predicted on 2008 EV₅; however the nature of these flat areas at the spatial scale of the landing pads (~1 m) requires careful consideration (see response on Surface Geotechnical Properties). For a landing velocity exceeding the crushing stress of the particulate regolith surface, the asteroid material might fluidize and slide out of the way of the lander legs, instead of holding in place to support it, so care must be taken that the landing is done with minimal deceleration and little vibration.

What is the expected distribution in depth of burial for ~1–5 m boulders on 2008 EV₅?

- **Based on the theories of how asteroids and boulders form and evolve, is there anything that can be said about the likely range or distribution of burial depths?**

This document is a NASA working document and is subject to further revision. This document has been reviewed for release to the public and is not export controlled.

Due to the nature of spacecraft images of Eros and Itokawa, there is minimal information with regard to the burial of boulders on their surfaces. Regolith does migrate on asteroids, either from potential highs to lows (e.g., Itokawa) or via crater ejecta (probably less important on smaller objects, as a lot of ejecta is likely to exceed escape velocity).

A minimum regolith depth of 20–40 m on Eros has been estimated based on the excavated volume of all large craters [Thomas et al., 2001]. Geomorphic observations indicate 50–100 m regolith depth, possibly globally [Robinson et al., 2002]. On Itokawa, regolith depth estimates find a minimum of ~2.3 m in the lowlands, based on roughness measurements [Barnouin-Jha et al., 2008], transitioning to a global rubble pile [Fujiwara et al., 2006].

- **Is there a way to determine/estimate the depth of burial from the visual images from the characterization phase?**

Boulders formed in fragmentation events have an average aspect ratio a:b:c of 1:0.7:0.5 (2:√2:1) (Table 16). Assuming these shapes, burial estimates could be made based on three-dimensional images taken by the ARV. If the boulder's maximum dimension parallel to the ground does not coincide with the intersection with the regolith, a symmetric shape to the boulder could be assumed and a depth of burial estimated. Three-dimensional images of the boulder will be essential for this characterization. Observations of the distribution of regolith and surface slopes/potential could help to inform whether regolith has moved into/out of the area and may have buried boulders.

- **What other ways are there to determine/estimate the depth of burial from the visual images from the characterization phase? What other ways are there to determine/estimate the depth of burial *in situ*?**

Seismic shaking can dislodge and transport boulders from depth [Asphaug et al. 2001; Miyamoto et al. 2007] as part of a convective size-sorting (Brazil-nut effect and related mechanisms). Deflation can leave behind exposed surface structures like remnants and clods. Many such apparent clasts might not be suitable for ARRM boulder retrieval (too weak). Embedded boulders emerging from the subsurface could be more difficult to extract than boulders that have been tossed downhill onto existing regolith surfaces. Identifying boulders that have survived ejection or been scattered by landslide movements, and to avoid exclusively focusing on boulders buried in smooth sediments. Boulders found in rougher, higher-energy environments would be stronger on average than clasts found randomly in regolith, and would be subject to much lower possibility of small particulate cementation. Among these, boulders that further show evidence for meteoroid fragmentation and spallation would indicate greatest competency. A sampling approach that is able to operate in a boulder-strewn environment is likely to find very many strong, suitably sized boulders to choose from.

If a flat operational environment is required, such as a gravel-field with an isolated boulder or a wide margin, then cohesion of the regolith is more of a concern. Cementation of discrete boulders by regolith can possibly be detected by thermal imaging, as generally speaking, a boulder cohesively coupled to the regolith would also be thermally coupled. This might show up as conductive cooling on week-long timescales. In principle this rock/regolith thermal coupling can be investigated by thermal cameras before the sampling is conducted, to help in selecting among candidate boulders.

This document is a NASA working document and is subject to further revision. This document has been reviewed for release to the public and is not export controlled.

Laser altimeter data could also be used to measure the heights of boulders, thus measuring the short-axis ('c') dimension. This could be compared to the expected 'a' dimension, other boulders on 2008 EV₅, other boulders on Itokawa, and expected impact fragment dimensions (see Table 16) to place estimates on burial (e.g., Figure 24).

Ground Penetrating Radar (GPR) is another approach [e.g., Hamran et al., 2014] that is a promising tool for rock and hazard avoidance. Generally the technique is capable of imaging dielectric contrasts through a few meters of loose rocky material; however the imaging technique works best for a background material with relatively uniform dielectric properties. So it would be a good choice for imaging boulders embedded in beds of dust, for instance, but not for imaging the specific configurations of boulders within blocky landslides and ejecta deposits, for which multiple scattering effects diminish the signal. Seen as an added investigation, GPR would be of good value in that it would provide essential contrast and mitigate risks in dusty environments where the temptation will be to land (because it is flat), and because it can obtain subsurface context wherever the sample is acquired. The added mass and cost of such an instrument is not insubstantial, but the most critical operational aspect is the possibly low SNR of the measurements. The radar electronics and antenna have to be isolated from the spacecraft electronics, which can become a strong source of noise, especially when motors are involved. The spacecraft itself is a strong radar reflector, and due to the relatively omnidirectional nature of GPR, it is challenging to image boulders in close proximity if they are comparable in size to the major spacecraft elements. If 2008 EV₅ is the target asteroid, and if the CR-designation holds, then the high metallic content of analogous materials would lead to a radar response that might enhance meter-scale imaging by providing strong contrasts (e.g., a metallic lag beneath silicate dust) or obscure imaging by scattering and attenuation.

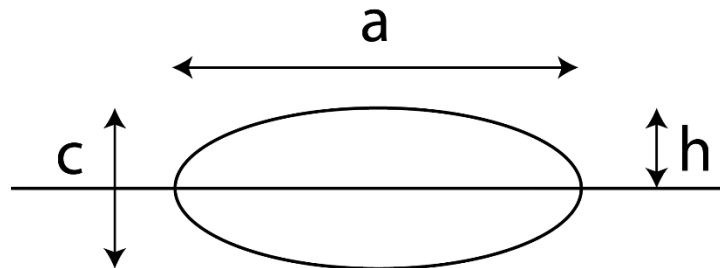


Figure 24: Example of a buried boulder. The dimension h could be measured with a laser altimeter and the dimension a could be measured with a camera. By assuming a typical $a:c$ ratio from other boulders on the body, from boulders on Itokawa, or from impact fragment experiments, the dimension c could be calculate, and the depth of burial estimated.

References:

- Arvidson, R. et al., 2008. Mars exploration program 2007 Phoenix landing site selection and characteristics, *Journal of Geophysical Research* 113, E00A09.
- Asphaug, E., King, P.J., Swift, M.R., Merrifield, M.R., 2001. Brazil nuts on Eros: Size-sorting of asteroid regolith. *LPSC 32*, #1708.
- Barnouin-Jha, O.S., Cheng, A.F., Mukai, T., Abe, S., Hirata, N., Nakamura, R., Gaskell, R.W., Saito, J., Clark, B.E., 2008. Small-scale topography of 25143 Itokawa from the Hayabusa laser altimeter. *Icarus* 198, 108–124.

- Benner, L.A.M., Busch, M.W., Giorgini, J.D., Taylor, P.A., Margot, J.-L., 2015. Radar observations of near-Earth and main-belt asteroids. In: Asteroids IV, in press. [http://http://echo.jpl.nasa.gov/asteroids/benner.etal.radar.chapter.20150728.pdf](http://echo.jpl.nasa.gov/asteroids/benner.etal.radar.chapter.20150728.pdf)
- Busch, M.W., Ostro, S.J., Benner, L.A.M., Brozovic, M., Giorgini, J.D., Jao, J.S., Scheeres, D.J., Magri, C., Nolan, M.C., Howell, E.S., Taylor, P.A., Margot, J.-L., Briske, W., 2011. Radar observations and the shape of near-Earth asteroid 2008 EV₅. *Icarus* 212, 649–660.
- Capaccioni, F., Cerroni, P., Coradini, M., Di Martino, M., Farinella, P., Flamini, E., Martelli, G., Paolicchi, P., Smith, P.N., Woodward, A., Zappala, V., 1986. Asteroidal catastrophic collisions simulated by hypervelocity impact experiments. *Icarus* 66, 487–514.
- Chapman, C.R., Merline, W.J., Thomas, P.C., Joseph, J., Cheng, A.F., Izenberg, N., 2002. Impact history of Eros: Craters and boulders. *Icarus* 155, 104–118.
- Cintala, M.J., McBride, K.M., 1995. Block distributions on the lunar surface: A comparison between measurements obtained from surface and orbital photography. NASA Technical Memorandum 104804, 1–41.
- Durda, D.D., Bagatin, A.C., Aleman, R.A., Flynn, G.J., Strait, M.M., Clayton, A.N., Patmore, E.B., 2015. The shapes of fragments from catastrophic disruption events: Effects of target shape and impact speed. *Planetary and Space Science* 107, 77–83.
- Ernst, C.M., Rodgers, D.J., Barnouin, O.S., Murchie, S.L., Chabot, N.L., 2015. Evaluating small body landing hazards due to blocks. LPSC 46, #2095.
- Fujiwara, A., Kamimoto, G., Tsukamoto, A., 1978. Expected shape distribution of asteroids obtained from laboratory impact experiments. *Nature* 272, 602–603.
- Fujiwara, A. et al., 2006. The rubble-pile asteroid Itokawa as observed by Hayabusa. *Science* 312, 1330–1334.
- Giblin, I., Martelli, G., Farinella, P., Paolicchi, P., Di Martino, M., Smith, P.N., 1998. The properties of fragments from catastrophic disruption events. *Icarus* 134, 77–112.
- Golombek, M., Rapp, D., Size-frequency distributions of rocks on Mars and Earth analog sites: Implications for future landed missions. *Journal of Geophysical Research* 102, 4117–4129.
- Golombek, M.P., Haldermann, A.F.C., Forsberg-Taylor, N.K., DiMaggio, E.N., Schroeder, R.D., Jakosky, B.M., Mellon, M.T., Matijevic, J.R., Rock size-frequency distributions on Mars and implications for MER landing safety and operations, *Journal of Geophysical Research* 108, 8086.
- Golombek, M.P., et al., 2008. Size-frequency distributions of rocks on the northern plains of Mars with special reference to Phoenix landing surfaces. *Journal of Geophysical Research* 113, E00A09.
- Golombek, M., Huertas, A., Kipp, D., Calef, F., 2012. Detection and characterization of rocks and rock distribution at the final four Mars Science Laboratory landing sites, Mars 7, 1–22.
- Hamran, S.E., Amundsen, H.E.F., Carter, L.M., Ghent, R.R., Kohler, J., Mellon, M.T., Paige, D.A., 2014. The RIMFAX ground penetrating radar on the Mars 2020 rover. AGU Fall Meeting, #P11A-3746.
- Hartzell, C.M., Scheeres, D.J., 2013. Dynamics of levitating dust particles near asteroids and the Moon. *Journal of Geophysical Research: Planets* 118, 116–125.
- Hirata, N., Barnouin-Jha, O.S., Honda, C., Nakamura, R., Miyamoto, H., Sasaki, S., Demura, H., Nakamura, A.M., Michikami, T., Gaskell, R.W., Saito, J., 2009. A survey of possible impact structures on 25143 Itokawa. *Icarus* 200, 486–502.
- Jiang, Y., Ji, J., Huang, J., Marchi, S., Li, Y., Ip, W.-H., 2015. Asteroid 4179 Toutatis: Boulders distribution as closely flew by Chang'E-2. IAU General Assembly Meeting 29, #2256175.
- JPL. http://echo.jpl.nasa.gov/asteroids/Toutatis2012/Toutatis2012_planning.html. 2012 Goldstone Radar Observations of (4179) Toutatis. Accessed November 19th, 2015.
- Küppers, M., Moissl, R., Vincent, J.-B., Besse, S., Hviid, S.F., Carry, B., Grieger, B., Sierks, H., Keller, H.U., Marchi, S., the OSIRIS team, 2012. Boulders on Lutetia. *Planetary and Space Science* 66, 71–78.

- Lee, S.W., Thomas, P., Veverka, J., 1986. Phobos, Deimos, and the Moon: Size and distribution of crater ejecta blocks. *Icarus* 68, 77–86.
- Lee, P., Veverka, J., Thomas, P.C., Helfenstein, P., Belton, M.J.S., Chapman, C.R., Greeley, R., Pappalardo, R.T., Sullivan, R., 1996. Ejecta blocks on 243 Ida and on other asteroids. *Icarus* 120, 87–105.
- Mazrouei, S., Daly, M.G., Barnouin, O.S., Ernst, C.M., DeSouza, I., 2014. Block distributions on Itokawa. *Icarus* 229, 181–189.
- Michikami, T., Nakamura, A.M., Hirata, N., 2010. The shape and distribution of boulders on Asteroid 25143 Itokawa: Comparison with fragments from impact experiments. *Icarus* 207, 277–284.
- Michikami, T., Yoshida, A., Shimada, A., Tsuchiyama, A., Hasegawa, S., 2014. The shapes of fragments and the impact energy: Implications for asteroid Itokawa. *Asteroids, Comets, and Meteors*.
- Miyamoto, H. et al., 2007. Regolith migration and sorting on asteroid Itokawa. *Science* 316, 1011–1014.
- Nolan, M.C., Magri, C., Howell, E.S., Benner, L.A.M., Giorgini, J.D., Hergenrother, C.W., Hudson, R.S., Lauretta, D.S., Margot, J.-L., Ostro, S.J., Scheeres, D.J., 2013. Shape model and surface properties of the OSIRIS-REx target asteroid (101955) Bennu from radar and lightcurve observations. *Icarus* 226, 629–640.
- Noviello, J.L., Barnouin, O.S., Ernst, C.M., Daly, M., 2014. Block distribution on Itokawa: Implications for asteroid surface evolution. *LPSC 45*, #1587.
- Pajola, M. et al., 2015. Size-frequency distribution of boulders ≥ 7 m on comet 67P/Churyumov-Gerasimenko. *Astronomy and Astrophysics*, <http://dx.doi.org/10.1051/0004-6361/201525975>.
- Robinson, M.S., Thomas, P.C., Veverka, J., Murchie, S.L., Wilcox, B.B., 2002. The geology of 433 Eros. *Meteoritics and Planetary Science* 37, 1651–1684.
- Rodgers, D.J., Ernst, C.M., Barnouin, O.S., Murchie, S.L., Chabot, N.L., 2015 (submitted). Methodology for finding and evaluating small body landing sites. *Planetary and Space Science*, submitted.
- Thomas, P.C., Robinson, M.S., 2005. Seismic resurfacing by a single impact on the asteroid 433 Eros. *Nature* 436, 366–369.
- Thomas, P.C., Veverka, J., Bell, J.F., Clark, B.E., Carcich, B., Joseph, J., Robinson, M., McFadden, L.A., Malin, M.C., Chapman, C.R., Merline, W., Murchie, S., 1999. Mathilde: Size, shape, and geology. *Icarus* 140, 17–27.
- Thomas, P.C., Veverka, J., Sullivan, R., Simonelli, D.P., Malin, M.C., Caplinger, M., Hartmann, W.K., James, P.B., 2000. Phobos: Regolith and ejecta blocks investigated with Mars Orbiter Camera images. *Journal of Geophysical Research* 105, 15091–15106.
- Thomas, P.C., Veverka, J., Robinson, M.S., and Murchie, S., 2001. Shoemaker crater as the source of most ejecta blocks on the asteroid 433 Eros. *Nature* 413, 394–396.
- Turcotte, D.L., 1997. *Fractals and chaos in geology and geophysics*. Cambridge University Press, Cambridge, 398p.
- Veverka, J. et al., 2001. The landing of the NEAR-Shoemaker spacecraft on asteroid 433 Eros. *Nature* 413, 390–393.
- Zou, X., Li, C., Liu, Wang, J.W., Li, H., and Ping, J. The preliminary analysis of the 4179 Toutatis snapshots of the Chang'E-2 flyby. (2014) *Icarus*, 229, 348-354.
- Zuber, M.T., et al., 2000. The shape of 433 Eros from the NEAR-Shoemaker laser rangefinder. *Science* 289, 2097–2101.

This document is a NASA working document and is subject to further revision. This document has been reviewed for release to the public and is not export controlled.

Appendix B2: Input from Michael Busch concerning Boulders on 2008 EV₅

Note: Input from non-FAST members have not been edited and are included as they were received.

Boulders on the Surface of 2008 EV₅

Michael W. Busch
SETI Institute, Mountain View, California
Prepared 2015 September 17

The near-Earth asteroid (NEA) 2008 EV₅ was discovered on 2008 March 4 by the Catalina Sky Survey. EV₅ made an 8.4 lunar distance (0.022 AU, 3.2 million km) flyby of Earth on 2008 December 23, and was observed with ground-based astronomical radars over 2008 December 16-27. The highest-resolution radar images were obtained with Arecibo during 2008 December 23-27 and have resolution of 7.5 m in range from Earth.

Details of the radar observing campaign and discussion of EV₅'s trajectory, spin state, and shape are given in Busch et al. 2011 (Icarus 212, 649-660, available at <http://echo.jpl.nasa.gov/asteroids/2008EV5/busch.etal.2011.2008ev5.pdf>). EV₅'s overall shape is a 400-m spheroid with an equator-aligned ridgeline broken by a single ~150 m concavity. Infrared spectroscopy suggests a composition analogous to CM meteorites (Reddy et al. 2012, Icarus 221, 678-681, available at <http://arxiv.org/abs/1209.1207>).

Boulders on NEAs

Boulders or blocks of a wide range of sizes, from ~100 m to sub-meter cobbles, are present in large numbers on the surfaces of all three NEAs so far visited by spacecraft (Eros, Itokawa, and Toutatis). This is consistent with NEAs being derived from products of the collisional cascade in the main asteroid belt: NEAs larger than 100-200 m in diameter are predominately rubble pile aggregates.

Boulders are evident in radar images of a large number of NEAs. They appear as single or small clumps of radar-bright pixels that track with a target asteroid's rotation, indicating features on the asteroid's surface, and that are offset from the rest of the radar echo, indicating that they are high-standing relative to the surface around them. The interpretation of such radar-bright features as boulders is verified by comparison between 2012 radar images of Toutatis and optical images of Toutatis from the Chang'E-2 spacecraft.

Boulders have been seen on more asteroids as the resolution of radar images has improved. For a review of radar images of boulders on NEAs, see Benner et al. 2015 (Asteroids IV, in press, available at <http://echo.jpl.nasa.gov/asteroids/benner.etal.radar.chapter.20150728.pdf>).

Radar observations also provide very approximate information on the presence of cobbles on the scale of the radar wavelength, 0.035 m for the Goldstone Solar System Radar and 0.126 m for the Arecibo Radar, by measuring the radar scattering properties of the surface. See Nolan et al. 2013 for discussion (Icarus 226, 629-640, available at <http://echo.jpl.nasa.gov/asteroids/nolan.etal.2013.bennu.pdf>).

Boulders on 2008 EV₅

This document is a NASA working document and is subject to further revision. This document has been reviewed for release to the public and is not export controlled.

Candidate boulders can be identified in Arecibo radar images of EV₅ from 2008 December 23, 26, and 27. On 2008 December 24, a problem with the transmitter power supply at Arecibo limited the transmit power to about 1/7 what it was on the other three days. The much lower echo signal-to-noise of the resulting radar images made identifying small features difficult.

The candidate boulders visible in the radar images from 2008 December 23, 26, and 27 appear as unresolved single bright pixels or as two adjacent bright pixels (Figure 25). Given a range resolution of 7.5 m, an unresolved boulder is less than 15 m in diameter – only the Earth-ward side of each boulder was illuminated by the radar. Some boulders are visible more than 50 m behind the trailing limb of EV₅, implying that they are at least 7 m higher than their surroundings. These boulders are described as “10 m scale”.

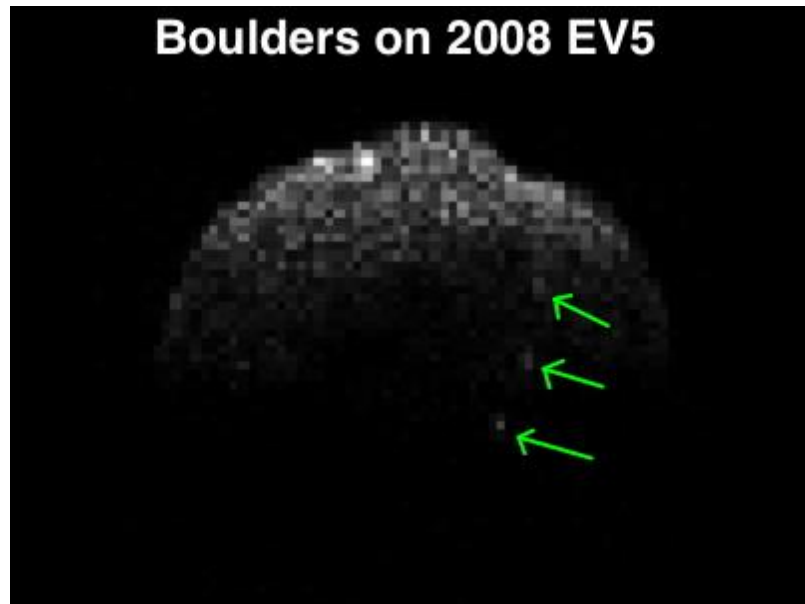


Figure 25: Range-Doppler radar image of 2008 EV₅, obtained at Arecibo Observatory at 2008 December 23 07:41 UT. Range from Earth increases from top to bottom. Image resolution is 7.5 m/pixel in range. The large concavity at EV₅'s equator is visible at upper right. Green arrows denote three candidate 10-m-scale boulders.

The radar images from 2008 December were all obtained with the subradar point just south of EV₅'s equator. I therefore cannot identify candidate boulders near the asteroid's north pole. Nor can I identify boulders at equatorial latitudes. Near the equator, larger areas of the EV₅'s surface fall within a given range-Doppler radar pixel and small boulders are lost to confusion with the surface around them. I can only identify 10-m-scale boulders over about ½ of EV₅'s surface. Finally, the range-Doppler projection has a north-south ambiguity. For most of the candidate boulders I identify, I cannot determine which hemisphere they are located in. The exception is a prominent boulder near the asteroid's south pole (lowest arrow in Figure 25, see also Figure 26).

With these caveats, I identify 6 distinct candidate 10-m-scale boulders on EV₅'s surface by visual inspection of the radar images. I estimate there to be at least 10 such boulders over the asteroid's entire surface.

This document is a NASA working document and is subject to further revision. This document has been reviewed for release to the public and is not export controlled.

Based on EV₅'s radar scattering properties and the highest-resolution images of asteroid surfaces from spacecraft (Eros and Itokawa), there are millions of 10-cm scale cobbles on EV₅.

If there is a power-law distribution between the two size ranges sampled by the available radar data, as seen on Itokawa and Eros, there are a few hundred 3-m scale boulders on EV₅'s surface. There should be an abundant number of choices for the ARV.

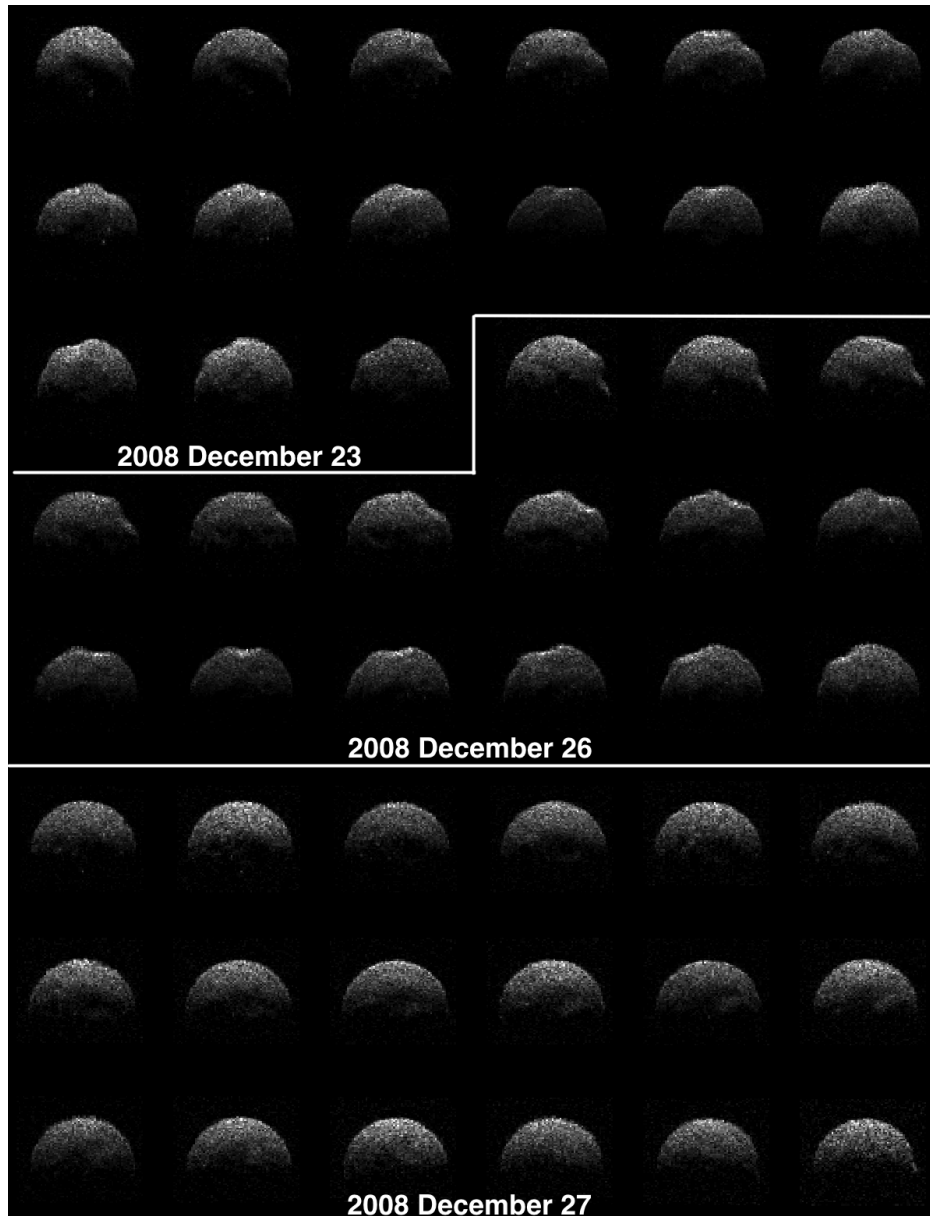


Figure 26: Collage of EV₅ radar images from Arecibo, obtained on 2008 December 23, 26, and 27. Resolution is 7.5 m/pixel in range in all images. Time increases from left to right and top to bottom. EV₅ appears to rotate counter clockwise and the image enlarged in Figure 25 is first on the left in the second row of the collage. Candidate 10-m-scale boulders appear as bright pixels. The boulder near EV₅'s south pole is visible in images on all three days, appearing well behind the trailing limb of the radar echo and near the center.

This document is a NASA working document and is subject to further revision. This document has been reviewed for release to the public and is not export controlled.

Appendix C: Full Surface Geotechnical Properties Response

What are the expected surface regolith geotechnical properties of the parent asteroid? For example: What is the expected range in the coefficient of friction between the parent asteroid surface regolith and the CRS contact pads? How uniform is this expected to be?

Coefficient of friction is a function of a magnitude of cohesive forces between regolith and contact pads. The main sources of cohesive forces are van der Waals and electrostatic forces.

Smaller particles have higher van der Waals forces per unit volume than larger particles and therefore friction between fine regolith and contact pads will be greater. For example a 1 micron grain would have a strength of less than 300 Pa, a 10 micron grain would have a 30 Pa strength, while a 100 micron grain would have a strength of 3 Pa [Sánchez and Scheeres, 2014].

Additionally, both the regolith and the spacecraft will be charged, due to their interactions with the solar wind plasma. The electrostatic force on a dust grain is the product of the grain charge and the local electric field. A calculation of the electrostatic force on the dust grain is described by Hartzell and Scheeres [2011]. Using simple approximations for the charge on the dust grain as well as the electric field between the dust grain and the spacecraft gives the following expression for electrostatic force:

$$F_{es} = 4\pi\epsilon_0 r_d U \frac{|U - U_{sc}|}{l}$$

where r_d is the radius of the dust grain, U is the potential of the regolith (approximately 5V in sunlight), U_{sc} is the potential of the spacecraft (varies with location on spacecraft and lighting conditions, but probably on the order of 10V), l is the length scale (separation between the dust grain and spacecraft), and ϵ_0 is the permittivity constant. For a 1 mm grain at 5 V, assuming a 10 V potential difference and a length scale of 1 mm, this results in a force on the order of 10^{-9} N. Although the electrostatic force will increase under certain lighting conditions and as the length scale decreases, it is unlikely to be more significant than van der Waals cohesion. A comparison of van der Waals cohesion and the electrostatic forces is reported by Scheeres et al., [2010].

During the Apollo program extensive work was conducted to acquire fundamental scientific and engineering knowledge of lunar-mineral resources through testing a simulated lunar environment. Karafiath and Mohr [1994] measured the friction between a rotating steel disc and a bed of fine (38-62 μm) and coarse (250-500 μm) crushed basalt (i.e. they investigated material-regolith interface). They found that the resistance between the steel disc and crushed basalt for both the coarse and the fine samples was higher under ultrahigh vacuum (below 10^{-10} kPa) than in air. However, it was found the coefficient of friction is not affected by the ultrahigh vacuum (Table 17). Ultra-high vacuum increase the total frictional resistance by an adhesion which is essentially constant over the range of normal loads in the experiment (455-910 gram).

This document is a NASA working document and is subject to further revision. This document has been reviewed for release to the public and is not export controlled.

Table 17: Coefficient of friction between steel disc and crushed basalt in vacuum and at 1 g [Karafiath and Mohr, 1969].

	Between steel disc and crushed coarse basalt (250-500 micron)		Between steel disc and crushed fine basalt (38-62 micron)		Between steel disc coated with coarse basalt and crushed basalt	
	Vacuum	Air	Vacuum	Air	Vacuum	Air
Initial Coefficient of Friction (effect of regolith dilation to allow grain displacement)	0.35	0.35	No Data	No Data	No Data	No Data
Kinetic Coefficient of Friction	0.28	0.27	0.20	0.18	0.28	0.20

What is the expected range of surface compaction and porosity of the regolith surrounding the boulder? How uniform is this expected to be?

The asteroid surface is more likely to be a pebble-rich lag depleted of fines and as such the surface porosity should be higher and compaction lower than asteroid’s bulk compaction and porosity. Whatever the porosity and compaction, it is likely that the same processes apply all around the target area, so it should be fairly uniform. In turn, this should be applicable to all ARRM targets. The exceptions are “low” areas observed for example on Eros and Itokawa that were filled with relatively fine material. These areas may be less consolidated than the surrounding terrain. However, the NEAR spacecraft landed on Eros in one of the fine-grained pond areas without making much of a noticeable impression on the pond or the spacecraft (impact velocity was approximately 1.5 to 1.8 m/s). Probably the consolidation (perhaps driven by thermal cycling) is enough to support a spacecraft in microgravity. Even with the mineralogy difference between Eros and EV₅ similar processes of consolidation should produce similar results.

For reference, properties of Itokawa (S-type), Bennu (B-type), and 253 Mathilde (C-type) are:

- Itokawa: bulk density of 2.0 g/cc; bulk porosity of 40.6%, or packing fraction of 0.59. [Abe et al., 2006; Gaskell et al., 2008]
- Bennu: bulk density = 1.260 ± 0.070 g/cc (1-sigma uncertainty) [Chesley, 2014]
- 253 Mathilde: 1.34 g/cc [Veverka, 1999]

Figure 27 and Figure 28 shows asteroids macroporosities and densities [Consolmagno et al., 2008; Britt et al., 2002].

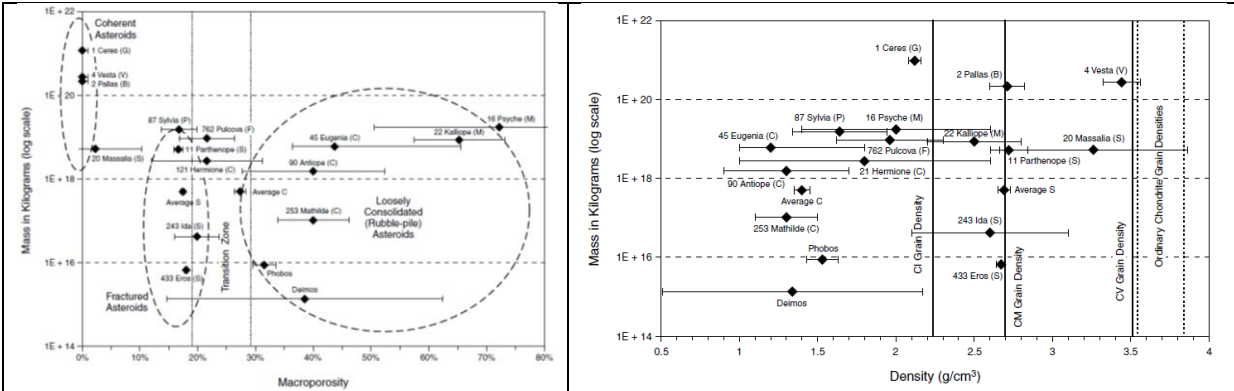


Figure 27. Macroporosities and densities of asteroids. [Britt et al., 2002]

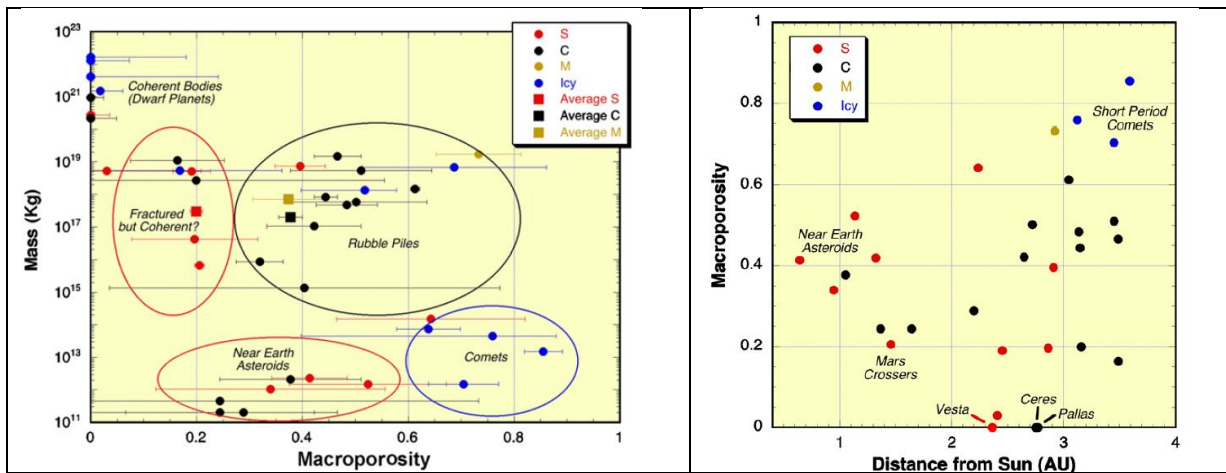


Figure 28. Macroporosities of asteroids [Consolmagno et al., 2008]

What is the expected particle size-frequency distribution of the regolith, and how does this influence the design of the CRS contact pads and geological context samplers?

Cumulative size distribution of coarse and fine regolith has a power-index of $d^{-2.8}$. This is based on particles size-frequency distribution of rocks and boulders on Itokawa in the millimeter to tens of meters size [Michikami, 2008] and grains from less than 100 micron down to 1 micron sizes returned by Hayabusa [Tsuchiyama, 2011].

Coarse gravel (1 cm or greater) is expected to exist on the surface overlaying fine grained material with the fraction of fines increasing with depth. The combination of low surface acceleration and solar radiation pressure tend to strip off fine particles, generated by comminution processes, and leave lags of larger, harder to move materials.

Since forces during the boulder extraction will be reacted through the CRS contact pads back to the asteroid, the pads need to be designed to prevent excessive sinkage. If regolith is rich in fines, its cohesion and in turn bearing strength will be greater and thus contact pads could be made smaller. The same is true if regolith is more compact. If regolith is coarse, cohesion will be lower and in turn contact pads would need to be larger. The same is true if regolith has low density/high porosity. Contact pads also need to leave the surface when spacecraft departs with the boulder. These two steps (boulder extraction and contact pads extraction from the surface) have competing requirements: for boulder extraction contact

This document is a NASA working document and is subject to further revision. This document has been reviewed for release to the public and is not export controlled.

pads need to be large and for contact pads extraction, the contact pads need to be small. Therefore, mission risk is likely reduced if the three contact pads are oversized (with appropriate margin) to prevent excessive sinkage. The issue of detaching of contact pads from the surface could be eliminated by implementing 'decoupling' subsystems that would leave the pads behind.

It is challenging to design a regolith sampler that will work with any and all particle sizes. The sampler would therefore benefit by being designed for specific particle sizes.

What is a set of earth analog surfaces (e.g. concrete, sand) that could be used to bound the expected range of surface variability for use in validating the design of the landing system?

From a regolith interaction standpoint, analog material should be 'designed' to match the regolith geotechnical properties. As such, parameters that are important include particle size distribution, particle shape, particle strength, magnetic moment, and particle density. All other material bulk properties, such as bulk density, porosity, shear strength (cohesion and friction angle), are directly influenced by these grain properties. Environmental parameters such as vacuum and gravity could have a much greater effect on geotechnical properties of granular material, and this needs to be taken into account.

The OSIRIS-REx team has developed several asteroid simulants, including Tagish Lake 7c (TL7c) [Hildebrand, 2015]. University of Central Florida [Dan Britt] is currently developing several asteroid simulants with a range of strengths and particle sizes.

What is the expected bearing strength of surface regolith? This is needed to determine if ARV requires dampers within the three legs.

Regolith bearing strength is highly dependent on the degree of regolith consolidation, internal friction angle, and cohesion. The four common bearing capacity failures are shown in Figure 29 (Jerry Johnson UAF, personal communication).

Four possible modes of regolith failure under a landing pad

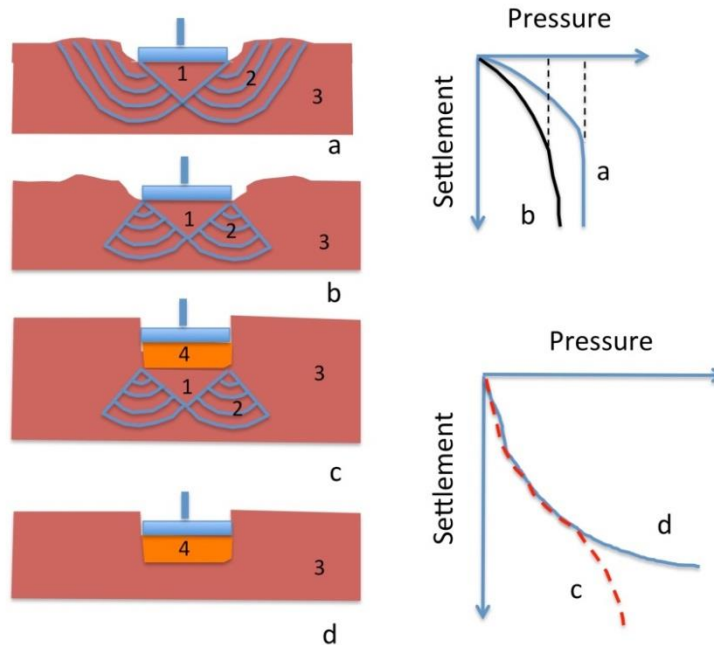


Figure 29: Bearing strength failure modes for soils. General shear failure (a), local shear failure (b), compaction with local shear failure (c), and compaction (d).

General shear failure occurs in well-consolidated regolith that has little pore space for particles to move into when subjected to compression. Failure occurs as a plug of regolith is pushed into the regolith (Figure 29a, #1) forcing regolith to displace laterally via slip planes to form a mound around the landing pad (Figure 29a, #2). When regolith is poorly consolidated with a loose to medium packing density, shear slip planes may not extend to the surface. While some mounding likely occurs at the surface, much of the regolith deformation is accommodated by filling pore space through grain rearrangement (Figure 29b). For very low density material (especially for cohesive regoliths), initial regolith settlement occurs through compaction that can either transition to local shear failure (Figure 29c) or continue compacting (Figure 29d), depending on the gradient of density and strength with depth [Das, 1998, Apfelbeck et al., 2011]. The pressure–settlement function differs for each of the different failure modes.

As a note, bearing strength failure is not necessarily a catastrophic event as long as the magnitude of settling is small enough such that adjustments to the spacecraft can be made to complete the capture operations. It is important to estimate the amount of expected settling that will occur during an initial bearing strength failure as it is highly likely that after the initial failure a high strength regolith will be encountered at depth.

Since asteroid gravity is negligible, Terzaghi’s equation [Terzaghi, 1943] for circular or square footing could be used to obtain a first order bearing capacity of the regolith. The bearing capacity of the regolith is defined as $\sigma = 1.3 * (c+c') * N_c$, where c is the regolith cohesion due to van Der Waals forces, c' is the apparent cohesion due to particles interlocking, and N_c is the bearing capacity factor.

The low limit for bearing strength can be calculated assuming the friction angle $\varphi=0^\circ$ ($N_c=5.7$), $c=25$ Pa and $c'=0$ Pa. Hence $\sigma=1.3 * (25+0) * 5.7 = 185$ Pa.

This document is a NASA working document and is subject to further revision. This document has been reviewed for release to the public and is not export controlled.

The upper limit for bearing strength can be calculated assuming $\phi=10^\circ$ ($N_c=9.6$), $c=250$ Pa and $c'=100$ Pa. Hence $\sigma=1.3 * (250+100) * 9.6 = 15,600$ Pa.

These are very rough estimates of the lower and upper limits of the bearing strength. Numerical modeling should be used to provide better estimates and sensitivities to different regolith and spacecraft parameters.

It should be noted that additional information with respect to regolith bearing strength will be available once OSIRIS-Rex- and Hayabusa2 missions performed their sampling operations.

What is the expected distribution in cohesion between ~1-5 meter boulders and the surface of 2008 EV₅?

Fine grains will preferentially attach to larger grains, and thus larger grains embedded in a matrix of fine grains would be held in place by the strength of the matrix itself. Hence, the cohesion between large boulders and regolith will be driven by cohesion between fine particles estimated to be in the range of 25-250 Pa [Sánchez and Scheeres, 2014].

Rozitis et al. [2015] reported that near-Earth asteroid (29075) 1950DA, whose bulk density ranges from 1.0 g/cc to 2.4 g/cc, is a rubble pile and requires a cohesive strength of at least 44–76 Pa to keep from failing due to its fast spin period.

Hirabayashi et al., [2014] determined possible cohesive values of a main belt comet P/2013 R3 which experienced a breakup, probably due to rotational disruption, to be 40–210 Pa).

Lunar surface regolith has cohesion in the range of 440 to 620 Pa [Heiken et al., 1991]. Since lunar regolith contains significant fraction (up to 50%) of agglutinates which provide apparent cohesive strength due to their interlocking nature, it is highly probable that cohesive strength without apparent cohesion would be much lower and in the range what's been suggested for asteroids at 25-250 Pa.

- **How does cohesion translate into the required extraction force for a given sized boulder?**

Regolith bearing capacity for shear failure is a function of cohesion (c) and friction angle (ϕ), while regolith tensile strength is primarily a function of cohesion. Cohesion is gravity independent. Friction angle, on the other hand, is normal force dependent, and it is zero at zero gravity, unless pressure is applied on confined regolith. Cohesion sometimes is due to particles interlocking, and is called apparent cohesion or c' (e.g. lunar regolith has extremely high apparent cohesion). Cohesion is density dependent; that is, denser the regolith, higher the cohesion. Bearing capacity compaction failure is a function of porosity and it is low at high porosity.

$F_{\text{extraction}}$ is a sum of two forces: cohesive force and inertial force. Cohesive force is attributed to boulder-regolith cohesion which is driven by regolith's matrix and can vary from 25 Pa to 250 Pa [Sanchez and Scheeres, 2014]. Inertial force is a function of the acceleration the boulder achieves during the process of lifting it off the surface. Hence, $F_{\text{extraction}} = \text{cohesion} * A_{\text{boulder}} + \text{Force}_{\text{inertia}}$. The extraction force could potentially be reduced by 'peeling' the boulder off the surface [Johnson et al., 2015]. However, this needs to be traded against operational complexity and time.

This document is a NASA working document and is subject to further revision. This document has been reviewed for release to the public and is not export controlled.

To remove the boulder from the asteroid surface, extraction force or $F_{\text{extraction}}$ is reacted through a pad into regolith: F_{pad} . In other words, $F_{\text{pad}} = F_{\text{extraction}}$ as shown in Figure 30.

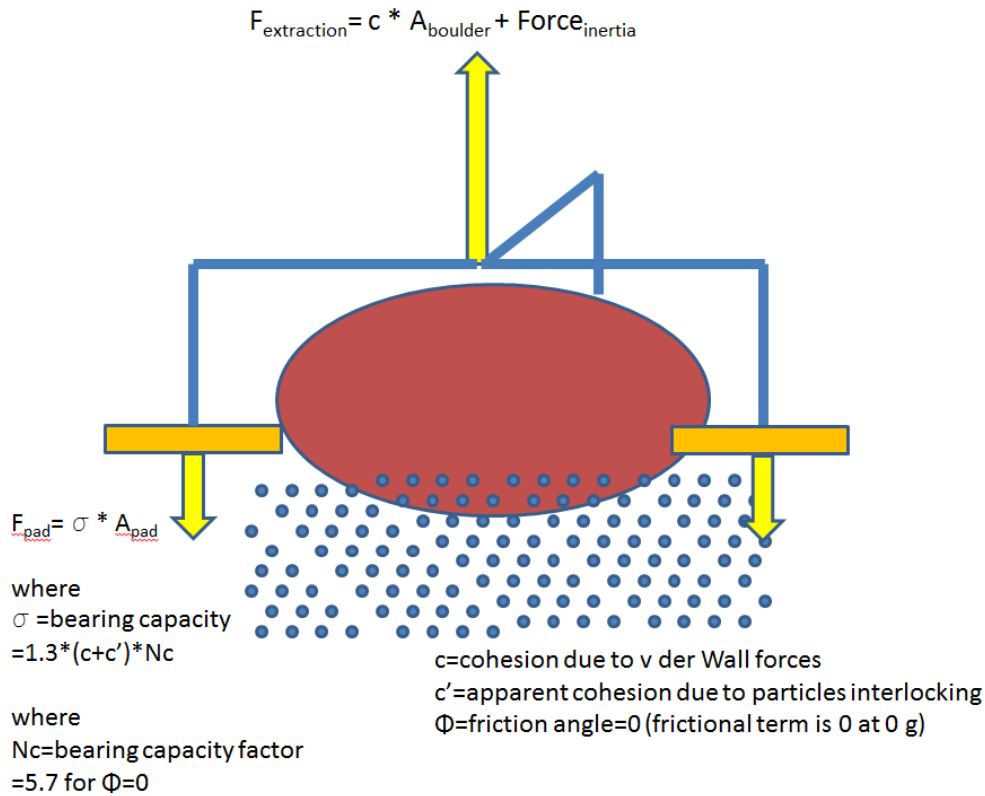


Figure 30: Balance of forces during boulder extraction.

For the pad not to sink, the regolith underneath needs to resist the boulder extraction force. In other words, regolith bearing strength, σ , needs to be high enough to support the contact pad: $F_{\text{pad}} = \sigma * A_{\text{pad}}$. To determine regoliths bearing strength, σ , a number of equations can be used but the most widely accepted is Terzaghi's bearing capacity formula. It combines fundamental strength equations and adds empirically derived factors. Since asteroid gravity is 0, the bearing capacity equation for circular or square footing becomes:

$$\sigma = 1.3 * (c + c') * N_c,$$

where c is regolith's cohesion (c) and/or apparent cohesion (c') and $N_c = 5.7$ for $\phi = 0$ and 9.6 for $\phi = 10^\circ$.

It should be noted that this equation assumes the pad is perpendicular to the regolith surface, no consolidation of the regolith occurs, and regolith fails in shear. Hence caution needs to be exercised when applying the bearing capacity equations to this particular case.

If the asteroid density is assumed to be very low, at say 30% Relative Density (D_r), then based on Figure 31, c' is approximately 100 Pa.

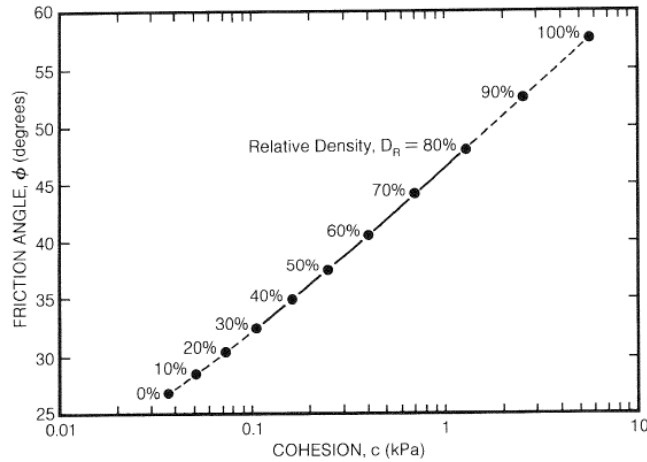


Figure 31: Measured shear strengths of a basaltic simulant of lunar regolith (showing friction and cohesion) as a function of relative density [Heiken et al., 1991].

To calculate the size of a contact pad, the following equation could be used:

$$F_{pad} = A_{pad} * 1.3 * (c + c') * Nc = F_{extraction} = (A_{boulder} * c + m * a) * f$$

$$A_{pad} = \frac{A_{boulder} * c + m * a}{1.3 * (c + c') * Nc} * f$$

For example:

- Boulder size and shape: 1 m diameter sphere
- Boulder area (1/3rd buried), $A_{boulder} = 2 \pi * r * h = 1 \text{ m}^2$
- Mass at ~2.9 g/cc density, $m = 1500 \text{ kg}$
- Boulder acceleration during extraction, $a = 0.001 \text{ m/s}^2$
- $Nc = 5.7$ for $\phi = 0$
- Cohesion, $c = 250 \text{ Pa}$
- Apparent cohesion, $c' = 100 \text{ Pa}$ ($D_r = 30\%$, for loose regolith)
- $f = 1/\text{number of pads} = 1/3$

The above assumptions lead to 21 cm contact pad diameter.

It is important to keep the boulder acceleration to minimum as this will keep inertial forces low and in turn reduce requirements on regoliths bearing capacity to support contact pads. Figure 32 shows an example of force required to accelerate a boulder of various size and mass. In this case, it was assumed the boulder is perfectly spherical and has a density of 2.9 g/cc. In calculating forces, it was assumed the boulder is accelerated at 0.001 m/s². With these parameters, it will take 14 seconds to move boulder 10 cm. The final boulder velocity will be 14 mm/sec.

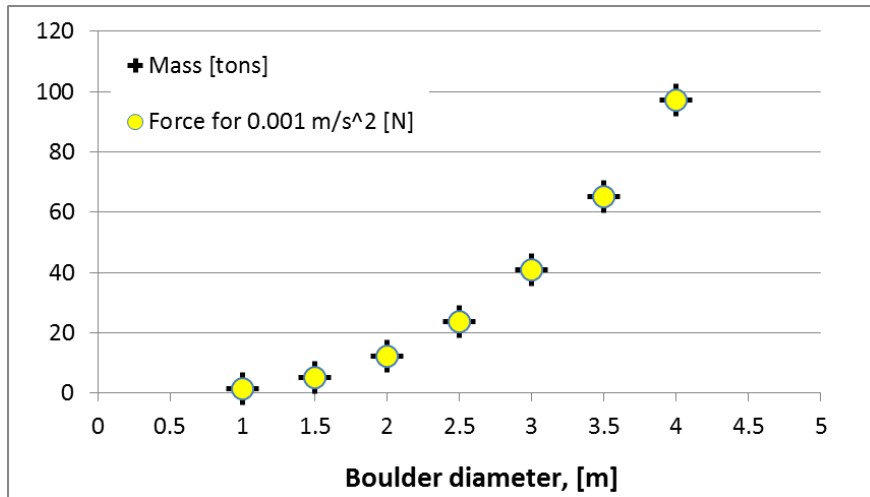


Figure 32: Acceleration Force and Mass of a boulder as a function of boulder diameter. The following assumptions were made: acceleration: 0.001 m/s²; distance: 10 cm; boulder density 2.9 g/cc; boulder shape: sphere.

Figure 33 shows relationship between contact pad diameter and boulder diameter for $c'=100$ Pa (loose regolith) and $\phi=10^\circ$. Inertia force was taken from Figure 32 for various boulder diameters. The calculations assumed spherical boulder with density of 2.9 g/cc (e.g. igneous rock) and 33% buried. If a required contact pad diameter is ~ 0.8 m ($1/3^{\text{rd}}$ buried 3 m boulder, $c=250$ Pa and $c'=100$ Pa), the total surface area of the three contact pads is ~ 9 m². The required spacecraft thrust is 2250 N.

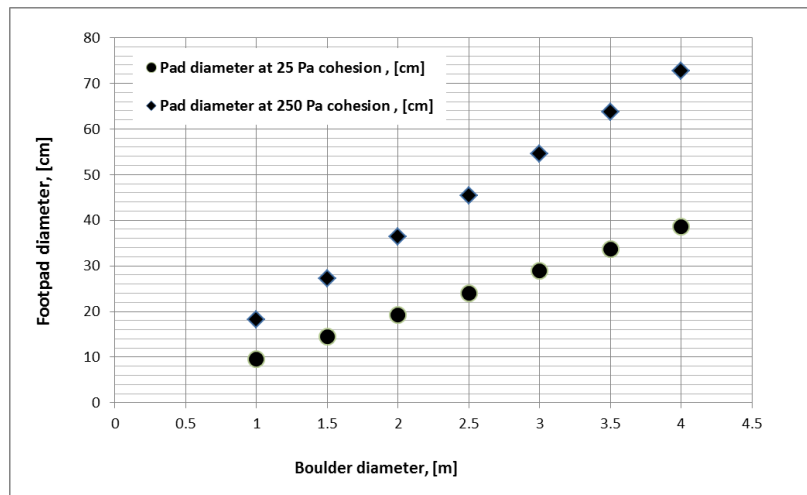


Figure 33: Pad diameter as a function of boulder diameter.

- Is there a way to estimate (or narrow the uncertainty in) the cohesion between the surface and boulder based on the visual images from the in situ characterization phase?

It is not possible to estimate with great certainty the cohesion between the surface and the boulder from visual imagery. However, the regolith strength (which drives cohesion between the boulder and the surface) can be determined by deploying geotechnical instruments. The geotechnical data could

This document is a NASA working document and is subject to further revision. This document has been reviewed for release to the public and is not export controlled.

then be used analytically or with an aid of numerical models such as DEM, to estimate cohesion between the surface and the boulder.

- How do we expect the cohesive force to “break” during boulder extraction?

The extraction of a boulder from a regolith with a size distribution ranging down to microns to 100’s of microns requires the breaking of cohesive bonds within the regolith. Based on DEM simulations [Sanchez and Scheeres, 2014] this occurs in two phases, a quasi-elastic phase followed by a plastic phase when the bonds between individual grains are broken (Figure 34). Due to the physics of cohesion, fine particles will preferentially adhere to a larger boulder, meaning that extraction occurs by breaking cohesive forces within the regolith.

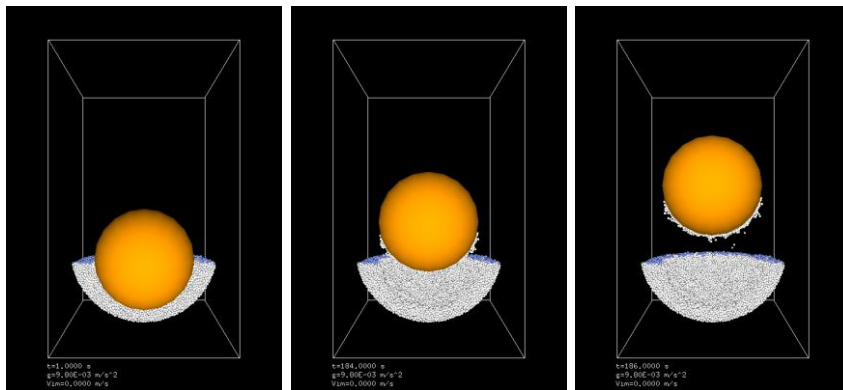


Figure 34: Shows the results of a DEM simulation of a boulder extraction from a cohesive regolith [Sanchez and Scheeres 2014]. Note that the cohesive regolith preferentially adheres to the boulder, meaning that extraction occurs by breaking the cohesive forces within the regolith.

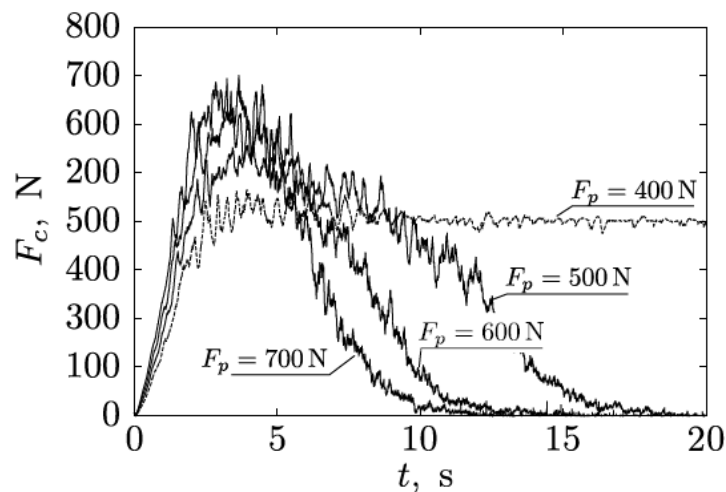


Figure 35. Resistance force profiles for different pull forces F_p in “peeling” test and regolith cohesive strength $c = 100 \text{ Pa}$. F_c is a DEM computed force that needs to be exceeded to remove the boulder from the surface. In this example 400 N pulling force is not sufficient to separate the boulder from the regolith [Kulchitsky et al., 2015].

This document is a NASA working document and is subject to further revision. This document has been reviewed for release to the public and is not export controlled.

Figure 35 gives an example of a general shape of the Pull Force, F_p , as a function of time [Kulchitsky et al., 2015]. The exact shape will depend on the cohesive values as well as extraction methods (e.g. constant acceleration, peeling etc.).

Are there any other likely physical properties or mechanisms that would prevent a boulder from being extracted?

Unless boulder can be inspected underneath, there will always be a risk that another rock could be wedging the boulder in place. The boulder could be buried in the regolith along its long axis.

There is also some uncertainty related to the effect that phyllosilicate minerals have on the strength of regolith and forces between the regolith and boulder. This could be investigated further.

References:

- Abe et al. (2006). Mass and local topography measurements of Itokawa by Hayabusa. *Science* 312:1344–1347.
- Apfelbeck, M., S. Kuř, B. Rebele, B. Schäfer. 2011. A systematic approach to reliably characterize soils based on Bevameter testing, *Journal of Terramechanics*, 48:360-371, <http://dx.doi.org/10.1016/j.jterra.2011.04.001>
- Chesley, S.R., Farnocchia, D., Nolan, M.C., Vokrouhlický, D., Chodas, P.W., Milani, A., Spoto, F., Benner, L.A.M., Busch, M.W., Emery, J., Howell, E.S., Lauretta, D., Margot, J.-L., Rozitis, B., Taylor, P.A., 2014. Orbit and bulk density of the OSIRIS-REx target asteroid (101955) Bennu. *Icarus* 235, 10-22.
- Das, B. M. (1998). Principles of geotechnical engineering. 4th ed., Boston, PWS Publishing Co., ISBN: 0-534-95179-1, 712 p.
- Gaskell et al., (2008). Itokawa shape model v1. 0. NASA Planetary Data System, 92
- Hartzell C., and D. Scheeres. “The Role of Cohesive Forces in Particle Launching on the Moon and Asteroids”(2011), *Planetary and Space Sciences*. 2011. Vol 59, pp 1758-1768.
- Heiken, G., D. Vaniman, B. French, (1991), *Lunar Sourcebook*, Cambridge University Press
- Hildebrand et al., (2015), An Asteroid Regolith Simulant for Hydrated Carbonaceous Chondrite Lithologies, 78th Annual Meeting of the Meteoritical Society (2015)
- Karafiath L., and G. Mohr, Effect of Ultrahigh Vacuum on the Friction between Metals and Granular Soils, *J. Vac. Sci. Technol.* 6, 198 (1969); <http://dx.doi.org/10.1116/1.1492659>
- Kulchitsky et al. (2015). Resistance forces during boulder extraction from an asteroid. *Acta Astronautica* AA_2015_93 (Submitted).
- MarcoPolo-R (2015) <http://us-marcopolor.jhuapl.edu/mission/docs/Potential%20NASA%20contribution.pdf>
- Mazrouei et al., (2014). Block distributions on Itokawa. *Icarus* 229:181–189.
- Michikami et al. (2008). Size-frequency statistics of boulders on global surface of asteroid 25143 Itokawa. *Earth, Planets and Space* 60:13–20.
- Sánchez, P. and D. J. Scheeres (2014). The strength of regolith and rubble pile asteroids, *Meteoritics & Planetary Science* 49, Nr 5, 788–811 (2014), doi: 10.1111/maps.12293
- Scheeres, D., C. Hartzell, P. Sánchez, M. Swift. “Scaling Physics to Asteroid Surfaces: The Role of Cohesion” *Icarus*. 2010. Vol 210, pp 968-984.
- Tsuchiyama et al., (2011). Three-dimensional structure of Hayabusa samples: Origin and evolution of Itokawa regolith. *Science* 333:1125–1128.

This document is a NASA working document and is subject to further revision. This document has been reviewed for release to the public and is not export controlled.

Appendix D: Additional Boulder Physical Property Information

Meteorite Physical Properties Papers:

- Consolmagno G.J., Macke R.J., Rochette P., Britt D. T, and Gattacceca J. (2006) Density, Magnetic Susceptibility, and the Characterization of Ordinary Chondrite Falls and Showers. *Meteoritics and Planetary Science* 41, 331-342.
- Consolmagno G.J., Britt D.T., and Macke R.J. (2008) The Significance of Meteorite Density and Porosity. *Chemie der Erde-Geochemistry* 68, 1-29
- Macke R. J. 2010. Survey of meteorite physical properties: Density, porosity and magnetic susceptibility. Ph.D. thesis, University of Central Florida. 310 p.
- Macke R.J., Consolmagno G.J., Britt D.T. and Hutson M.L. (2010) Enstatite chondrite density, porosity and magnetic susceptibility *Meteoritics & Planetary Science* 45, 1513-1526
- Macke R.J., Britt D.T. and Consolmagno G.J. (2011) Density, porosity and magnetic susceptibility of achondritic meteorites. *Meteoritics & Planetary Science* 46, 311-326.
- Macke R. J., Consolmagno G. J. and Britt D. T. (2011) Density, porosity and magnetic susceptibility of carbonaceous chondrites. *Meteoritics & Planetary Science* 46, 1842-1862.

Meteorite Thermal Properties Papers:

- Ali-Lagoa V., Lionni L., Delbo M., Gundlach B., Blum J., and Licandro J. (2014) Thermophysical properties of near-Earth asteroid (341843) 2008 EV₅ from WISE data. *Astronomy and Astrophysics* 561, A45.
- Opeil C.P., Consolmagno G.J., Safarik D.J., and Britt D.T. (2012) Stony meteorite thermal properties and their relationship to meteorite chemical and physical states. *Meteoritics & Planetary Science*, 47, 319-329.
- Opeil C.P., Consolmagno G.J., and Britt D.T. (2010) The Thermal Conductivity of Meteorites. New Measurements and Analysis. *Icarus* 208,449-454.
- Brodsky N.S., Riggins M., and Connolly J. (1997) Thermal Expansion, Thermal Conductivity, and Heat Capacity Measurements at Yucca Mountain. *Int. J. RockMech. &Min. Sci.* 34:3-4, Paper No. 040
- Delbo M., Libourel G., Wilkerson J., Murdoch N., Michel P., Ramesh K.T., Ganino C., Verati C. and Marchi S. (2014) Thermal fatigue as the origin of regolith on small asteroids. *Nature*, Vol 50, 233.
- Ghabezloo S. (2012) Micromechanical analysis of the effect of porosity on the thermal expansion coefficient of heterogeneous porous materials. *International Journal of Rock Mechanics & Mining Sciences* 55, 97-101
- Nagihara S, Hedlund M, Zacny K, and Taylor P.T. (2014) Improved data reduction algorithm for the needle probe method applied to in-situ thermal conductivity measurements of lunar and planetary regoliths. *Planetary and Space Science* 92, 49-56.
- Sevostianov I. (2012) On the thermal expansion of composite materials and cross-property connection between thermal expansion and thermal conductivity. *Mechanics of Materials* 45, 20-33.
- Vosteen H., and Schellschmidt R. (2003) Influence of temperature on thermal conductivity, thermal capacity and thermal diffusivity for different types of rock. *Physics and Chemistry of the Earth* 28, 499–509

Acronym List

AGC – Asteroid Grand Challenge	LEO – Low Earth Orbit
APXS – Alpha particle X-ray Spectrometry	LiBS – Laser-induced Breakdown Spectroscopy
ARCM – Asteroid Redirect Crewed Mission	MOC – Mars Orbiter Camera
ARM – Asteroid Redirect Mission	MEX – Mars Explorer
ARRM – Asteroid Redirect Robotic Mission	MGS – Mars Global Surveyor
ARV – Asteroid Redirect Vehicle	MPC – Minor Planet Center
AU – Astronomical Unit	MRO – Mars Reconnaissance Orbiter
BRDF – Bidirectional Reflectance Distribution Function	Myr – Megayear
C2 – Type 2 carbonaceous chondrites	NEA – Near-Earth Asteroid
CB – Bencubbin-type carbonaceous chondrites	NEAR – Near Earth Asteroid Rendezvous
CI – Ivuna-type carbonaceous chondrite	NEO – Near-Earth Object
CK – Karoonda-type carbonaceous chondrite	OC – Ordinary Chondrite
CLASS – Center for Lunar and Asteroid Surface Science	OSIRIS-REx – Origins, Spectral Interpretation, Resource Identification, Security-Regolith Explorer
CM – Mighei-type carbonaceous chondrite	PAH – Polycyclic Aromatic Hydrocarbon
CME – Coronal Mass Ejection	RADF – Radiance Factor
CapM – Capture Module	SEP – Solar Electric Propulsion
CO – Ornans-type carbonaceous chondrite	SFD – Size-Frequency Distribution
CR – Renazzo-type carbonaceous chondrite	SPE – Solar Particle Event
CRS – Contact and Restraint Subsystem	TAGSAM – Touch-And-Go Sample Acquisition Mechanism
CV – Vigarano-type carbonaceous chondrite	TBD – To Be Determined
DEM – Discrete Element Method	TL7c – Taggish Lake 7c simulant
DSAC – Deep Space Atomic Clock	TRL – Technology Readiness Level
DSI – Deep Space Industries	UV – Ultraviolet
EGT – Enhanced Gravity Tractor	UT – Universal Time
EOM – End-of-Mission	VLBI – Very Long Baseline Interferometry
EVA – Extra-vehicular Activity	VNIR – Visible Near-Infrared
FAST – Formulation Assessment and Support Team	XRD – X-ray Diffraction
FTIR – Fourier Transform Infrared Spectroscopy	YORP – Yarkovsky–O'Keefe–Radzievskii–Paddack
GCR – Galactic Cosmic Radiation	
GPR – Ground Penetrating Radar	
GPS – Global Positioning System	
Gyr – Gigayear	
HEOMD – Human Exploration and Operations Mission Directorate	
IAU – International Astronomical Union	
IMC – Intermediate-source Mars-Crossing region	
IMU – Inertial Measurement Unit	
IR – Infrared	
ISRU – In-situ Resource Utilization	
ISS – International Space Station	
IT – Investigation Team	
LDRO – Lunar Distant Retrograde Orbit	